Analysis of IGCC-Based Plants with Carbon Capture for an Efficient and Flexible Electric Power Generation

vorgelegt von
Diplom-Ingenieur, geb. in Berlin

Max Sorgenfrei

von der Fakultät III – Prozesswissenschaften
der Technischen Universität Berlin
zur Erlangung des akademischen Grades

Doktor der Ingenieurwissenschaften
-Dr.-Ing.-

genehmigte Dissertation

Promotionsausschuss

Vorsitzender:	Prof. Dr.-Ing. F. Ziegler
Gutachter:	Prof. Dr.-Ing. G. Tsatsaronis
Gutachter:	Prof. Dr.-Ing. H. Spliethoff

Tag der wissenschaftlichen Aussprache: 15.03.2016

Berlin 2016

Acknowledgement

This work was generated during the period of time I was working as a research associate at the *Department of Energy Engineering and Environmental Protection* of the *Berlin Institute of Technology* (Technische Universität Berlin). I really enjoyed the teaching and supervision of students as well as the pleasant and constructive atmosphere.

I am very thankful to Prof. George Tsatsaronis for having offered the supervision of this thesis. He always had an open door and supported me at all times. I would also like to thank Prof. Hartmut Spliethoff for having reviewed this thesis as a specialist in the field of electric power generation from solid fuels.

I truly appreciate the enjoyable and fruitful discussions with my colleagues Berit Erlach, Jan Eggers, Andreas Christidis, Mathias Hofmann, Sebastian Spieker, Mathias Penkuhn, Timo Blumberg, Pieter Mergenthaler, Peter Sahlmann, and the students Daniela Koch, Victor Adolfo Romo Ibarra. I will always miss the time we spent together.

I am also grateful to Suzanne Linehan Winter for having reviewed the spelling and grammar. I learned a lot and appreciate the warm and constructive atmosphere.

Finally, I would like to thank my family. Thanks to my lovely wife Eva, my son Leonard, and my daughter Elisabeth for always supporting me and giving me the strength to carry on. I would like to thank my beloved mother for having given me this opportunity and for her unconditional love, support, and encouragement.

Zusammenfassung

In der vorliegenden Arbeit werden Potentiale zur effizienten und flexiblen Stromerzeugung auf Basis von kohlegefeuerten Gas- und Dampfkraftwerken (IGCC - Integrated gasification combined cycle) mit CO_2-Abscheidung untersucht.
Als Bewertungsgrundlage dient sowohl ein effizientes als auch ein kostengünstiges kommerziell verfügbares IGCC. Thermodynamische Ineffizienzen werden zuerst basierend auf einer konventionellen Exergieanalyse für das effiziente IGCC identifiziert. Die Ergebnisse zeigen, dass der Vergaser und danach die synthesegasgefeuerte Gasturbinenbrennkammer wichtige Komponenten für den Gesamtprozess darstellen. Im Rahmen der erweiterten Exergieanalyse werden die Irreversibilitäten einerseits in einen vermeidbaren und unvermeidbaren Anteil sowie andererseits in einen endogenen und exogenen Anteil untergliedert. So wird etwa die Hälfte der Ineffizienzen des Vergasers durch andere Anlagenkomponeten verursacht (exogener Anteil). Abschließend werden die Kombinationen aus beiden Unterteilungen ermittelt und bewertet. Aufgrund des großen Einflusses der Gasturbine, wird diese detailliert nach dem aktuellen Stand der Technik modelliert. Zum besseren Verständnis wurden 12 charakteristische Ineffizienzen der Gasturbine identifiziert und bewertet.
Eine vielversprechende Weiterentwicklung der verfügbaren IGCC-Technologie stellt die Verbrennung nach dem Verfahren *Chemical-Looping Combustion* (CLC) dar. Dabei wird der Luftsauerstoff mittels Metallpartikel, die als Sauerstoffträger dienen, über einen Redox-Kreislauf an den Brennstoff abgegeben. Dadurch werden die Irreversibilitäten der Verbrennung gesenkt und die CO_2-Abscheidung erfolgt inherent. In dieser Arbeit werden die für Synthesegas potentiell geeignetsten Sauerstoffträger Nickel- und Eisenoxid bei verschiedenen Temperaturen untersucht und verschiedene Vergasertypen sowie Konfigurationen des CLC-Verfahrens analysiert. So kann etwa die Regeneration des Sauerstoffträgers mittels Wasserdampf und Luft erfolgen. Durch die Reduktion des Wasserdampfes entsteht Wasserstoff, welcher anschließend in einer Gasturbine genutzt wird. Im Besonderen liegt ein Schwerpunkt auf der Optimierung des integrierten Wärmemanagements. Die Ergebnisse zeigen ein relativ geringes Potential zur Steigerung des Gesamtwirkungsgrades.
Der wirtschaftliche Betrieb von IGCC-Anlagen kann durch eine Flexibilisierung verbessert werden. Dabei wird die Produktion des Synthesegases kontinuierlich betrieben und lediglich die Stromerzeugung wird flexibel in Abhängigkeit des Stromerlöses gefahren. Nach einer weiteren Aufreinigung des Synthesegases, besteht das Synthesegas nahezu ausschließlich aus Wasserstoff und bietet damit ein hohes wirtschaftliches Potential. Der Gewinn wird basierend auf relevanten Einflussfaktoren abgeschätzt.

Abstract

In this work, systems based on the *Integrated gasification combined cycle* (IGCC) technology with carbon capture are analyzed regarding an efficient and flexible electric power generation.

All analysis are related to a high-efficiency or low-cost IGCC base case with carbon capture which are both commercially available. In the high-efficiency base case, thermodynamic inefficiencies are determined based on a conventional exergy analysis. The gasifier followed by the combustion chamber of the gas turbine running on syngas are rated to the largest inefficiencies. Based on an advanced exergy analysis, the inefficiencies are split into an avoidable and unavoidable part as well as an endogenous and exogenous part. For example, it was found that about half of the inefficiencies within the gasifier are caused by other components of the overall system (exogenous part). Further investigations on the combination of both splitting types are presented. The gas turbine system is identified to be a major component and therefore a detailed model was developed using state-of-the-art technologies. Based on this model, 12 types of characteristic inefficiencies were determined and rated by their exergy destruction.

Chemical-Looping Combustion (CLC) is one of the most promising technologies to enhance the available IGCC design. CLC uses composite metal particles acting as an oxygen carrier to transport oxygen from the air to the fuel gas through a redox-cycle. Thus, the inefficiencies associated with the combustion process decrease and the application of physical absorption for capturing CO_2 is replaced by an inherent CO_2-capture. In this work, the most suitable oxygen carriers for CLC using syngas (nickel oxide and iron oxide) are analyzed at different temperatures. Moreover, different types of gasifier as well as CLC reactor designs are analyzed. Regenerating the oxygen carrier by steam and air, produces additional hydrogen from the reduction of steam which is further combusted within the gas turbine. Particularly, the development of the novel process design focuses on optimizing the heat exchanger network under specific constraints. The final results show a minor potential for improvement.

Economic benefits are potentially generated by a transition from a base load to a flexible operation of IGCC plants. In this process, the operation of the syngas production path remains constant while the generation of electricity depends on the market price. Subsequent to an additional purification of the common syngas, the product gas consists of almost pure hydrogen which can be sold in times of low electricity prices. The profit is estimated considering major relevant impact factors.

Contents

Nomenclature

Roman symbols

A	m^2	heat transfer area
b	-	coefficient NTU method
c^*	-	coefficient NTU method
$\dot{C}$	kW/K	heat capacity flow rate
cga	%	cold gas efficiency
D	m	diameter
$\dot{E}$	MW	exergy flow rate
$\dot{E}_\mathrm{D}$	MW	rate of exergy destruction
$\dot{E}_\mathrm{L}$	MW	rate of exergy loss
h	kJ/kg	mass-specific enthalpy
$\bar{h}$	kJ/kg	mole-specific enthalpy
H_i	MJ/kg	lower heating value (inferior)
H_s	MJ/kg	higher heating value (superior)
$\dot{H}$	MW	enthalpy flow rate
m	-	number of system components
$\dot{m}$	kg/s	mass flow rate
n	-	polytropic exponent
$\dot{n}$	kmol/s	mole flow rate
p	bar	pressure
$\dot{Q}$	MW	rate of heat transfer
$\bar{R}$	kJ/(kmol K)	universal gas constant
Re	-	Reynolds number
$\bar{s}$	kJ/(kg K)	mole-specific entropy
S_L	-	longitudinal pitch
S_T	-	transversal pitch
T	°C, K	temperature
U	W/(m^2 K)	heat transfer coefficient
v	m^3/kg	specific volume
$\dot{W}$	MW	mechanical or electrical power
x	kmol/kmol	mole fraction
x	kg_{steam}/kg_{tot}	steam quality
y_D	%	exergy destruction ratio

Greek symbols

α	-	correction factor wetness
Δ	-	difference
ε	%	exergetic efficiency
ϵ	%	heat transfer effectiveness
η_{pol}	%	polytropic efficiency
η_{s}	%	isentropic efficiency
μ	-	exponent for off-design correlation

Subscripts

0	refers to ambient or design conditions
ar	as-received
c	compressor
cv	control volume
el	electric
F	fuel
g	gaseous
i	element index
j	stream of matter or heat transfer index
k	system component index
l	liquid
maf	moisture- and ash-free
P	product
r	system component index
ref	reference
SKE	german standard coal trading unit
t	turbine
tot	total

Superscripts

AV	avoidable
CH	chemical

EN	endogenous
EX	exogenous
mexo	mexogenous
PH	physical
sat	saturated
UN	unavoidable

Abbreviations

abLA	german apportionment for interruptible loads
AC	air compressor
AGR	acid gas removal
AR	air reactor
ASU	air separation unit
BAFA	german federal office for economic affairs and export control
BGL	British Gas Lurgi
CC	combined cycle
CC	combustion chamber
CCS	carbon capture and storage
CCU	carbon capture and utilization
CEPCI	Chemical Engineering plant cost index
CFD	computational fluid dynamics
CLC	chemical-looping combustion
CNG	compressed natural gas
COT	combustor outlet temperature
DCL	direct chemical-looping
DEPG	dimethyl ether of polyethylene glycol
DOE	U.S. Energy Information Association
ECBM	enhanced coal bed methane
Eco	economizer
EEG	german renewable energies law
EES	Engineering Equation Solver
EGR	enhanced gas recovery
EIA	U.S. Department of Energy
EOR	enhanced oil recovery
FGD	flue gas desulfurization

FR	fuel reactor
GEE	General Electric Energy
GT	gas turbine
HGCU	hot gas cleaning unit
HGD	hot gas desulfurization
HP	high pressure
HRSG	heat-recovery steam generator
HT-WGS	high-temperature water gas shift
IAPWS	International Association for the Properties of Water and Steam
IEA	International Energy Agency
IGCC	integrated gasification combines cycle
IGFC	integrated gasification fuel cell
IGT	Institute of Gas Technology
IP	intermediate pressure
ISO	International Organization for Standardization
LNG	liquefied natural gas
LP	low pressure
LPG	liquefied petroleum gas
LT-WGS	low-temperature water gas shift
M	metal
MCFC	molten carbonate fuel cell
MO	metal oxide
NETL	U.S. National Energy Technology Laboratory
NGGT	gas turbine running on syngas
NIST	National Institute of Standards and Technology
NTU	number of transfer units
O&M	operating and maintenance
OTM	oxygen transfer membrane
PBI	polybinzimidazole polymer membrane
PC	pulverized coal
PC-SAFT	perturbed chain statistical association fluid theory
PSA	pressure swing adsorption
R&D	research and development
RKS-BM	Redlich-Kwong-Soave with Boston-Matthias alpha function
SCOT	Shell Claus off-gas treating
SGT	gas turbine running on natural gas

SMR	steam methane reforming
SNG	substitute natural gas
SOFC	solid oxide fuel cell
SPECO	specific exergy costing
SR	steam reactor
STIG	steam-injected gas turbine
TBC	thermal barrier coating
TCI	total capital investment
TIT	turbine inlet temperature
TREMP®	Topsøe's recycle methanation process
WGS	water gas shift

List of Figures

List of Tables

Chapter 1

Introduction

1.1 Challenges of Clean Electricity Production

One of today's major challenges is represented by the reduction of greenhouse gas emissions to the environment as well as the depletion of fossil fuels. On that account, CO_2 was identified as being a pollutant which significantly facilitates global warming. In the past, the CO_2 emissions growth accelerated due to a higher energy demand associated with rapid economic growth and an increase in the share of coal in the global fuel mix. In the year 2012, about 45 % of the worldwide CO_2 emissions from fuel combustion derived from the combustion of carbon intensive coal [1]. On that account, especially bituminous coal accounts for nearly half of the world's coal reserves [2], and will continue to play an important role in the future. The future trend in the field of electricity generation tends to increase the worldwide share of low-emission renewable energies while the use of low-emission nuclear energies strongly depend on the governmental policy, respectively.

In 2010, the energy supply sector was responsible for approximately 35 % of the total anthropogenic greenhouse gas emissions. Reducing the carbon intensity of the electricity generation is a key component of cost-effective mitigation strategies in achieving low-stabilization levels as decarbonization happens more rapidly than in the industry, buildings, and transport sectors. [3]

Based on the scenario of global electricity production published by the International Energy Agency (IEA), the future share of coal should in fact decrease by 6.7 %-points from the year 2011 to the year 2030 but the absolute coal consumption should increase by 29.7 %. The overall consumption is strongly affected by the growth of the non-OECD nations, where the demand for electricity will increase significantly by 54 % [4]. The U.S. Energy Information Association (EIA) expects the world primary

energy consumption to increase by about 30 % by the year 2030, while the electricity generation doubles [5]. Today a lot of energy providers intensify their investments into technologies using natural gas as prices have decreased the last couple of years which is mainly maintained by an increasing shale gas production. However, coal is still the most abundant and least expensive fossil fuel for electric power generation.

A reduction of greenhouse gas emissions can be realized by multiple options, like e.g. efficiency improvements in energy conversion, transmission, distribution, as well as fuel switching. Another suitable solution is represented by using carbon capture. The effect of storing the captured CO_2 depends on the type of storage. In the long term, a conversion into carbonates can be a useful option. The storage in depleted fossil fuel mining areas and other underground regions represents another possibility but still a competition to other storage materials, such as natural gas, and potentially high emission rate to the environment remain. In this process, public acceptance is one of the major challenges because leakages potentially cause rapid CO_2 emissions that substitute oxygen and in this way may cause fatalities. Further utilization of CO_2 should be preferred in order to replace carbon from fossil sources but still a lot of research is required to find proper solutions. While all components of carbon capture system are in use today by the fossil fuel extraction and refining industry, the success of large-scale carbon capture technologies is subject to the price of CO_2 emission certificates.

Regarding the efficiency of coal-fired plants with CO_2 capture, the U.S. Department Of Energy (DOE) recommends that an electric power generation by Integrated Gasification Combined Cycle (IGCC) power plants should be preferred over Pulverized Coal (PC) steam power plants [6]. The U.S. DOE has further investigated different setups and components of an IGCC plant with carbon capture. Using a Shell gasifier and a dry syngas quench was found to be the most efficient option. From an economic point of view, using a GEE radiant gasifier and a water quench represents the best option [7].

1.2 Motivation and Scope of This Work

This work focuses on the future trend analysis of the IGCC technology. The results of this analysis provide the fundamentals for generating an ecologically and economically worthwhile policy framework. Accordingly, the overall efficiency and the economic feasibility are the major challenges.

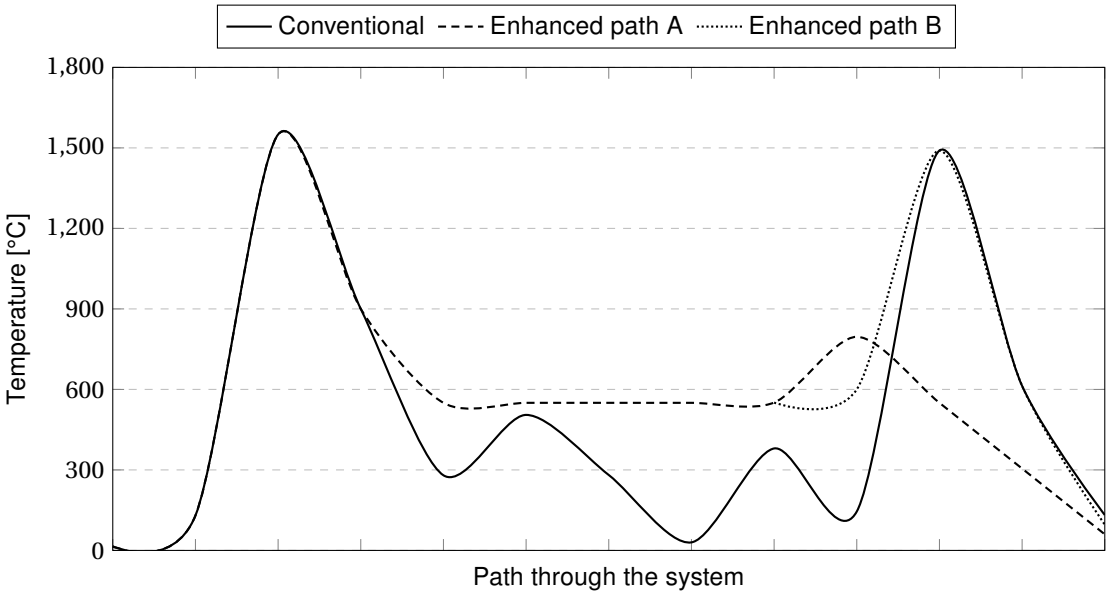

Figure 1.1: Temperature development through the IGCC-based systems.

Efficiency Approach

From a thermodynamic point of view, the temperature development through a conventional state-of-the-art IGCC plant with carbon capture holds some potential for further improvements. Figure 1.1 shows the temperature drop between the gasifier and the combustion chamber of the gas turbine system as the removal of pollutants takes place at low temperatures. In order to handle this temperature development, a suitable integrated heat management is required. Even in the best case, thermodynamic inefficiencies occur due to temperature differences within the heat exchangers. The dashed and dotted curves show the resulting temperature development of an enhanced IGCC plant using a Hot Gas Cleaning Unit (HGCU) and Chemical-Looping Combustion (CLC). As two gas streams exit the CLC unit, the dotted line represents the path of the other stream in parallel. From the diagram it becomes visible that a smaller temperature drop occurs in the case of the enhanced IGCC plant when compared to the conventional IGCC plant. Finally, the proof of this approach will be rated by the overall net efficiency of the analyzed cases. Furthermore, the exergy analysis is a suitable tool in order to identify the distribution of inefficiencies within the systems.

Flexibility Approach

The economic viability of an IGCC plant is strongly influenced by the governmental regulations of the market and other market players. Figure 1.2 shows the qualitative

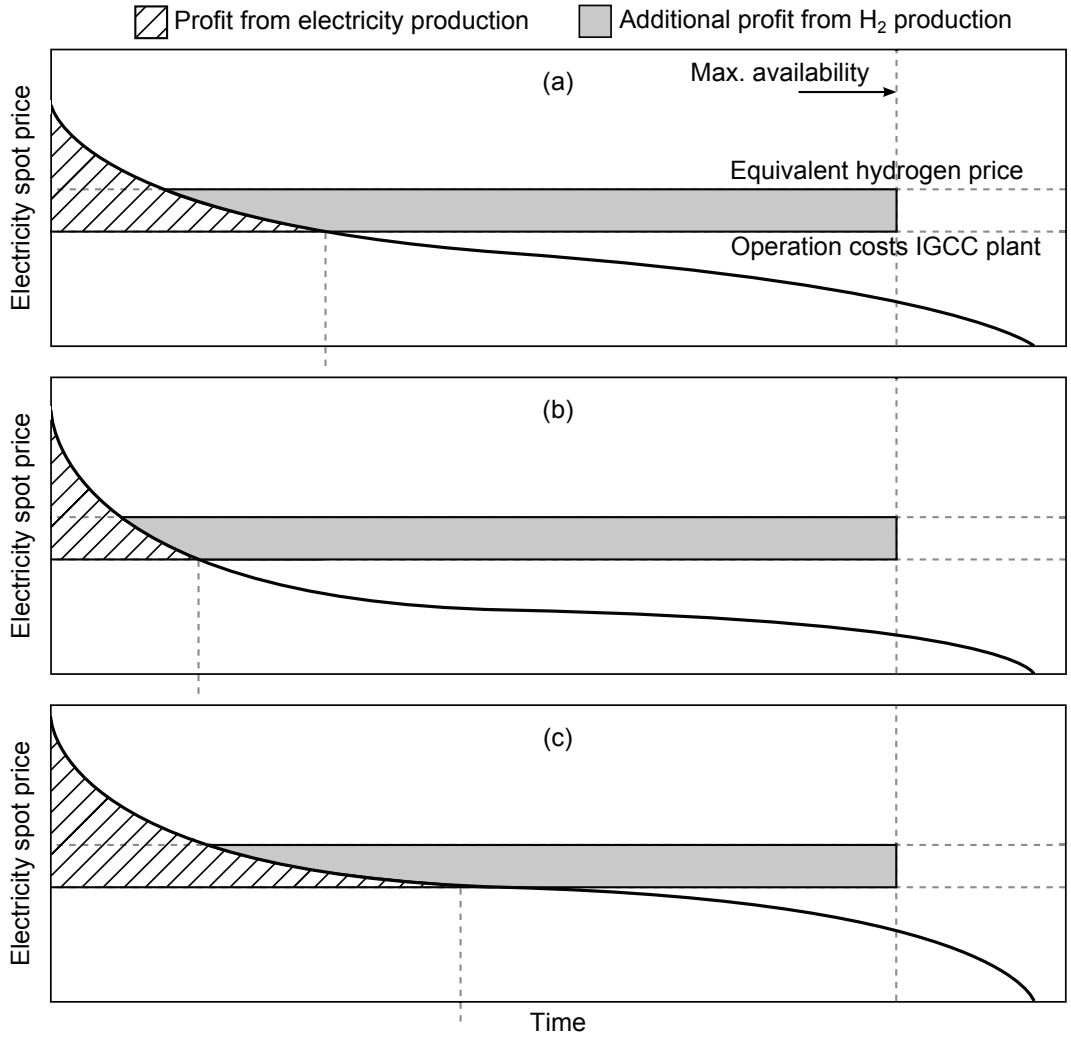

Figure 1.2: Annual load curve of a flexible IGCC plant producing electricity or hydrogen in a (a) conventional fossil-based market, (b) market with growing renewable energies quota and (c) market with increasing CO_2 certificate costs.

operation potential of an IGCC plant for different market conditions. Case (a) represents the annual load curve of electricity spot prices induced by a conventional centralized fossil-based market. Typically, the peak prices represent the operation of stand-alone gas turbines running on natural gas or oil, followed by combined cycle power plants. The mid range represents steam power plants using bituminous coal followed by lignite. Smaller prices are generated by nuclear power plants. In this market, the operation of an IGCC plant ranges in the area of steam power plants using a similar type of coal since the minimum operation costs mainly depend on the fuel costs as well as on the overall efficiency. The lower dashed line represents the operation costs of an IGCC plant which also may include the return on investment. The profit is

generated by the difference of the electricity spot price and the operation costs as long as the electricity spot prices is higher. In addition, some technical limitations causing down time may further reduce the availability of units assumed in this diagram.

The upper dashed line represents the equivalent hydrogen price determined by the hydrogen market price and the ratio of efficiencies producing either electricity or hydrogen. The corresponding value strongly depends on the costs of natural gas as today most of the available hydrogen is produced by Steam Methane Reforming (SMR). In Germany, the resulting price is higher when compared to the operation costs of an IGCC plant. By assuming a constant production of syngas, purified hydrogen can be sold at times right to the intersection limited by the maximum availability of the IGCC plant. In this way, additional profit can be generated by a flexible production.

Considering a market with growing renewable energies quota (case (b)), typically the electricity spot prices decrease but the peak prices increase. This reduces the operation time and, simultaneously, the profit of an IGCC plant which only generates electric power. Finally, this scenario even more favors a flexible co-production of hydrogen.

Case (c) represents an electricity market with increasing CO_2 certificate costs. In general, the prices increase due to the CO_2 emissions of the technologies, respectively. Particularly, the emissions depend on the fuel carbon fraction and the overall efficiency. The increase of stand-alone gas turbines and steam power plants using bituminous coal is supposed to be almost the same. Using lignite is even worse. Combined-cycle power plants feature the highest efficiency resulting in a very small increase and nuclear power plants operate with almost no CO_2 emissions. The higher electricity spot prices left to the intersection increase the profit from the electricity generation. A flexible co-production of hydrogen is still advantageous but the additional profit is smaller compared to the other scenarios.

Cases (b) an (c) show an opposing trend. Depending on the future policy framework, the profit of commercial IGCC plants as well as the commitment of a flexible hydrogen co-production can be advantageous.

Chapter 2

State of Research

2.1 Carbon Capture and Utilization

Generally, there are two strategies how to handle captured carbon dioxide. Carbon Capture and Storage (CCS) refers to the storage in geological rock formations, depleted oil and gas fields (on- and offshore), as well as saline aquifers. Carbon Capture and Utilization (CCU) refers to the reuse of CO_2 for synthetic products.

Carbon Capture

In the power industry, CO_2 arises from the combustion or oxidation of hydrocarbons. Especially processes using fossil fuels that have high specific CO_2 emissions have great potential to decrease the global CO_2 emissions using carbon capture. Depending on the overall efficiency and the carbon content of the fuel, lignite and bituminous coal should be considered first. Commercially available capturing systems decrease the overall efficiency by 8-10 %, including the transport to a storage location [8].

In general, CO_2 capture can be performed by applying absorption, adsorption or membranes. Pressure Swing Adsorption (PSA) is the most experienced process and the use of membranes is still under research. The capture technologies are divided into three superior groups:

- Pre-combustion capture:
  CO_2 gets captured from a reformed synthesis gas of an upstream gasification unit prior to combustion. Typically, physical absorption is used at a high partial pressure of CO_2. Common physical solvents or processes are namely Selexol®, Rectisol®, Purisol®, Sepasolv MPE, Fluor solvent, Sulfolane, and Estasolvan [6].
- Post-combustion capture:
  CO_2 gets captured from the flue gas stream subsequent to combustion. Typically,

chemical absorption is applied at a low partial pressure of CO_2. Common chemical reagents are namely MEA, DEA, DGA, TEA, DIPA, MDEA, and other amines or carbonates [6]. Compared to pre-combustion capture, a larger unit size is needed based on a larger volumetric flow rate, and the regeneration of the acid gases from the solvent is more costly [9].

- Oxyfuel combustion:
  The combustion process uses almost pure oxygen instead of air. Hence, the combustion gas mainly consists of CO_2 and H_2O. By cooling and thereby condensing the water vapor, CO_2 can easily be separated. Usually, oxygen is provided by an Air Separation Unit (ASU), and the CO_2-rich flue gas stream is recycled to avoid thermal damage within the steam generator [8].

Applying hybrid solvents is another possibility. They combine the high treated-gas purity offered by chemical solvents with the flash regeneration ability and lower energy requirements of physical solvents (e.g. Sulfinol®, Flexsorb® PS, and Ucarsol® LE) [6].

IGCC-based concepts apply pre-combustion capture which has been studied in several demonstration projects. Since 2008, the Nakoso IGCC power station in Japan has been conducting a feasibility study injecting the captured CO_2 below the ocean in a depleted gas reservoir. In 2009, the Polk Power IGCC plant started a CCS pilot project capturing CO_2 from a 30 % syngas side stream. The CO_2 gets injected into a saline formation more than 1500 m below the power station. In 2010, a R&D project investigating the capture of CO_2 was started at the Puertollano IGCC power plant. In order to investigate an industrial-scale operation and obtain reliable economic data, 2 % of the coal-derived syngas was used. A stream of 99.99 % pure hydrogen was produced while 90 % carbon capture efficiency was obtained. [10]

Carbon Utilization

A significant amount of CO_2 emissions can be avoided by using CCU when applying a mix of several technologies. CO_2 could be used as a source for the synthesis of platform or bulk chemicals, as well as for increasing the utilization of manufacturing polymers and fine chemicals. The production of urea and synthetic fuels, like e.g. methanol, are already commercially available. Another option is represented by refining the polyoligomer Oxymethylether-4. The synthesis is simple and, compared to diesel, has the same properties, such as temperature stability. Since no particles are formed during combustion, particulate filters are obsolete [11]. Usually, a high purity of the exit CO_2 stream is required when it is used in the chemical industry

because impurities may poison catalysts. Using unicellular organisms represents another option to reuse captured CO_2. Blue algae additionally needs solar radiation to directly produce ethanol which can be used to substitute conventional gasoline. Other organisms producing ethanol without the need for solar radiation are already under research. Under certain circumstances, the production of Synthetic Natural Gas (SNG) for the transport industry has some potential benefits. For the synthesis process additional hydrogen is required, which could be produced by excessive renewable energies.

Today, CO_2 is used for Enhanced Oil Recovery (EOR), Enhanced Gas Recovery (EGR), and Enhanced Coal Bed Methane (ECBM). By increasing the pressure within the production field, the discharge flow rate increases when applying EOR or EGR. The ECBM technology uses CO_2 injected into a bituminous coal bed to occupy pore space, and, subsequently, methane gets displaced for recovery. This technology is particularly used for unminable coal seams. Today, in the western USA more than 2500 km of CO_2 pipelines are operating to transport CO_2 from natural gas sources to EOR projects [12]. During the transport, the ambient temperature is decisive for the aggregate state of CO_2. Above the critical point it behaves like a liquid with respect to its density and flow characteristic.

2.2 Integrated Gasification Combined Cycle

2.2.1 Process Design and Benchmark

General

The Integrated Gasification Combined Cycle (IGCC) combines the advantages of a coal-fired steam plant and a gas-fired combined cycle plant. Comparing both technologies, coal-fired steam plants use low-cost fuel, but offer a low overall efficiency. In contrast, gas-fired combined cycle plants use high-cost fuel, but offer a high overall efficiency. Figure 2.1 presents the schematic of an IGCC. At first, solid or liquid fuel is prepared (e.g. crushing, drying) and then converted into raw syngas by gasification. Commercial IGCC power plants use coal, residual oil, petroleum coke, and biomass as fuel. The gasifier uses a dry or slurry feed and the oxidant is either air or oxygen provided by an Air Separation Unit (ASU). The raw syngas is then cooled through quenching or heat transfer, in order to decrease the temperature for the following units. On the cold side of the cooler, water is heated to the saturation state instead

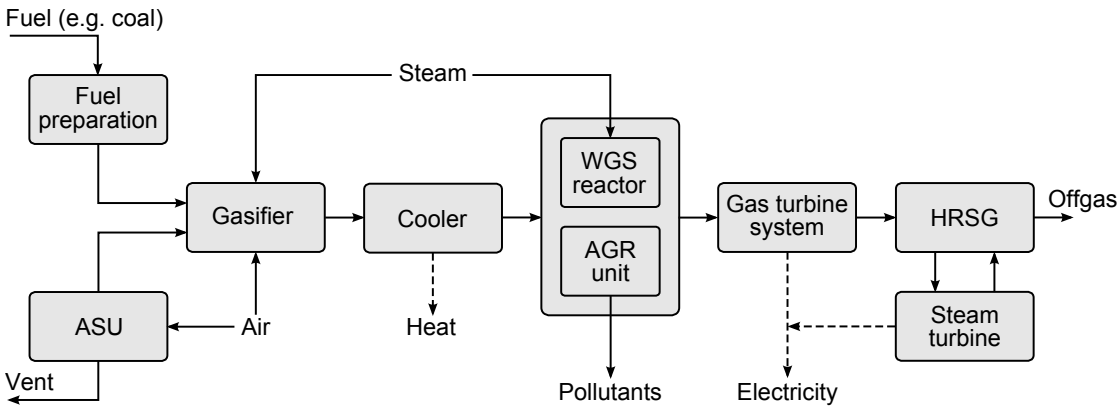

Figure 2.1: Schematic of an Integrated Gasification Combined Cycle (IGCC).

of producing thermodynamically preferred superheated steam. This decreases the average temperature of the tube materials and thereby reduces the capital costs. The relatively high fraction of sulfur and hydrogen within the product gas may also cause serious problems with corrosion. Subsequently, an Acid Gas Removal (AGR) unit removes pollutants like particulates, mercury, hadrogen sulfide (H_2S), carbonyl sulfide (COS), and optionally CO_2 from the syngas. In case of applying carbon capture, CO generated by the gasification process is shifted into CO_2 and H_2 through a Water Gas Shift (WGS) reactor by additionally injecting steam. The arrangement of AGR unit and WGS reactor depends on the application of a clean or sour shift configuration which refers to the contact of H_2S and the catalyst of the WGS reactor. The cleaned syngas then gets fired in a gas turbine system producing electricity. Finally, the hot flue gas of the gas turbine system is used to produce steam through a Heat-Recovery Steam Generator (HRSG) in order to run a steam turbine.

An exergy-based rating of inefficiencies of an IGCC plant was performed several times before [13–16]. In this work, a very detailed analysis is performed in order to understand the shift of inefficiencies when novel technologies are integrated into the conventional process. An advanced exergy analysis of the conventional process has only been performed by the author.

System Integration

Generally, the ASU should be integrated into the IGCC process as much as possible to increase the overall efficiency [8]. Thereby the air flow needed by the ASU is completely provided by the gas turbine compressor, and the nitrogen product flow is totally expanded in the gas turbine. However, this yields a decrease in operational flexibility. The advantage of the degree of integration depends on the operating pres-

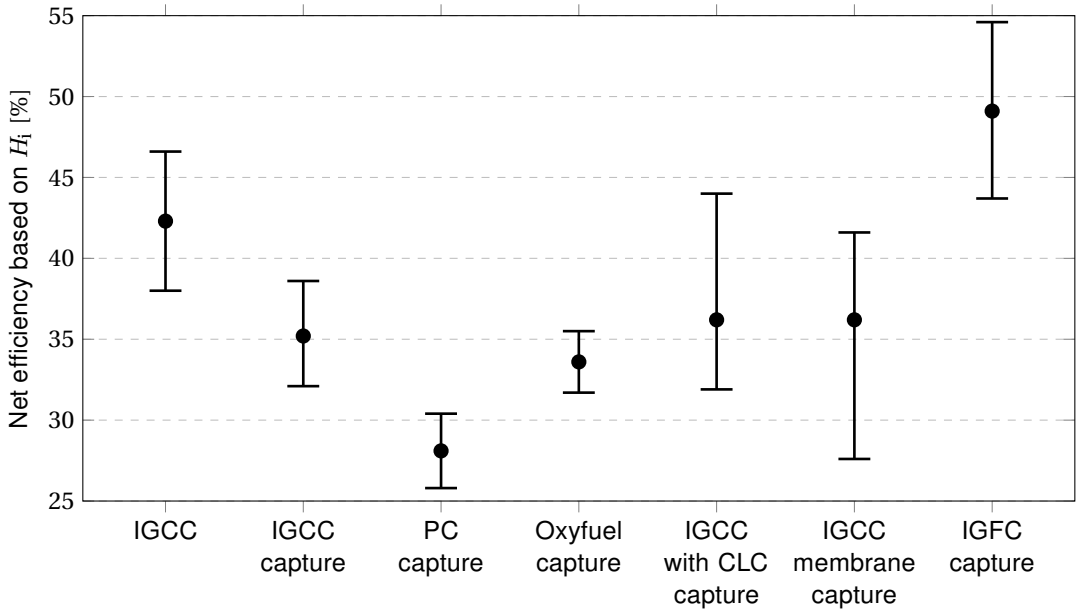

Figure 2.2: Range of overall net efficiencies (based on H_i) for coal-based technologies: IGCC without carbon capture [6, 8, 12, 19–22], IGCC with carbon capture [6, 12, 15, 19–25], pulverised coal (PC) combustion with post-carbon capture [12, 21, 26], Oxyfuel combustion with carbon capture [12, 21], IGCC using Chemical-Looping Combustion (CLC) with carbon capture [27–30], IGCC using membranes with carbon capture [23, 27, 31–33], IGFC with carbon capture [34, 35].

sure of the ASU and if oxygen exits at the gaseous or liquid state [17]. Liszka and Tuka [18] conclude an integration is not advantageous when the ASU uses an intercooled multistage air compressor in combination with an adiabatic gas turbine compressor. Generally, the feed air flow to the ASU might become too small, based on the operating conditions of the gas turbine system. The operating Puertollano IGCC power plant uses a fully integrated ASU, and operators recommend an external air compressor to decrease the start-up time of five days when starting from ambient conditions [10]. During the start-up, the combined cycle gets fired by cost-intensive natural gas. In this work, a low-pressure ASU using an intercooled multistage air compressor is used which does not favor an integration.

Benchmark

Compared to other conventional technologies, the major advantages of IGCC plants are represented by a high overall efficiency and the ability to produce several products (polygeneration). On the contrary, high investment costs as well as low availability and reliability are still challenges for the IGCC technology. Figure 2.2 gives a literature

overview of the overall net efficiencies based on the lower heating value H_i of the IGCC compared to other competing coal-fired technologies. The presented efficiency range incorporates different configurations and assumptions, such as the type of gasifier or heat integration concept. Each mark represents the arithmetic average. The average difference between the IGCC with and without carbon capture results to 7.1 %-points. Considering carbon capture, the IGCC outperforms thermodynamically the Pulverized Coal (PC) technology used in conventional steam plants, as well as the Oxyfuel concept. Increasing the overall efficiency of a conventional IGCC with carbon capture is feasible by applying Chemical-Looping Combustion (CLC). From the literature, a maximum efficiency of 44 % indicates the high potential of this technology. However, a large-scale operation has not been tested so far. Further discussions are presented in Section 2.4. Still being under research, the use of membranes within the IGCC potentially increases the overall net efficiency to an upper limit of 41.6 %. In general, membranes could be used in different subsystems. An Oxygen Transfer Membrane (OTM) replaces the thermal separation column within the ASU [23, 32]. Other studies investigate the application within the WGS reactor or AGR unit [27, 31, 32]. By separating H_2 through a high-temperature membrane, the steam demand of the WGS reaction will decrease significantly [8]. Applying a Polybinzimidazole Polymer Membrane (PBI) in order to separate CO_2 from the syngas has been investigated by Krishnan et al. [33]. However, the development of membranes is still challenging since the almost similar size of molecules poses a huge obstacle for the development of molecular sieve and dense polymer membranes. Additionally, the major challenge for dense ceramic and metallic membranes are tolerances to syngas impurities, high operating temperatures, and material instability [36].

Replacing the gas turbine system of an IGCC by a fuel cell significantly increases the overall net efficiency [34, 35]. The resulting concept is called Integrated Gasification Fuell Cell (IGFC). Due to the preferred high-temperature operation, systems using a Solid Oxide Fuel Cell (SOFC) or Molten Carbonate Fuel Cell (MCFC) are potentially useful. In literature, mostly concepts using SOFCs are analyzed. In the long term, the use of SOFCs is reasonable, but in the near term, SOFCs in large-scale plant size are not commercially available and combining a large number of SOFCs increases the investment costs significantly. On the contrary, the largest fuel cell plant using MCFCs has a net output of 59 MW [37]. Catalytic gasification is another promising long-term technology. Compared to conventional gasification, the methane content of the product gas increases which is advantageous for fuell cells like the SOFC [34].

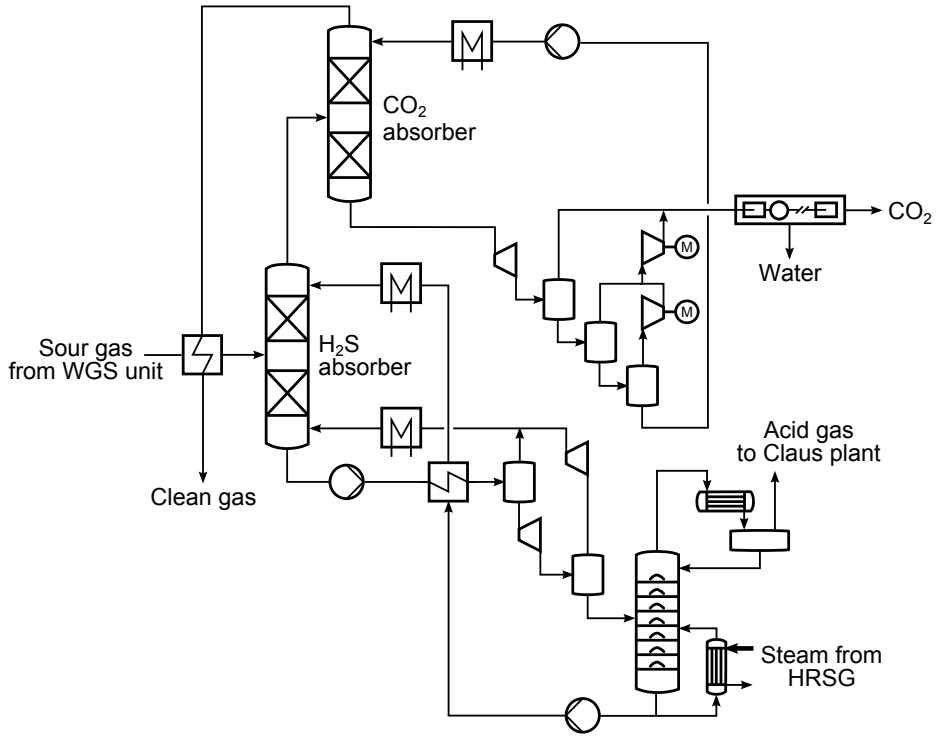

Figure 2.3: Flow diagram of the Selexol® process (according to [38, 39]).

Conventional Gas Cleaning

Compared to conventional PC steam plants, the removal of pollutants is much more simple and cost-effective due to a smaller gas volume flow [6]. The major pollutants of the raw syngas produced by gasification are mercury, ammonia, H_2S, and COS. Fine particulates are already captured by using a cyclone as well as a scrubber. For the removal of mercury, usually activated, sulphur-impregnated carbon bed adsorption is used prior to the H_2S capture unit. In this work, the removal of mercury is not part of the simulation because it has no significant impact on the syngas conditions. The WGS reactor operates in the so-called *sour CO shift*, which denotes the removal of H_2S subsequent to the WGS reactor.

Figure 2.3 shows the flow diagram of the AGR unit used in this work. Depending on the particular case, either the first stage or both stages are used. Within the first stage, H_2S is removed from the sour shift gas in a separation column by applying physical absorption. In this work, the physical solvent Selexol®, licensed by the Union Carbide Corporation, is applied as it has been used in a number of gasification applications [9]. In general, there are many process designs possible. A H_2S-rich acid gas stream can be accomplished by using a H_2S concentrator, which includes two flash stages and a compressor to recycle the flash gas. A regeneration column has to be used to separate the acid gas from the Selexol® solvent. The temperature of the solution

within the reboiler is about 100 to 150 °C [9, 38]. The steam demand of the regeneration column is calculated according to Doctor and Molburg [38]. Calculations based on data published by NETL [39] and Bryan Research & Engineering, Inc. [40] show almost the same result.

In the second stage, the clean gas from the H_2S absorber enters the CO_2 absorber and is finally released with a mole fraction of 0.05 % CO_2. The treated gas contains less than 1 ppmv H_2S to avoid poisoning of catalysts used subsequently [9]. The desorption of CO_2 from the rich solvent employs a three-stage flash. In order to mix the flashed CO_2 streams, two compressors are needed. Finally, the CO_2 is pressurized for transport by an intercooled three-stage compressor. Generally, the design of the compressor is very challenging. After pressurization of the gaseous CO_2, the supercritical state is reached which changes the density to the typical area of liquids. This leads to a large reduction in the volume flow when passing the following compressor stages. In this process, using a gear-type compressor is preferred over a single axial type because the efficiency was found to be higher [41]. For absorption, the lean Selexol® solvent is cooled to -1 °C [38] by ambient air and a refrigeration machine in order to achieve high removal rates. Due to the low temperature, the use of carbon steel instead of stainless steel is suitable. The single-stage refrigeration machine uses CO_2 as the working fluid.

The acid gas has a H_2S mole fraction of about 35 % and is transported to a Claus plant in order to convert the captured H_2S into elemental sulfur. To ensure good kinetics within the Claus plant, the combustor temperature should be about 1050 °C, and the mole ratio of H_2S to SO_2 at the combustor outlet should be 2:1 [42]. In the case of relatively low H_2S concentration in the acid gas, almost pure oxygen provided by the ASU is needed for the combustion process. In this work, a three-stage Claus plant is used, which results in an overall sulfur recovery exceeding 99 %. For further purification usually a Shell Claus Off-gas Treating (SCOT) plant is applied.

Hot Gas Cleaning

Typically, syngas derived from the gasification of bituminous coal contains H_2S, particulates, mercury, COS, and minor contaminants like hydrogen chloride (HCL), hydrogen fluoride (HF), ammonia (NH_3), and hydrogen cyanide (HCN) [8]. Separating H_2S from syngas is conventionally performed at temperatures below 50 °C [9, 43]. Thus, in IGCC applications the temperature between the high-temperature gasifier and gas turbine system must decrease by cooling which causes higher inefficiencies. In contrast, the Hot Gas Desulfurization (HGD) unit operates at temperatures ranging from 260 to

600 °C. The HDG unit is part of the Hot Gas Cleaning unit (HGCU), which represents the overall section for gas cleaning. Compared to the conventional cold gas cleaning, the application of an HGCU increases the overall efficiency by about 2.5 %-points [44]. Typically, the HGD unit consists of a redox cycle where a metal circulates among two interconnected fluidized-bed reactors. The oxides of the metal Zn, Fe, Cu, Mn, Mo, Co and V are potentially promising but no single metal performs optimally as a desulfurization sorbent [45]. Zinc oxide (ZnO) represents a highly suitable metal for H_2S capture because concentrations below 10 ppmv are obtainable and reactions feature a high equilibrium constant. However, kinetics are very slow and ZnO may get reduced at high temperatures leading to zinc contamination in the syngas [8]. Using zinc ferrite ($ZnFe_2O_4$) increases the kinetics by its component iron oxide and the properties of zinc oxide are still valid. In the following, the major reaction equation for the reduction is presented in Eq. 2.1, sulfidation in Eq. 2.2, and regeneration in Eq. 2.3.

$$3\,ZnFe_2O_4 + H_2 \rightarrow 3\,ZnO + 2\,Fe_3O_4 + H_2O \tag{2.1}$$

$$3\,ZnO + 2\,Fe_3O_4 + 9\,H_2S + 2\,H_2 \rightarrow 3\,ZnS + 6\,FeS + 11\,H_2O \tag{2.2}$$

$$ZnS + 2\,FeS + 5\,O_2 \rightarrow ZnFe_2O_4 + 3\,SO_2 \tag{2.3}$$

The separation of zinc ferrite to ZnO and Fe_3O_4 occurs at temperatures around 600 °C and above. The sulfided zinc ferrite particles are regenerated by using air and steam at about 650 °C [45, 46]. Zinc titanate is another promising sorbent but it becomes brittle after several circulations [46]. In 2014, a 50 MW demonstration project at Tampa Electric Polk Power plant achieved the mechanical completion [47]. The project involves long-term testing of sulfur removal and other contaminants at high temperatures ranging from 315 °C to 538 °C using ZnO [48]. However, for several reasons the governmental interest in the HGCU development in Europe and the USA has declined. The attrition of the studied sorbents is one major challenge. The removal of mercury (Hg), ammonia or HCN and COS has never been demonstrated to be satisfying and a prior engineering analysis has found that an operation above 425 °C is not worth the additional capital costs. Only particulates removal, such as candle filters, have been demonstrated successfully. The development of an HGCU appears to be commercially ready in the long-term, if at all achievable [49].

2.2.2 Gasification Technology and Polygeneration

Classification of Gasifiers

In general, three reactor types are used for gasification: moving-bed (sometimes called fixed-bed), fluidized-bed, and entrained-flow. About 75 % of the worldwide gasified coal is converted into gas by moving-bed gasifiers with dry ash removal [50]. Moving-bed gasifiers are characterized by long residence times, thereby the hot sythesis gas of the gasification zone preheats and pyrolyzes the coal in a counter-current arrangement. Compared to other gasfier types, the oxygen demand and temperature is very low and the pyrolysis products are present in the product gas. The discharge of ash is either dry or molten (slagging type) [51].

IGCC power plants mostly use entrained-flow gasifiers. The residence time of the coal particles is short which leads to a smaller unit size. The major advantages compared to other types are represented by the use of different types of coal, low steam demand, production of almost oil and tar-free gases, high carbon conversion, low methane fraction in the product gas, high flow capacity based on high reaction rates, as well as easy discharge of molten slag [51]. On the other hand, additional components like a mill and a dryer or slurry tank, are required. Compared to other gasifier types, the cost of entrained-flow gasifiers may increase due to a high oxygen demand and high operating temperature [51].

Fluidized-bed gasifiers offer a limited carbon conversion because a good mixing of oxidant and feed ensures an even distribution of the material in the bed. Hence, a lot of fluidized-bed gasifiers use a recycle. The temperature is moderate and stays below the softening point of the ash, since ash slagging will interrupt the fluidized bed. Recent IGCC power plants apply gasifiers of the moving-bed or entrained-flow type.

Polygeneration

According to the IGCC technology, polygeneration refers to systems that use gas derived from coal or biomass gasification to generate basic products, secondary energy products or electricity. Figure 2.4 gives an overview of potential gasification applications. Rectangular items represent processes, whereas round items represent material products. The final product determines the process design and requirements. With respect to a market with small peak electricity prices, the generation of electricity may be enhanced by the production of a by-product. One of the most suitable options is represented by the production of Substitute Natural Gas (SNG) because worldwide

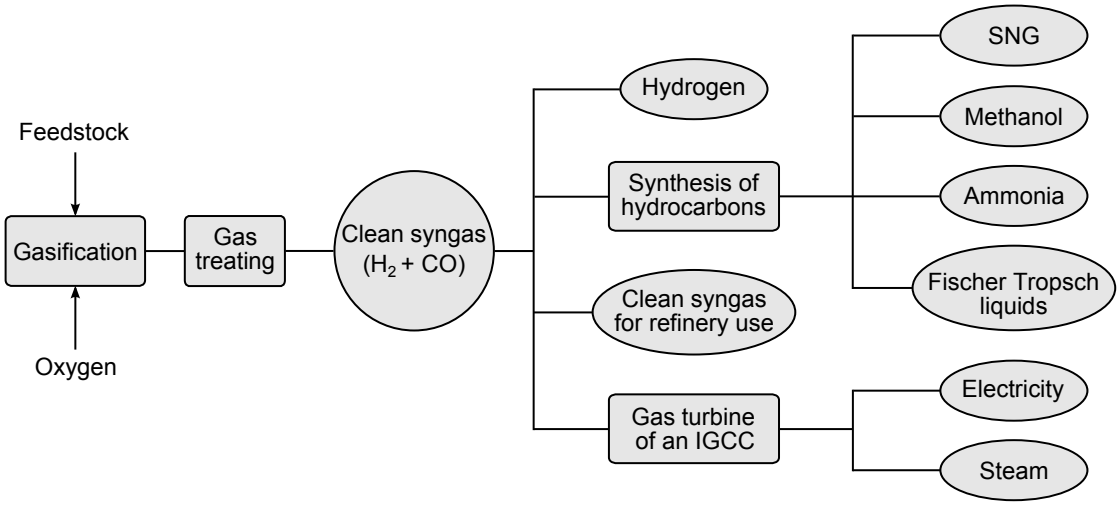

Figure 2.4: Applications of gasification technology.

the existing infrastructure for natural gas can be used for transport and storage. This reduces the obstacles for a market entry. Among others, the author analyzed a poly-generation concept either producing electricity or SNG [52, 53] based on the TREMP® process [54]. Likewise, the production of synthetic gasoline by applying the Fischer Tropsch synthesis also results in low obstacles for a market entry. However, the major disadvantage of hydrogen is the bad volumetric energy density. Compared to SNG and synthetic gasoline, only a small infrastructure is available. Generally, each conversion results in a reduction in the overall efficiency.

2.2.3 Experiences of Commercial IGCC Power Plants

In the 1970s/1980s, the first generation of IGCC power plants for coal-based applications was build. The second generation of power plants were build in the 1990s, using the experiences from the first generation. An overview, including major plant properties for current operating power plants worldwide is given by the Gasification Technologies Council [55] and the National Energy Technology Laboratory (NETL) [56].

Recent operating experiences from commercial IGCC power plants are presented by the IEA Clean Coal Centre [10]. The report indicates that the refractory lifetime of the vertical hot face of the slurry-fed gasifier at the Polk and Wabash River power plant typically does not exceed two years. Especially when using a slurry feed gasifier, the lifetime of the fuel injector tip of the gasifier does not exceed 90 days. In case of a dry-feed gasifier, the lifetime increases to more than one year. Power plants using a slagging gasifier should use blended coal. Otherwise the change in ash properties

may cause serious problems blocking the slag trap. Another option to overcome this blockade is represented by the installation of a slag crusher to avoid outages of several days. When applying a syngas cooler subsequent to the gasifier, the installation of flexible tube connectors is recommended because vibration caused by changes in the gasifier parameters may indicate leakages in the tubes. Particularly during the start-up the top part of the syngas cooler can be blocked by fly ash deposits.

The Buggenum IGCC power plant has a considerable experience in biomass co-gasification. The maximum biomass contribution of untreated wood was approximately 15 %, based on the heating value. When using biomass, the cold gas efficiency of a high-temperature gasifier decreases because biomass gasification favors low temperatures. Using a thermal pre-treatment of the biomass producing torrefied wood increased the maximum contribution to 70 % [10]. The plant was shut down in April 2013 for economic reasons [55].

2.3 Gas Turbine System

In general, gas turbines are used for propulsion or electricity generation. For stationary gas turbines, the electrical power generation ranges from only a few kW to more than 350 MW. Larger heavy-duty gas turbines are typically used in a simple or a combined cycle mode for centralized electrical power generation. In the combined cycle mode, the highest electrical net efficiency among all thermal energy conversion systems is available, which is approximately 60 % based on the lower heating value [57]. Another important ability is represented by its fast change in electricity generation due to a worldwide increasing volatile production of renewable energies.

Compared to the well-known combustion of natural gas, the combustion of hydrogen and carbon monoxide involves a higher flame velocity, higher flame temperature and wide flammability range, along with low ignition energy and low density which may cause blowouts or flashbacks [10, 58]. The combustion of H_2-rich fuel in gas turbine systems has been demonstrated by General Electric in a full-scale combustor, but the turbine design needed further development [59]. Until the year 2010, the maximum volumetric content of hydrogen by volume used in F-class operation was 45 %, and in industrial operation up to 95 % [60]. Syngas produced by gasification in common IGCC plants without carbon capture typically contains 12-38 vol-% of H_2. Problems concerning vibration and hot spots were detected and eliminated. Generally, the firing temperature of a gas turbine running on syngas is about 110-170 °C lower compared to the equivalent running on natural gas [10].

Several studies [61–65] report on the exergy analysis of the compressor, combustion chamber and turbine based on a simple gas turbine model according to ISO 2314 [66]. A more detailed conventional exergy analysis was performed by El-Masri [67] who focused on the inefficiencies associated with the cooling system based on a simplified three-stage gas turbine model. The results showed the trade-offs between decreasing combustion losses and increasing turbine cooling losses affecting the overall efficiency. Another study on the cooling system was performed by Khodak and Romakhova [68]. The inefficiencies were determined by splitting the total system into a topping cycle producing electricity and a bottoming cycle representing the process management of the cooling air flows. It was found that the inefficiencies within the cooling system are caused by heat transfer between the main gas and coolant, the bottoming cycle itself as well as mixing at different compositions. Staudacher and Zeller [69] evaluated different setups of the secondary air system of an aircraft turbine supported by data from Rolls-Royce. The study presents the results of a conventional exergy analysis based on grouping characteristic inefficiencies focusing on the secondary air system.

This work focuses on the detailed modeling and evaluation of a heavy-duty gas turbine system running on syngas derived from the gasification of bituminous coal using subsequent CO_2 capture. The detail level of the model is selected to give a distribution of inefficiencies among all components divided by its characteristic sources. To account for the real cooling system, the bleed air of the compressor is further split into cooling and sealing parts. Basically, the developed model can be applied for the combustion of any gaseous fuel which provides a sufficient heating value in order to reach the firing temperature presented in Section 4.4.3.

2.4 Chemical-Looping Combustion

2.4.1 Fundamentals

Principle of CLC

The idea of using a redox cycle to decrease the inefficiencies of a combustion process has been proposed by Knoche and Richter [70]. This technology is based on the principle of energy conversion within the human organism. The human organism uses a lot of organic intermediate reactions to convert food and oxygen into mechanical work performed by the muscles. In technical applications, an inorganic matter should be used. The technical fundamentals were introduced by the steam-iron process

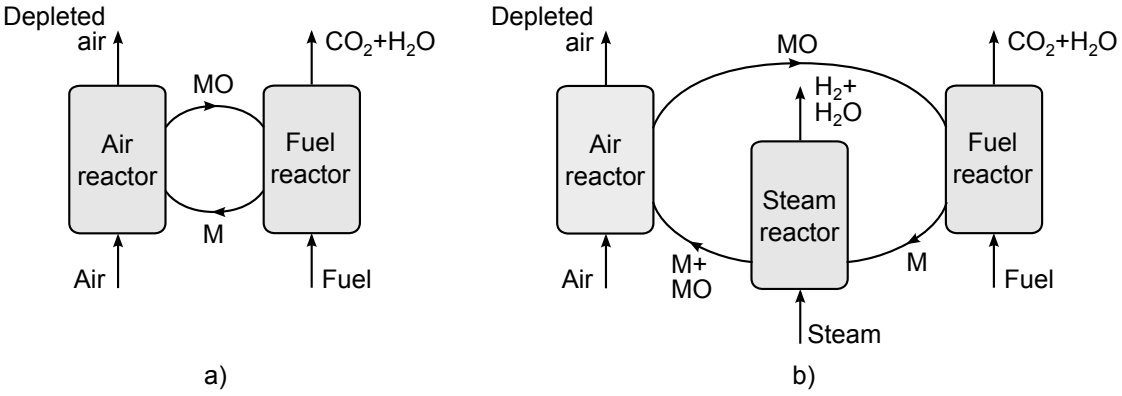

Figure 2.5: Schematic of CLC using a) two-reactors and b) three-reactors.

[71] in the late 19th century. In this process, metallic fixed-bed reactors were used to produce hydrogen from gaseous fuels. In 1949, Lewis and Gilliand [72] applied a patent using a metal-based redox cycle in interconnected reactors for the production of pure carbon dioxide. For the reduction of the metal oxides, a fluidized-bed or moving-bed reactor can be potentially used. In 1987, Ishida et al. [73] introduced the term Chemical-Looping Combustion (CLC), which can be understood as an oxyfuel combustion without the need for air separation. Simultaneously, an inherent capture of CO_2 is possible which enables a higher carbon capture efficiency compared to a post-combustion capture with a typical efficiency of 80 to 95 %. Higher efficiencies require a larger unit size, causing higher costs and a greater loss in the overall net efficiency [74]. Investigations on CLC started using gaseous fuels such as natural gas and syngas produced by gasification of solid fuels. A general overview about the development is given by Adanez et al. [75]. Later, the direct use of solid fuel like coal and biomass was investigated [76]. Both also present the experimental status of CLC. Chemical-Looping Combustion replaces the conventional combustion by a redox cycle that uses a metal oxide as an oxygen carrier. Figure 2.5 shows the principle of two different CLC systems analyzed in this work and discussed below. On the reduction side, natural gas or coal-derived syngas reduces the metal oxide (MO) to metal (M) in the fuel reactor, as shown in Eq. 2.4 to 2.6.

$$MO + H_2 \rightarrow M + H_2O \tag{2.4}$$

$$MO + CO \rightarrow M + CO_2 \tag{2.5}$$

$$4\,MO + CH_4 \rightarrow 4\,M + 2\,H_2O + CO_2 \tag{2.6}$$

On the oxidation side, the reduced metal is re-oxidized into a metal by using air or steam, see Eq. 2.7 and 2.8. Using steam is preferred for the oxidation due to the co-production of H_2. However, a full regeneration of the metal is not possible when using steam, therefore, further oxidation with oxygen or air is needed, resulting in a three-reactor system. The minimum residual oxygen in the flue gas of an air reactor is 4 mol-% [77]. In this work, most of the reactors use a fluidized-bed, which has been demonstrated in the pilot plant scale by the Institute of Gas Technology (IGT) [78].

$$M + H_2O \rightarrow MO + H_2 \tag{2.7}$$

$$2M + O_2 \rightarrow 2MO \tag{2.8}$$

Unlike conventional combustion, at least two streams exit the CLC unit. Depleted air exits a cyclone subsequent to the air reactor, and a mixture of CO_2 and H_2O exits the fuel reactor. Due to the highly exothermic reactions taking place in the air reactor, the hot depleted air can be used to produce steam or dilute the combustion gas of a gas turbine system. It has to be taken into consideration that air reactor temperatures above 1000 °C require the use of cost-intensive ceramic materials in the subsequent cyclone instead of alloy steel which is more common. When using the three-reactor system, an additional mixture of H_2 and H_2O exits the steam reactor because only part of the steam can be converted into hydrogen. Depending on the reactor temperature, the maximum conversion of H_2O to H_2 is 74.8 %, if only Fe was consumed [79]. By cooling the mixture of CO_2 and H_2O in a heat-recovery steam generator (HRSG), the water vapor condenses. Finally, high-purity CO_2 exits the HRSG without the need for a conventional absorption process. After compression, the CO_2 is ready for transport and sequestration. Usually the air reactor is operating as a riser, transporting the oxygen carrier particles to the top level of the CLC unit. After being separated by a cyclone, the particles drop to the fuel and steam reactor, forced by gravity. The fuel gas and steam enter the reactor in the counter-current direction. Experimental studies on CLC often use nitrogen or steam for sealing the interconnections among the reactors. In this work, no auxiliaries for sealing are assumed because, so far, a realistic estimation underlies large uncertainties.

Oxygen Carrier

A number of oxygen carriers have been proposed and tested for CLC. The oxygen carrier particles mostly consist of a metal oxide and a support material. Some of

Table 2.1: Physical properties of the oxygen carriers in reduction reactions [30, 80].

Reaction	Enthalpy of reaction (at 1000°C, and 1 atm) [kJ/kmol]	Melting point of the reduced metal form [°C]	Melting point of the oxidized metal form [°C]
$NiO + H_2 \rightarrow Ni + H_2O$	-15.0	1453	2000
$NiO + CO \rightarrow Ni + CO_2$	-47.2	1453	2000
$4\,NiO + CH_4 \rightarrow 4\,Ni + CO_2 + 2\,H_2O$	133.5	1453	2000
$Fe_2O_3 + H_2 \rightarrow 2\,FeO + H_2O$	27.5	1420	1560
$Fe_2O_3 + CO \rightarrow 2\,FeO + CO_2$	-4.7	1420	1560
$4\,Fe_2O_3 + CH_4 \rightarrow 8\,FeO + CO_2 + 2\,H_2O$	303.7	1420	1560
$3\,Fe_2O_3 + H_2 \rightarrow 2\,Fe_3O_4 + H_2O$	-9.9	1538	1560
$3\,Fe_2O_3 + CO \rightarrow 2\,Fe_3O_4 + CO_2$	-42	1538	1560
$12\,Fe_2O_3 + CH_4 \rightarrow 8\,Fe_3O_4 + CO_2 + 2\,H_2O$	154.2	1538	1560

the most desired properties of the particles are the following: good oxygen carrier capacity, good gas conversion in all reactors, high rates of reaction, satisfactory long-term recyclability, good mechanical strength, suitable heat capacity, high melting points, low investment costs, easy synthesis procedure, suitable particle size, and low environmental impact [30]. Several promising particles have been identified [81–83].

The most promising oxygen carrier in case of producing electricity and hydrogen is iron (Fe) and its oxides hematite (Fe_3O_4), wüstite (FeO), and magnetite (Fe_2O_3). This has been introduced by Velazquez-Vargas et al. [84] and applied to a three-reactor system. Mattisson et al. [81] performed experimental investigations on iron using aluminium oxide (Al_2O_3) as an inert support material, and identified iron as a suitable oxygen carrier for the reduction of carbon monoxide (CO) and hydrogen (H_2). Iron and its oxides are nontoxic and very inexpensive. Generally, the melting temperature of the oxygen carrier is a limiting factor, namely 1560 °C for Fe_2O_3, 1538 °C for Fe_3O_4, 1420 °C for FeO, and 1275 °C for cast Fe (with pure iron melting at 1535°C) [85]. In this work, a small amount of Fe occurs only in one analyzed case. Using an oxygen carrier consisting of 60 % nickel oxide (NiO) and 40 % aluminium spinel ($MgAl_2O_4$) showed a conversion efficiency of 99 % when using syngas while reaching chemical equilibrium for both H_2 and CO at reactor temperatures above 950 °C [86]. The melting temperature of Ni is 1453 °C and is 2000 °C in the case of NiO [80]. In this work, nickel oxide was selected for the two-reactor system, and iron oxide for the three-reactor system.

The physical properties of the oxygen carriers NiO and Fe_2O_3 used in this work are presented in Table 2.1. The single reactions including CO or H_2 have an exothermic characteristic except the reaction of Fe_2O_3 and H_2. Reactions including H_2 are merely slightly exothermic compared to the reactions including CO. The syngas includes methane (CH_4) at relatively low concentrations only when using a BGL gasifier. The reactions including CH_4 have an endothermic characteristic.

2.4.2 Research on CLC-Based Systems

Anheden and Svedberg [87] conclude that a power plant using the two-reactor CLC system has approximately the same efficiency compared to a conventional IGCC plant without carbon capture. An exergy analysis of a CLC unit combined with a gas turbine system was performed. Compared to a conventional combustion of the same fuel, the exergy destruction decreases by about 12 % when using nickel oxide or iron oxide as the oxygen carrier for the reduction of syngas which has a mole fraction of 51.7 % CO and 29.2 % H_2, provided by coal gasification [88]. Erlach and the author of this work [89, 90] complemented this study by comparing the power plant using CLC with a conventional IGCC plant with carbon capture. This work includes some further changes in the assumptions and the flow diagram to satisfy a suitable comparison of all analyzed cases based on stringent input parameters.

Figure 2.6 presents the overall net efficiencies for CLC-based IGCC concepts found by other researchers. When using a two-reactor system consisting of a fuel and an air reactor, higher efficiencies can be obtained when nickel oxide is used as the oxygen carrier. The average efficiency is calculated to 33.9 %. The air reactor temperature varies from 920 °C [28] to 1200 °C [27]. Mantripragada and Rubin [91] performed an analysis of this system design by using an additional CO_2 turbine subsequent to the fuel reactor. Rezvani et al. [27] applied this system by using a double-stage CLC unit and found an increase of the efficiency of about 1.5 %-points. In this case, additional investment costs have to be considered. Cormos [28, 29] analyzed a CLC-based IGCC concept using a two-reactor system which consisted of a fuel and a steam reactor. Iron oxide is used as the oxygen carrier for the co-production of electricity and hydrogen. When producing only electricity, the overall net efficiency increases to an average value of 36.2 %. The efficiency mainly depends on the choice of gasifier type as well as concept for cooling the syngas. Romano et al. [22] present a CLC-based IGCC concept, using two fixed-bed reactors. The best pressure of a co-current reactor system was found to be 20 bar. The overall net efficiency increased by 5.7 %-points, compared

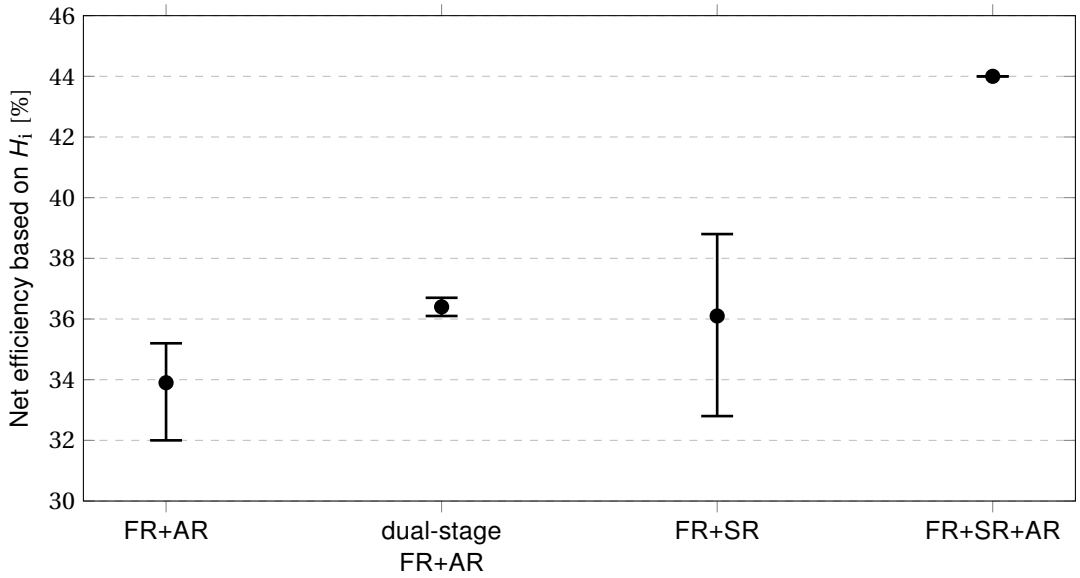

Figure 2.6: Range of overall net efficiencies (based on H_i) for CLC systems: a) two-reactor system: Fuel Reactor (FR) and Air Reactor (AR) [27, 28], FR and Steam Reactor (SR) [28, 29], dual-stage FR and SR [27], b) three-reactor system: FR, SR and AR [30].

to a current IGCC with carbon capture. Further experimental investigations on the oxygen carrier behavior are needed to confirm this high potential. The overall net efficiency presented for the three-reactor system consisting of a fuel reactor, steam reactor and air reactor is significantly higher compared to other system designs, but it has to be mentioned that the underlying simulation is based on a crude model. This is the only concept using a counter-current five-stage moving-bed fuel reactor instead of fluidized type to improve the gas and solid conversion [30]. The temperature of the air reactor is 1044 °C. Based on Fig. 2.6, it is concluded that the three-reactor system exhibits the highest potential. However, when using coal-derived syngas, higher concentrations of CO in the fuel gas may lead to an undesired formation of soot, Fe_3C and iron carbonate. Pressurized conditions during the reduction will potentially enhance these formations [92].

Xiang et al. [93] analyzed a CLC-based IGCC concept, using iron oxide as the oxygen carrier in a three-reactor system for the co-production of electricity and hydrogen. A combination of the oxygen carriers nickel oxide and subsequent iron oxide has been investigated [94] as well. In both studies the steam reactor for the production of hydrogen was used. Chiesa et al. [95] present an analysis using a three-reactor system and iron oxide as the oxygen carrier in a natural gas-fueled combined cycle concept, producing electricity and hydrogen. An analysis of a Steam-Injected Gas Turbine (STIG) concept, using the same system design but other oxygen carriers like nickel

Table 2.2: Abilities of various large-scale power plants (PC: Pulverized Coal, CC: Combined Cycle, GT: Gas Turbine) [102, 103].

Ability	Definition	Unit	PC bituminous coal	PC lignite	CC	GT
Hot start-up	< 8 h stop	min	50-150	90-120	30-60	5-9
Cold start-up	> 48 h stop	min	170-230	300-360	120-180	10
Load gradient		%/min	2-6	2-5	4-9	10-25

oxide, has been performed by Wolf and Yan [96]. Gnanapragasam et al. [97] present a double-stage three-reactor CLC unit. A comparison to a Direct Chemical-Looping (DCL) system showed disadvantages for the production of hydrogen. So far, the use of a CLC unit in combination with a HGD unit has only been investigated by the author himself [98–101].

2.5 Flexible Electric Power Generation

Flexibility

Generally, the flexibility of conventional large-scale power plants can be arranged in a characteristic order. Table 2.2 presents the start-up period and load gradient, respectively. The best results can be obtained by using a Gas Turbine (GT) system which offers start-up periods of around 5-10 minutes. The load gradient also clearly outperforms the other plant types. The particular load change depends on the GT size. An IGCC plant has very long start-up periods as well as a small load gradient except when the power unit is uncoupled from the gasification island. Without linking the gasification island it acts like a Combined Cycle (CC) plant. Bypassing the HRSG makes the IGCC act like a single gas turbine.

Increasing the flexibility of a conventional IGCC plant could be realized by adding a syngas storage since the gasifier should operate under continuous conditions. The temperature and pressure of the stored syngas may vary depending on the storage mechanism. Cocco et al. [104] presented a plant that includes a larger gasification island as well as an additional peak gas turbine system compared to a conventional plant. It was found that the overall efficiency drops by about 1-6 percentage points and the energy production costs increase by about 5-20 %. Douglas and Dunn [105] found that an IGCC plant featuring a syngas storage that compensates 12 hours of

operation economically outperforms a PC plant. Adding a natural gas fuel switching capability significantly enhances the profitability by roughly 20 % [106].

Hydrogen Transport and Storage

The storage of H_2 faces the challenge that a) the energy density is only about one third of the natural gas density, b) H_2 makes most metals brittle and c) enables diffusion through the storage chamber wall. Alternatively, H_2 can potentially be transported or stored by using high-pressure tubes or spheric tanks, cryogenic liquid vessels, as well as underground salt or excavated rock caverns. Typically, H_2 is stored at low-pressure (about 170 bar) tubes for a moderate period of time. This option is well known from the storage of Liquefied Petroleum Gas (LPG), Liquefied Natural Gas (LNG), and Compressed Natural Gas (CNG). Generally, the capacity of H_2 increases at higher pressures. Regarding the transport of H_2, trailers are loaded at the processing facility and off-loaded at the fueling station. In this work, the produced H_2 is pressurized and distributed to a pipeline network which usually operates at low pressure (20 to 80 bar). The storage mechanism may be enhanced by using alternative H_2 carriers which are roughly presented in the following.

Alternative liquid hydrogen carriers include pure liquids, solutions, or slurries. For example, liquid hydrocarbons like ethylcarbizole, a solution including chemical hydrides like aqueous sodium borohydride, or a slurry including metal hydrides like magnesium are potentially useful. It was found that the H_2 carriers have far more impact on the overall costs than, for example, trailer capital costs. Moreover, the alternative carriers have the potential to be less expensive than the transport of pure liquid H_2. [107]

Unlike liquid carriers, solid-state H_2 carriers remain on the trailer usually in form of powders. Potential materials are carbon sorbents such as AX-21 or complex hydrides like sodium alanate (NaA1H4). In comparison of both carriers, the carbon sorbent features faster kinetics which supports a rapid desorption. Unlike liquid carriers, the powder remains on the trailer for transport. From an economic point of view, it was found that dropping off the trailer is much more expensive than off-loading the H_2 [107]. In general, finding a suitable carrier depends on factors such as energy consumption, greenhouse gas emissions, total costs, and potential hazard. It might be advantageous to use different carriers depending on the scale, available infrastructure, and time frame.

Chapter 3

Methodology

3.1 Thermodynamic Analysis

This section provides the fundamentals of the energy analysis as well as the conventional and advanced exergy analysis. Particular definitions are given in Appendix B, Eq. 2.1 to 2.12.

3.1.1 Energy Analysis

Energetic state variables are calculated by solving the global energy balance. In this work, the global energy balance is simplified by assuming only stationary processes and neglecting differences in kinetic and potential energy. The remaining energy balance for an open system control volume of the k-th component contains enthalpy flow rates $\dot{H}_j$ of the inlet (index in) and outlet (index out) streams, mechanical or electrical power $\dot{W}_{\mathrm{cv}}$ and rate of heat transfer $\dot{Q}_{\mathrm{cv}}$ of the control volume (index cv).

$$0 = \dot{Q}_{\mathrm{cv}} + \dot{W}_{\mathrm{cv}} + \sum_j \dot{H}_{j,\mathrm{in}} + \sum_j \dot{H}_{j,\mathrm{out}} \tag{3.1}$$

The characteristics of turbomachinery components, such as compressors (index c) and turbines (index t), are represented by either using the isentropic efficiency η_{s} or the polytropic efficiency η_{pol}. Therefore, the term $h_{\mathrm{s,out}}$ represents the exit specific enthalpy determined by the inlet specific entropy and exit pressure.

$$\eta_{\mathrm{s,c}} = (h_{\mathrm{s,out}} - h_{\mathrm{in}}) / (h_{\mathrm{out}} - h_{\mathrm{in}}) \tag{3.2}$$

$$\eta_{\mathrm{s,t}} = (h_{\mathrm{in}} - h_{\mathrm{out}}) / (h_{\mathrm{in}} - h_{\mathrm{s,out}}) \tag{3.3}$$

$$\eta_{\mathrm{pol,c}} = \int_1^2 v\,\mathrm{d}p / (h_{\mathrm{out}} - h_{\mathrm{in}}) \tag{3.4}$$

$$\eta_{\mathrm{pol,t}} = (h_{\mathrm{out}} - h_{\mathrm{in}}) / \int_1^2 v\,\mathrm{d}p \tag{3.5}$$

The energetic conversion of a solid feedstock through gasification within a gasifier is rated by the cold gas efficiency *cga*. In this work, the lower heating value H_{i} is used instead of the higher heating value.

$$cga = H_{\mathrm{i,product}} / H_{\mathrm{i,fuel}} \tag{3.6}$$

The rating of the overall system is performed by applying the overall net efficiency η_{tot}. In this work, the product under design operations is consistently net electric power $\dot{W}_{\mathrm{el,net}}$ and the total fuel depends on the mass flow rate and lower heating value of the fuel.

$$\eta_{\mathrm{tot}} = \dot{W}_{\mathrm{el,net}} / (\dot{m} \cdot H_{\mathrm{i}})_{\mathrm{fuel}} \tag{3.7}$$

3.1.2 Conventional Exergy Analysis

The exergy analysis is a convenient and powerful tool to quantify inefficiencies of thermal systems from a thermodynamically unbiased point of view. The exergy concept has proven to be advantageous, with its methodology and capabilities being well established [108–110]. Exergy is defined as the maximum theoretical useful work obtainable as the system is brought into complete thermodynamic equilibrium with the thermodynamic environment while the system interacts with this environment only [110]. The exergy flow rate of a stream of matter $\dot{E}_j$ is given by the physical, chemical, magnetic, kinetic, and potential exergy flow rate. The contribution of kinetic, potential as well as magnetic exergies is neglected in the following.

$$\dot{E}_j = \dot{E}_j^{\mathrm{CH}} + \dot{E}_j^{\mathrm{PH}} \tag{3.8}$$

$$\dot{E}_j^{\mathrm{PH}} = \dot{n} \cdot \left((\bar{h} - \bar{h}_0) - T_0 \cdot (\bar{s} - \bar{s}_0) \right) \tag{3.9}$$

$$\dot{E}_j^{\mathrm{CH}} = \dot{n} \cdot \left(\sum_i x_i \bar{e}_i^{\mathrm{CH}} + \bar{R} T_0 \cdot \sum_i x_i \ln(x_i) \right) \tag{3.10}$$

The calculation of the chemical exergy flow rate $\dot{E}_j^{\mathrm{CH}}$, according to Eq. 3.10, is only valid for a mixture of ideal gases. The chemical exergy of a stream, including a gas and liquid phase, is calculated by their phase fractions if condensation occurs at ambient

conditions (15 °C and 1 bar). The model of Szargut [108] is used as the reference environment.

The chemical and physical exergies were calculated by directly using the simulation environment Aspen Plus®. Based on internal Fortran routines, each stream is flashed to ambient conditions whereas physical properties are taken from the simulation database. Particularly the condensation of water has to be considered. However, the exergies of solids were calculated outside of the simulation. The determination of the physical exergies of solids was carried out based on fitting polynoms also using physical properties supplied by the simulation database. Thereby the coefficients were adapted closely to the temperature range needed within the simulations in order to provide a good accuracy.

Under steady state conditions, the rate of exergy destruction within the k-th component $\dot{E}_{\mathrm{D},k}$ is calculated as the difference between the exergy transfer associated with heat (first summand of Eq. 3.11), mechanical or electric power, exergy flow rates at the inlet to the exergy flow rates at the exit. The temperature T_j represents the average temperature of the rate of heat transfer at the location on the boundary of the control volume. However, the exergy destruction quantifies the thermodynamic irreversibilities within the component in regard and is only caused by chemical reaction, heat transfer, friction, and mixing.

$$\dot{E}_{\mathrm{D},k} = \sum_j \left(1 - \frac{\dot{Q}_j}{T_j}\right) + \dot{W}_{\mathrm{cv}} + \sum_j \dot{E}_{j,\mathrm{in}} - \sum_j \dot{E}_{j,\mathrm{out}} \tag{3.11}$$

$$y_{\mathrm{D},k} = \dot{E}_{\mathrm{D},k} / \dot{E}_{\mathrm{F,tot}} \tag{3.12}$$

The exergy destruction ratio $y_{\mathrm{D},k}$ is a dimensionless variable representing the exergy destruction rate within the k-th component related to the exergy rate of the total plant fuel $\dot{E}_{\mathrm{F,tot}}$. In general, dimensionless variables ease the interpretation of results compared to absolute values. The exergetic efficiency ε_k of the k-th component is calculated by the ratio of the exergy rate associated with the fuel $\dot{E}_{\mathrm{F},k}$ and the exergy rate associated with the product $\dot{E}_{\mathrm{P},k}$. The SPECO approach [111] is used to define $\dot{E}_{\mathrm{F},k}$ and $\dot{E}_{\mathrm{P},k}$.

$$\varepsilon_k = \dot{E}_{\mathrm{P},k} / \dot{E}_{\mathrm{F},k} = 1 - \dot{E}_{\mathrm{D},k} / \dot{E}_{\mathrm{F},k} \tag{3.13}$$

The difference between $\dot{E}_{\mathrm{F},k}$ and $\dot{E}_{\mathrm{P},k}$ equals the sum of $\dot{E}_{\mathrm{D},k}$ and the rate of exergy loss $\dot{E}_{\mathrm{L},k}$. The exergy loss refers to losses of the overall system to the environment, for

example hot flue gases or heat losses, whereas the exergy destruction to components only. Applying an exergy analysis provides information which is not available through a conventional energy analysis. Thereby, possible means to improve the system are easily derived. However, it does not become clear whether the modifications proposed by a conventional exergetic evaluation lead to an improved overall system [112] as no implications caused by the structure of the overall system are taken into account. The real available improvement potential can only be determined by conducting an advanced exergy analysis.

3.1.3 Advanced Exergy Analysis

The advanced exergy analysis concept [113] provides the framework for the identification of the thermodynamic interactions of each system component, as well as their real improvement potentials. Thus, the exergy destruction within the system component is split into its endogenous and exogenous parts as well as its avoidable and unavoidable parts, respectively. A general overview is given by Fig. 3.1, including all options for splitting the exergy destruction of a component.

Splitting the exergy destruction of the k-th component into its endogenous (index EN) and exogenous (index EX) parts reveals the thermodynamic interdependencies among the system components. Moreover, the substitution of a system component or changing the process arrangement is rated by this splitting.

$$\dot{E}_{\mathrm{D},k} = \dot{E}^{\mathrm{EN}}_{\mathrm{D},k} + \dot{E}^{\mathrm{EX}}_{\mathrm{D},k} \tag{3.14}$$

The endogenous exergy destruction $\dot{E}^{\mathrm{EN}}_{D,k}$ is associated with the irreversibilities of the k-th component operating with the default exergetic efficiency ε_k but the remaining components of the overall system operate in an ideal way without any exergy destruction [112]. In contrast, the exogenous exergy destruction $\dot{E}^{\mathrm{EX}}_{D,k}$ is defined as the part of the exergy destruction within the k-th component caused by irreversibilities of other system components. Calculating the endogenous exergy destruction does not need an additional simulation. The necessary set of equations includes the specific default exergies used in the definitions of the exergy rate of products and fuel as well as the leveling of every involved mass flow rate based on a characteristic mass flow rate. As an additional result, the productive mass flow rate of the component in regard is identified.

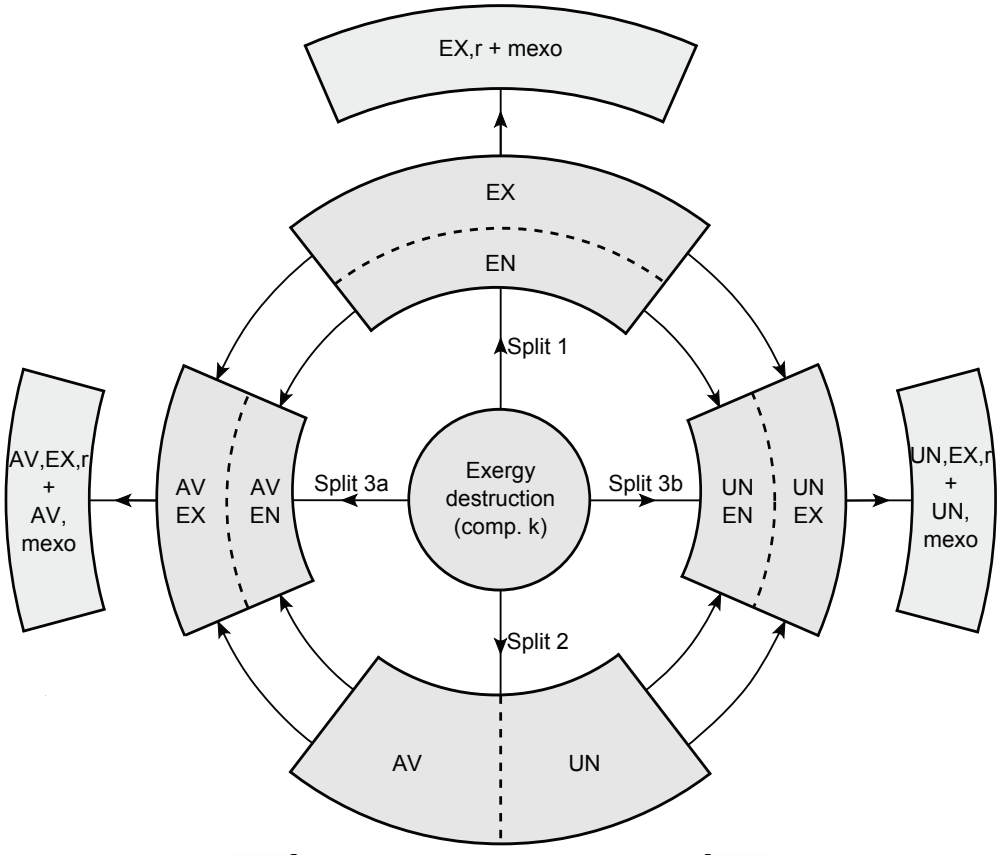

Figure 3.1: Options for splitting the exergy destruction within a component in an advanced exergy analysis.

The calculation of the endogenous exergy destruction has been performed by suggesting several approaches [114–116]. However, the suggested approaches are still tedious to be used for complex systems, face theoretical shortcomings [114, 115], and computational problems for chemical reactions [116]. On that account, a new concept [117] was developed using an aggregated superstructure model [118] in combination with inherent features of the exergy concept. In contrast to previous approaches, every mass and energy balance of the system is fulfilled and the computational load is highly reduced.

The real improvement potential of a particular fixed process arrangement is determined by splitting the exergy destruction into its unavoidable (index UN) and avoidable (index AV) parts (see Fig. 3.1). The unavoidable part is calculated from a simulation considering the unavoidable boundary conditions weighted by the default exergy rate of products [119].

$$\dot{E}_{\mathrm{D},k}^{\mathrm{UN}} = \dot{E}_{\mathrm{P},k} \cdot \left(\dot{E}_{\mathrm{D},k} / \dot{E}_{\mathrm{P},k}\right)^{\mathrm{UN}} \tag{3.15}$$

$$\dot{E}_{\mathrm{D},k} = \dot{E}_{\mathrm{D},k}^{\mathrm{UN}} + \dot{E}_{\mathrm{D},k}^{\mathrm{AV}} \tag{3.16}$$

The unavoidable exergy destruction $\dot{E}_{\mathrm{D},k}^{\mathrm{UN}}$ is associated with the amount of exergy destruction that cannot be further reduced. These constraints are set by techno-economic limitations such as availability, cost of materials, as well as manufacturing methods. This enables engineers to identify and quantify potential changes in design and operation for the particular component based on their knowledge, experience, and expectations. The remaining avoidable exergy destruction $\dot{E}_{D,k}^{\mathrm{AV}}$ represents the potential savings in irreversibilities of the k-th component.

The combination of both splittings of exergy destruction shows the final results of an advanced exergy analysis. The determination of the most promising modifications for improving the overall system is represented by the avoidable endogenous exergy destruction $\dot{E}_{\mathrm{D},k}^{\mathrm{AV,EN}}$ and avoidable exogenous exergy destruction $\dot{E}_{\mathrm{D},k}^{\mathrm{AV,EX}}$ (see Fig. 3.1).

$$\dot{E}_{\mathrm{D},k} = \dot{E}_{\mathrm{D},k}^{\mathrm{UN,EN}} + \dot{E}_{\mathrm{D},k}^{\mathrm{UN,EX}} + \dot{E}_{\mathrm{D},k}^{\mathrm{AV,EN}} + \dot{E}_{\mathrm{D},k}^{\mathrm{AV,EX}} \tag{3.17}$$

$$\dot{E}_{\mathrm{D},k}^{\mathrm{AV,EN}} = \dot{E}_{\mathrm{D},k}^{\mathrm{EN}} - \dot{E}_{\mathrm{D},k}^{\mathrm{UN,EN}} \tag{3.18}$$

$$\dot{E}_{\mathrm{D},k}^{\mathrm{AV,EX}} = \dot{E}_{\mathrm{D},k}^{\mathrm{AV}} - \dot{E}_{\mathrm{D},k}^{\mathrm{AV,EN}} \tag{3.19}$$

The unavoidable endogenous exergy destruction is calculated by taking the results of the simulation used for the unavoidable case, and assuming that the remaining system components operate in an ideal way without any exergy destruction. Hence, no additional simulation is needed.

In order to further improve the understanding of interdependencies among the components, the exogenous exergy destruction of the k-th component is further split in order to account for binary component interactions between component k and r [115] (see Fig. 3.1). Hence, component r is also operating at its default exergetic efficiency, while the other of the m system components operate ideally.

$$\dot{E}_{\mathrm{D},k}^{\mathrm{EX}} = \sum_{r \neq k}^{m} \dot{E}_{\mathrm{D},k}^{\mathrm{EX},r} + \dot{E}_{\mathrm{D},k}^{\mathrm{mexo}} \tag{3.20}$$

The remaining difference to the exogenous exergy destruction is called the mexogenous exergy destruction $\dot{E}_{\mathrm{D},k}^{\mathrm{mexo}}$, representing the simultaneous interactions among all

other components together. A large amount of the mexogenous exergy destruction indicates strong component interactions as a part of a highly integrated systems.

From the thermodynamic point of view, the components with the largest sum of the avoidable exergy destruction $\dot{E}_{\mathrm{D},k}^{\mathrm{AV},\Sigma}$ should be given the highest priority for improvement when the arrangement of the system components remains constant.

$$\dot{E}_{\mathrm{D},k}^{\mathrm{AV},\Sigma} = \dot{E}_{\mathrm{D},k}^{\mathrm{AV,EN}} + \sum_{r \neq k}^{m} \dot{E}_{\mathrm{D},k}^{\mathrm{AV,EX},r} \tag{3.21}$$

Based on simple rules, the simultaneous consideration of the different parts of exergy destruction identifies the real potential for improving the component in regard, as well as the overall system [113]. The results from the advanced exergy concept provide the system designer and operator with information that cannot be derived from any other method available. The calculation algorithm is given in the end of Appendix B.

3.2 Cost Estimation

In this work, an economic analysis is performed in order to valuate an additional H_2 production during periods of low electricity prices. The bare erected costs estimation of the conventional IGCC system components are taken from the same reference which was mainly used for the simulation [6]. The particular subsystem costs were adapted using cost degression exponents ranging from 0.75 to 0.93 [109, 120]. The calculation of additional costs for engineering, contingencies, operating and maintenance (O&M) and others are taken from Simbeck and Chang [120] in order to use the same economic boundary conditions as the competing steam methane reforming (SMR) plant. Table 3.1 presents the specifications of the cost analysis. Compared to the reference case IGCC-2, the production of hydrogen requires further purification using pressure swing adsorption (PSA) as well as an H_2 compressor to meet the transport pressure. The competing SMR plant requires an additional CO_2 compressor to satisfy the same pipeline transport pressure of the IGCC cases.

In order to estimate the operation costs, a price for coal is required. The average coal price in Germany is taken from the BAFA [123]. The average value of the year 2014 results in 72.9 €/t_{SKE} based on data given by German power plant operators. Within the result section, the coal prices are presented based on the standard trading unit (SKE). In the case IGCC-2, the prices were adjusted to the analyzed coal type (Illionois No.6) by weighting their heating value.

Table 3.1: Specifications for the cost analysis.

Variable	Unit	Value
General		
Availability [120]	%	90
CEPCI 2002 [121]	-	395.6
CEPCI 2008 [121]	-	539.5
CEPCI 2010 [121]	-	550.8
Exchange rate [122]	$(\$/€)^{2010}$	1.33
Capital charges [120]	%/a	18
Plant lifetime [120]	a	20
General facilities [120]	% of process units	20
Engineering, permitting, startup [120]	% of process units	15
Contingencies [120]	% of process units	10
Working capital, land & Misc. [120]	% of process units	7
Site specific factor [120]	% above US golf coast	110
Fixed O&M [120]	%/a of capital	5
Non-fuel variable O&M [120]	%/a of capital	1
IGCC-2		
Mass flow rate H_2 case IGCC-H2	kg/s	4.54
Mass flow rate H_2 case IGCC-H2i	kg/s	6.95
Electrical power demand case IGCC-H2i	MW	113.1
H_2 compressor case IGCC-H2	$T€^{2010}$	5628
H_2 compressor case IGCC-H2i ,3 compressors each 50% of duty ,lubricated 3-stage [107]	$T€^{2010}$	6836
PSA for H_2 purification [107]	$€^{2010}/kg_{H_2}$	0.077
SMR (central,H_2 pipeline)		
Inlet pressure H_2 pipeline [120]	bar	75
Operating costs [120]	$€^{2010}/kg_{H_2}$	0.67
Product costs [120]	$€^{2010}/kg_{H_2}$	0.98

Furthermore, an electricity price is required for the estimation of operation costs in some cases. The average electricity price for the German industry considers several elements: the full tax on electricity, apportionments for EEG, abLA, according to § 19, and wind offshore, combined heat and power law, concessions, grid charge, as well as procurement and distribution. The resulting average value amounts to 83 €/MWh for the year 2014 and a yearly consumption of more than 100 GWh [124].

3.3 Software and Simulation

The process simulations were undertaken using Aspen Plus® (Aspen) version 8.0 [125] and Engineering Equation Solver (EES) Professional [126]. Furthermore, the data

management and some additional calculations have been conducted using MATLAB® [127]. Each analysis in this work has been performed at steady-state conditions.

In Aspen, the property method Redlich-Kwong-Soave with Boston Matthias Alpha function (RKS-BM) was used for modeling the gas path. In the acid gas removal system, the property method based on the Perturbed Chain Statistical Association Fluid Theory (PC-SAFT) equation of state was used for the glycol Dimethyl Ether of Polyethylene Glycol (DEPG) representing the Selexol® solvent. The introduction of the corresponding model properties is available from the Aspen Technology, Inc. [128]. For the simulation of Chemical-Looping Combustion, the properties of solids were taken from the Aspen inorganic database. Especially for iron and its oxides, property coefficients were implemented in the Aspen software taken from the literature [129–131]. In Aspen, the material properties derive from the NIST database [132].

The steam cycle of each IGCC simulation has been implemented using the EES software. The properties of water and steam were calculated based on the steam table formulation IAPWS‘95 [133] which is the most accurate method available so far. Optimization has been performed using the non-linear Nelder-Mead Simplex method which is only available from the professional EES version.

Application of Aspen Plus®

Generally, the simulation has been run in the sequential modular mode. In order to specify the outlet conditions, a lot of internal modules called *design specification* have been used within the simulations. The internal module called *calculator* is useful for directly calculating characteristic parameters such as efficiencies and the equivalence ratio. Another internal module called *transfer* should be used in case the process design includes more than one loop which is mostly induced by recycle streams.

Most of the reactors were simulated by using the *RGIBBS* reactor model which minimizes the Gibbs free energy representing chemical equilibrium. In some cases, mostly at high amounts of excess agents, the simulation did not converge and therefore the reactor model was replaced by the *RSTOICH* reactor model. However, the residence time of coal particles within the moving-bed BGL gasifier does not satisfy the chemical equilibrium conditions. Hence, the equilibrium temperature of each reaction was corrected to adjust the product composition given by the literature (temperature approach, see Section 4.6.2). For Chemical-Looping Combustion, the component $Fe_{0.947}O$ is used instead of FeO because it is much more available in the real environment.

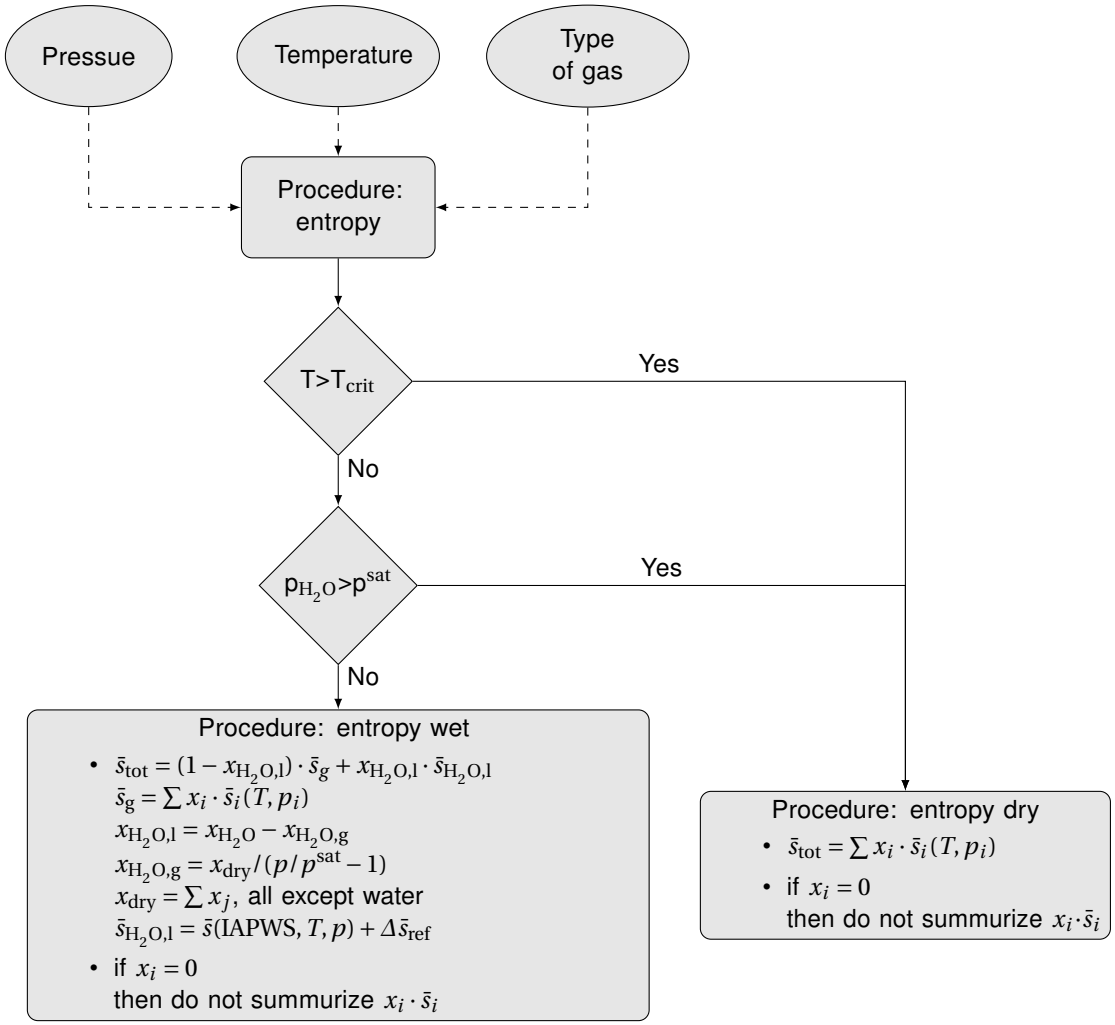

Figure 3.2: Structure chart of the entropy calculation in EES.

Apllication of EES

Using the EES software entails several advantages. The software enables the user to implement any set of equations because it is based on source code. The provided libraries satisfy the mathematical functions and physical properties needed in this work. It is based on a sequential simultaneous calculation algorithm and, additionally, the professional version provides a non-linear optimization tool. The maximum degree of freedom is set to three which satisfies the optimization of the three-pressure steam cycle performed in this work. However, a simultaneous optimization of the live steam temperature is not possible.

In general, setting the initial values is highly important for complex simulations, especially for exponents. Particularly, the initial values of off-design variables should be set by the corresponding design variable. Setting the variable boundaries might be

useful in some cases but for optimization this may lead to convergence problems. It is recommended to manually edit the accuracy of equations and number of iterations used by the solver. Optimization convergence problems may be overcome by starting at a low accuracy. The results from this first step are potentially useful to be used as initial values for further more accurate optimization steps.

Since only the properties of pure materials are available through the library, the state variables of mixtures have to be calculated by the user. In this work, external routines were generated. Particularly, the general formulation for computing the specific entropy of mixtures might be challenging for the user. Figure 3.2 presents the structure chart in regard. In general, logical operators such as if-else statements can be implemented in so-called *procedures*. In contrast to this sequential operation mode, the so-called *subroutines* use a simultaneous operation mode. When calling the entropy procedure, the pressure, temperature, and type of gas have to be assigned. The composition depends on the type of gas and is taken from values deposit within the procedure.

Checking the condensation of water is necessary for mixtures that include a large amount of water. Prior to that, the temperature should be below the critical temperature to avoid errors within the calculation. The final calculation of the entropy with or without condensation is performed sequentially. If a material component does not occur within the mixture, it should not be considered in the calculation algorithm because the partial pressure becomes zero, leading to an error message by the EES software. In case of liquid water, the entropy derives from the steam table formulation IAPWS'95 corrected by a reference point shift. Additionally, the composition of the gas phase has to be re-calculated based on the liquid fraction.

Adding inequalities to the model can help checking the results of a simulation. For example, an auxiliary variable is defined as the ratio of the component inlet and outlet temperature of a particular stream. In combination with the setting of the auxiliary variable limits between zero and one, this equation acts like an inequation. A direct implementation is not possible. The software constrains the equation if the ratio exceeds the limits and displays the constrained equations after finishing the calculations. For smaller simulations, the convergence does not depend on either the enthalpy is a function of the temperature or the other way around. However, in case of larger simulations this dependency may become important.

Chapter 4

Modeling

In this chapter, the assumptions and models used for the analysis in this work are presented.

4.1 Overview of Cases and Subsystems

The thermodynamic and economic assessment depends on characteristic cases given in Table 4.1 that are further introduced in the following sections. Each analysis uses an IGCC base case for the evaluation. All cases consider carbon capture. The base case IGCC-1 represents a high-efficiency conventional IGCC power plant using a Shell gasifier (see Section 4.5.1) and is used to analyze the thermodynamic potential. The second base case IGCC-2 is introduced in Section 4.5.2 and represents a low-cost conventional IGCC plant using a General Electric Energy (GEE) gasifier.

The cases IGCC-H2i and IGCC-H2 represent the off-design operation of the base case IGCC-2. The product switches from electrical power to hydrogen. In both cases, the steam cycle only provides the water streams required by the scrubber, quench unit, WGS unit as well as saturator if required and some electric power generated by the LP steam turbine. In the case IGCC-H2i, the electric power demand is satisfied by the steam turbine and external purchases. On the contrary, in the case IGCC-H2 the electric power demand is completely generated internally representing a stand-alone operation.

The IGCC plants including a Chemical-Looping Combustion (CLC) unit are separated into two categories depending on the reactor system design. The choice of the particular oxygen carrier depends on the thermodynamic characteristics presented in Section 2.4. In general, two different types of gasifiers are selected in the underlying cases. The selection is presented in the following detailed case description sections. The air reactor temperature is one of the major parameters and therefore a sensitivity

Table 4.1: Specifications of the analyzed cases.

Base cases IGCC	**IGCC-1**	**IGCC-2**			
Gasifier type	Shell	GEE			
Off-design IGCC	**IGCC-H2i**	**IGCC-H2**			
Gasifier type	GEE	GEE			
Two-reactor CLC	**CLC-Ni1**	**CLC-Ni2**	**CLC-Ni3**	**CLC-Ni4**	**CLC-Ni5**
Gasifier type	Shell	Shell	Shell	BGL	BGL
Air reactor temperature	1100 °C	1200 °C	1300 °C	1000 °C	1100 °C
CO_2 turbine	no	no	no	no	no
Three-reactor CLC	**CLC-Fe1**	**CLC-Fe2**	**CLC-Fe3**	**CLC-Fe4**	**CLC-Fe5**
Gasifier type	Shell	Shell	BGL	BGL	BGL
Air reactor temperature	900 °C	1000 °C	900 °C	1000 °C	900 °C
CO_2 turbine	no	no	no	no	yes

analysis was performed. The upper temperature limits were chosen according to the thermal limitation of the HRSG.

The cases CLC-Ni1 to CLC-Ni5 represent the plants using a two-reactor CLC unit and nickel oxide as the oxygen carrier. The plants using a three-reactor CLC unit and iron oxide as the oxygen carrier are represented by the cases CLC-Fe1 to CLC-Fe5. The application of a CO_2 turbine is only conducted is the case CLC-Fe5.

4.2 Basic Assumptions

Some of the major assumptions applied for each analysis performed in this work are listed in Tab. 4.2. Further assumptions for particular systems are given in the following sections.

Each IGCC plant is simulated in the large-scale size. The analysis of plants addressing the improvement of the overall efficiency have a coal input of 80 kg/s and the others 50 kg/s. All cases use the same bituminous coal (Illinois No.6) with a weight composition of 64.61 % C, 4.39 % H, 1.39 % N, 0.86 % S, 7.05 % O, 12.20 % ash and 9.50 % moisture. The lower heating value $H_{\mathrm{i,ar}}$ results to 25.97 MJ/kg and the higher heating value $H_{\mathrm{s,ar}}$ to 27.07 MJ/kg. Based on the heating values, the chemical exergy of the raw coal $e^{\mathrm{CH}}_{\mathrm{coal,ar}}$ yields to 31.97 MJ/kg. The ambient conditions as well as the exit conditions of the captured CO_2 are similar for each analysis. All heat exchangers consider a pressure drop that depends on the state of the cooled and heated fluids.

Table 4.2: Basic assumptions of all cases.

System/Component	Unit	Value
General		
Ambient temperature [134]	°C	15
Ambient pressure [134]	bar	1.013
Ambient air fractions of O_2 and N_2	%	21, 79
Mechanical efficiency of turbo-machinery	%	99 - 99.5
Electrical generator efficiency	%	99
Electric motor efficiency	%	95
CO_2 compressor isentropic stage efficiency [135]	%	81.5 - 77.4
CO_2 exit temperature	°C	45
CO_2 exit pressure	bar	110
Air, N_2 and O_2 compressor isentropic efficiency	%	85
ASU		
O_2 mole purity	%	98
Intercooler exit temperatur	°C	35
Outlet pressure HP/LP column	bar	5.8/1.3
Outlet temperature of N_2, O_2	°C	18
Steam cycle		
Steam turbine polytropic efficiency HP, IP, LP	%	90, 92, 87
Pumps isentropic efficiency	%	85
Condenser pressure	bar	0.035
Max. live steam temperature	°C	590
Pinch point temperature difference	°C	20, 10, 5
Gas/gas, gas/liquid, liquid/liquid		
Pressure loss liquid/gas per 100°C	%	2/3
Pressure loss evaporation	%	5

The calculation of the overall efficiency considers auxiliaries required by the major components. Table 4.3 shows the specific factors applied in this work for the major subsystems of an IGCC plant.

4.3 Steam Cycle

4.3.1 Equation-Based Model

In this section, the model of the system components is described by using the following subscripts: 0 = design state, 1 = inlet, 2 = outlet. The characteristic of turbomachinery is either presented by the isentropic efficiency η_s or polytropic efficiency η_{pol} (see Section 3.1.1). The implementation of the isentropic efficiency can be simply performed by defining the outlet enthalpy at isentropic state change as a function of the outlet

Table 4.3: Assumptions of the subsystem auxiliaries [6].

System	Unit	Value
Coal handling	kW/(kg/s) wet coal	7.85
Slag handling	kW/(kg/s) slag	93.67
Air separation unit	kW/(kg/s) air in	5.14
Cooling tower fans	% of cooling duty	0.65
Gas turbine	% of net power	0.216
Steam turbine	% of net power	0.048

pressure and inlet entropy. When implementing the polytropic efficiency, the use of the polytropic exponent n is necessary to solve the integral of $v \cdot \mathrm{d}p$. Hence, Eq. 4.1 is used to reformulate the definition of the polytropic efficiency into Eq. 4.2. In Eq. 4.2, the unit of the pressure is [kPa]. The limits of the polytropic exponent should be set very closely to the final value, e.g. $1.1 < n < 1.6$ in case of the steam turbine. Otherwise the solver of the EES software might not find a solution.

$$p_1 \cdot v_1^n = p_2 \cdot v_2^n \tag{4.1}$$

$$(h_2 - h_1) \cdot \left(1 - \frac{1}{n}\right) = \eta_{\mathrm{pol}} \cdot p_1^{\left(\frac{1}{n}\right)} \cdot v_1 \cdot \left(p_2^{\left(1-\frac{1}{n}\right)} - p_1^{\left(1-\frac{1}{n}\right)}\right) \tag{4.2}$$

Usually, within the low-pressure steam turbine some amount of steam condenses whereby the dry polytropic efficiency $\eta_{\mathrm{pol,dry}}$ has to be corrected resulting in the wet polytropic efficiency $\eta_{\mathrm{pol,wet}}$. The first approach was presented by Baumann [136] who found a factor for the correction of the dry efficiency as a function of the average steam quality. Later, this approach has been enhanced because is not likely that wet efficiency is proportional to dry efficiency. The approach by Smith [137] considers the correction factor as being independent of the dry efficiency (see Eq. 4.3). At high pressures, the correction factor α is 0.9, and it is 0.7 at low pressures.

$$\eta_{\mathrm{pol,wet}} = \eta_{\mathrm{pol,dry}} - \alpha \cdot \left(1 - \frac{x_1 - x_2}{2}\right) \tag{4.3}$$

The heat transfer within a heat exchanger is determined by the mass flow rates as well as enthalpies of the hot and cold stream, respectively. Thereby, the enthalpy is a function of the composition, temperature, and pressure, or rather the state of matter instead of temperature or pressure. As a result of the calculated rate of heat transfer $\dot{Q}$, the product of the heat transfer coefficient U and the heat transfer area A can be calculated by using the Fourrier law for a counter-current flow arrangement, as presented in Eq. 4.4. The resulting area is typically used for cost estimations or

off-design calculations. Mathematically, the logarithmic function comes along with convergence problems. Even though the logarithmic function is approximated by a polynom of the third order [138], the off-design calculations performed in the EES software sometimes did not converge for groups of heat exchangers larger than three. Using the arithmetic temperature difference solves this problem but the result is not acceptably precise.

$$\dot{Q} = UA \cdot \left(\frac{(T_{\text{hot},1} - T_{\text{cold},2}) - (T_{\text{hot},2} - T_{\text{cold},1})}{\ln\left(\frac{T_{\text{hot},1} - T_{\text{cold},2}}{T_{\text{hot},2} - T_{\text{cold},1}}\right)} \right) \tag{4.4}$$

Compared to the Fourrier law, applying the NTU method may improve the convergence due to the absence of a logarithmic function. However, the determination of the minimum heat capacity flow within a heat exchanger arises problems for a simultaneous operating solver.

4.3.2 Integrated Heat Management

In general, the overall efficiency of all analyzed cases in this work strongly depends on the design of the heat exchanger network that combines several objectives. The heat exchanger network is supposed to satisfy the cooling and heating demand of the syngas production path and the HRSG subsequent to the gas turbine system as well as the restrictions from the steam turbine. In this section, the base case IGCC-1 introduced in Section 4.5.1 is discussed representing the general approach for all other cases.

Superstructure

The heat exchanger network is implemented using the EES software presented in Section 3.3. Generally, using a mathematically simultaneous solver is favored compared to a sequential solver because several loops may cause severe convergence problems. Furthermore, constrains do not have to be implemented in a specific order which helps the user a lot.

The development of the heat exchanger network starts using a superstructure based on three pressure levels. Including all possible arrangement scenarios is mathematically unfavorable as this may result in a bad probability in finding a valid solution. Potentially, the heat transfer within the HRSG is separated into preheating, evaporation and superheating for each pressure. Additionally, a single reheat is applied to

increase the steam cycle efficiency. However, the sensible heat exchangers can be split into parts depending on the conditions needed by external sources. In this work, the superstructure already excludes some heat exchangers that are supposed to be improper.

The objective function of the mathematical optimization maximizes the net electric power output of the steam cycle by varying the live steam pressure of the three lines, respectively. The lower boundary of the particular pressure is determined by the extraction pressure if there is any. In case of a higher pressure which is found by the solver to be optimal, a throttling unit uncouples the extraction pressure. After running a first optimization using the superstructure, heat exchangers are disabled that only share a very small amount of the overall heat transfer and, accordingly, a very small water mass flow rate. This is an alternative approach to the optimization featuring a mixed-integer problem. In a second optimization run, the pressures are recalculated resulting in small differences compared to the first run.

Component Arrangement

Figure 4.1 presents the final flow diagram of the base case IGCC-1 and the corresponding temperature profiles are shown in Fig. 4.2. The higher temperatures of the hot gas streams at the inlet of the syngas cooler (900 °C) and the gasifier (1550 °C) are not presented to give a valuable overview about the other streams. Furthermore, the internal heat transfer from the Low-Temperature Water Gas Shift (LT-WGS) cooler to the saturator is not displayed.

Starting subsequent to the condensate pump, the liquid water is mixed with the make-up stream which substitutes the water demand of the gasifier, scrubber and WGS unit. The water is then preheated at a pressure of 2 bar by, primary, cooling the product gas of the LT-WGS unit, and, secondary, cooling the flue gas in the HRSG directly before entering the stack. On that account, the offgas temperature at the HRSG exit is limited by the low-temperature demand of the WGS unit. The saturated water is then pressurized by the pumps of the three pressure levels. The overall efficiency is mostly affected by the high pressure (HP) and intermediate pressure (IP). The mass flow rate of the HP section is determined by the cooling demand of the syngas cooler and How-Temperature Water Gas Shift (HT-WGS) unit cooler. Both heat exchangers at first preheat the HP water to the corresponding saturation temperature, and then evaporation takes place outside of the HRSG. The superheating of the HP steam within the HRSG is split into two parts to enable a high IP live steam temperature between

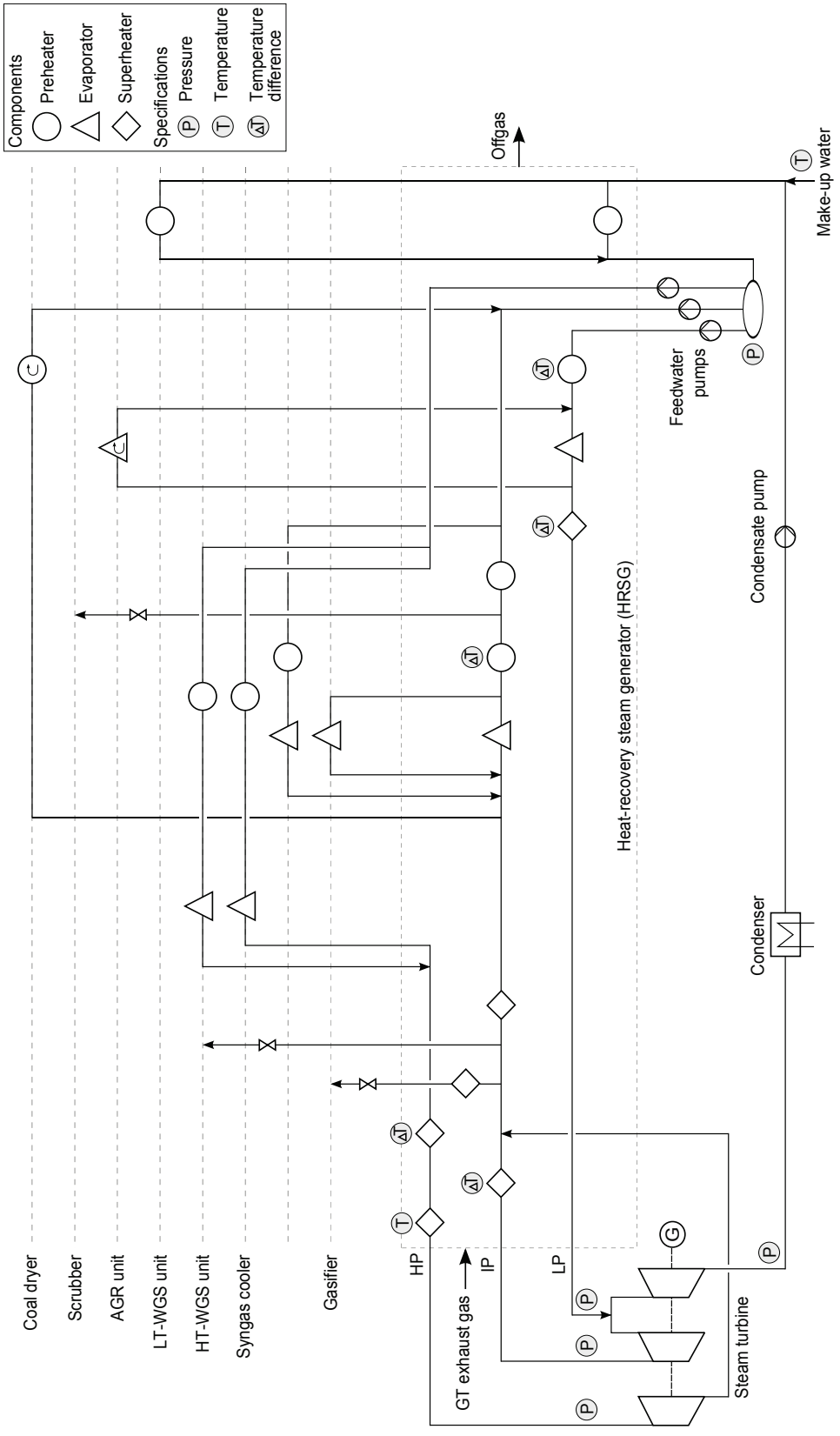

Figure 4.1: Flow diagram of the steam cycle of case IGCC-1.

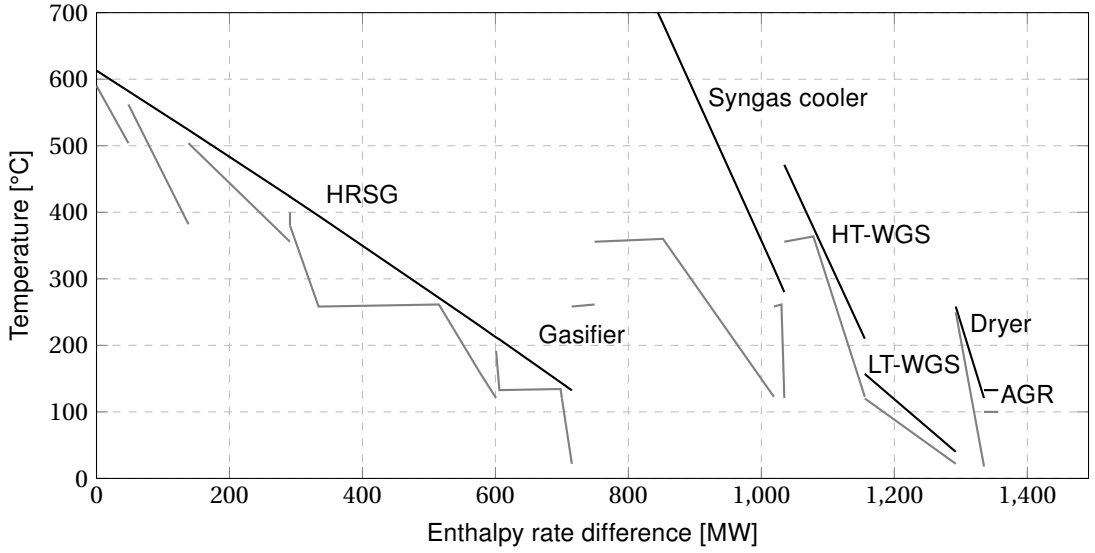

Figure 4.2: Temperature profiles of the heat transfer (case IGCC-1).

both superheaters. The HP live steam is fed to the HP steam turbine and the outlet pressure of this turbine is determined by the pressure of the IP line. Subsequently, the outlet stream is mixed into the IP main stream to further reheat the IP steam.

The arrangement of the IP section starts using a preheater, which supplies the temperature needed for the wet-type scrubber. The extract needed by the scrubber passes through a throttling unit to separate the scrubber pressure from the intermediate pressure determined by the results of the mathematical optimization. Based on the throttling process, a small temperature drop occurs. Prior to the scrubber extraction, the stream is split to produce saturated IP steam within the low-temperature part of the syngas cooler. The preheated IP water is then further preheated and evaporated within the HRSG. Evaporation takes place parallelly within the membrane wall of the gasifier to facilitate a high cooling demand restricted by the surface area as well as the isothermal heat transfer. The saturated IP steam is partly used to heat nitrogen required by the coal dryer. The corresponding recycle stream is then mixed into the main IP stream subsequent to the IP pump. The smaller part of the IP saturated steam is partly superheated to provide steam for the WGS unit. Afterwards, a small part is split from the main stream and is further superheated to provide steam needed for the gasification process. Like the extraction for the scrubber, a throttling unit uncouples the pressure needed by the shift reaction and gasification process from the optimized IP pressure.

After the expansion within the IP turbine, low pressure (LP) superheated steam is mixed into the off-steam to increase the power generation within the LP turbine. The

LP live steam is only produced within the HRSG. However, a part of the IP saturated steam is discharged to satisfy the heat demand of the AGR regeneration column. The recycle stream consists of boiling liquid and enters the LP evaporator within the HRSG again. Within the LP turbine, the steam quality should not underrun 85 % to avoid erosion caused by water droplets [139, 140]. In the case IGCC-1, the share of the HRSG on the overall heat transfer results to about 55%.

Specifications

Finding a proper set of specifications represents the most difficult part for the process engineer. The number of specifications needed is determined by the number and arrangement of the heat exchangers, mixers, splitters, and turbomachinery. Finally, the degree of freedom must be zero to start a calculation. Difficulties may occur in the process of placing the specifications. It is recommended to start assigning specifications to the components by their priority to the overall system. Finding proper assignings is supported by the *Computational Flow Window* in the EES software, which presents the grouped matrices that are sequentially used for solving the set of equations. Checking the temperature profile (see Fig. 4.2) can help the engineer if the software finds a solution.

In general, a preheater followed by an evaporator is specified to produce a boiling liquid. Moreover, all evaporators producing saturated steam have a smaller exit temperature compared to the inlet because the pressure drops decreases the corresponding saturation temperature. Figure 4.1 shows the specifications applied for the steam cycle of case IGCC-1. For obvious reasons, the inlet conditions as well as the exit temperature of the external gas streams outside of the HRSG have to be provided. The parameters of the extractions also have to be given. For the simulation of the HRSG the conditions of the gas turbine exhaust gas are provided.

Other important specifications are represented by the HP and IP live steam temperatures which are set to be max. 590 °C in this work. The HP live steam temperature is fixed to be 590 °C as the turbine exhaust temperature is about 613 °C. However, the LP and IP live steam temperature can be smaller determined by the minimum temperature difference between the exhaust gas and superheated steam (20 °C) as well as the gas turbine exhaust mass flow rate. The same temperature difference is used to determine the exit steam temperature of the first HP superheater. Typically, the pinch point occurs at the beginning of boiling of the liquid state. Thus, a temperature difference of 10 °C is specified for the exit of the IP and LP preheater which are both

producing boiling liquid. Finally, the LP steam turbine outlet pressure is determined by the ambient temperature and the temperature difference within the condenser. In this work, the pressure is fixed at 0.035 bar. The feedwater pressure is set to be 2 bar. However, the live steam pressures must be provided or determined by applying mathematical optimization.

In the case IGCC-1, the maximum electric power generation calculated by optimization occurs at live steam pressures of 164 bar/42 bar/3 bar, respectively. The corresponding live steam temperatures are found to be 590 °C/562 °C/192 °C, resulting in a vapor fraction of 87.4 % at the steam turbine outlet. The steam cycle produces about 38 % of the overall gross electric power.

Generally, under off-design conditions the steam cycle should work at fixed design pressures to ensure the same evaporation temperatures compared to the design case. In contrast, a sliding pressure may cause critical issues, for example to the membrane wall cooling within the gasifier. More detailed information are given in Section 5.4.1.

4.4 Gas Turbine System

The real gas turbine is a highly complex system. The design and a lot of parameters depend on the particular application. This section presents the modeling of a heavy-duty gas turbine at steady-state conditions. A lot of conditions depend on design constrains by the particular manufacturer. For a very detailed simulation featuring a high accuracy, CFD (Computational Fluid Dynamics) should be used but a lot of parameters and assumptions make the mathematical model very complex. In this work, the level of detail is chosen to determine the inefficiencies within the overall system and to confirm characteristic parameters that are typically given by the manufacturers. The process simulations were undertaken using the Aspen Plus® software.

4.4.1 Determination of Inefficiencies

Generally, exergy destruction is only caused by friction, mixing, heat transfer and chemical reactions. In this work, the following incorporated twelve processes are associated with characteristic inefficiencies in a heavy-duty gas turbine system:

- Compression,
- Stoichiometric combustion,
- Addition of excess air,

- Convective cooling in vanes/blades,
- Pressure drop (caused by the transport of working fluids),
- Expansion,
- Mixing at different pressures,
- Mixing at different temperatures,
- Mixing at different compositions,
- Heat loss,
- Transport of shaft work,
- Conversion of mechanical energy to electrical energy.

The characteristic inefficiencies are selected to provide a comprehensible overview among the components of the gas turbine system based on an exergy analysis. Particularly, the mixing processes are subdivided into three types: first, the high-pressure stream gets throttled by a hypothetical throttling unit to the minimum inlet pressure of the mixer. Then the temperature change at isobaric conditions follows which is represented by the difference in physical exergies. At last, the change in composition at isobaric and isothermal conditions takes place, represented by the difference in chemical exergies. The expansion process is modeled by using the isentropic efficiency which includes the friction losses associated with: a) surface friction of the housing, b) incidence caused by the angle between the air and blade, c) profile losses due to a negative velocity gradient in the blade boundary layer, d) surface friction on the blade and annular walls, e) clearance between the blade tip and the casing and f) wake produced at the end of the rotary [141].

4.4.2 Gas Turbine Model

In this section, the gas turbine model is introduced independently of the particular fuel. The flow diagram is shown in Fig. 4.3. Broadly, the gas turbine system consists of an air compressor (AC), a combustion chamber (CC) and a gas turbine (GT). The air compressor pressurizes ambient air at a pressure ratio of 1.255 for each of its 13 stages. In this work, the suction loss at the compressor inlet is incorporated by the polytropic efficiency. The pressure of the bleed air flows used for cooling and sealing the turbine is assumed to be at least 10 % higher than the pressure at the inlet of the gas turbine, but at least 1 bar [142]. Altogether, seven cooling and seven sealing flows are considered. Within the combustion chamber, the pressure loss (6.5 % of the inlet pressure) is separated into two parts: for combustion purposes, the exit air of the compressor needs to be throttled from almost sonic speed within the diffusor (T1).

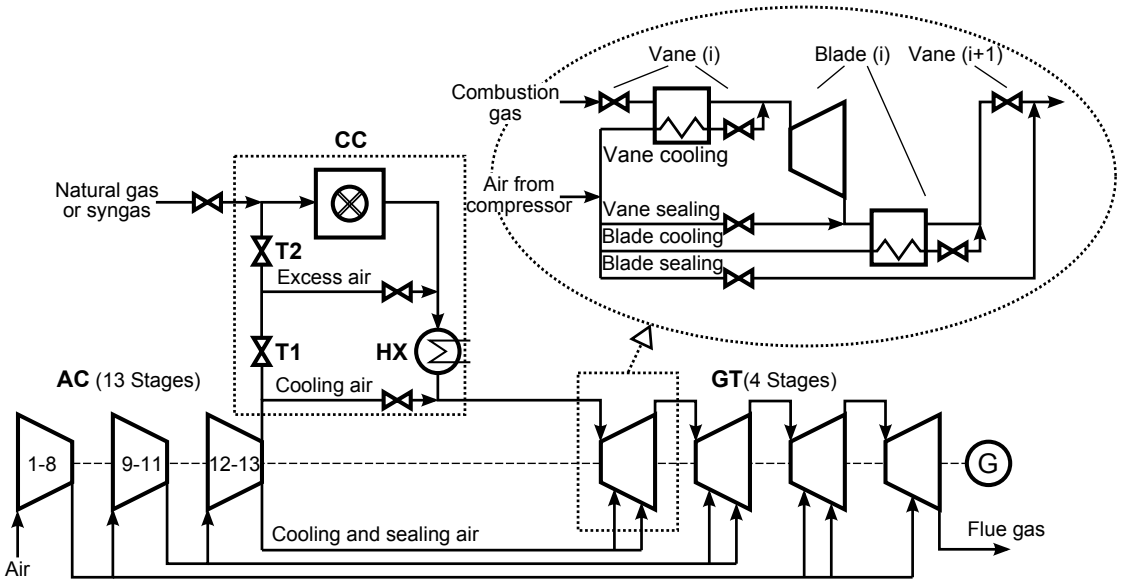

Figure 4.3: Flow diagram of the gas turbine system.

The larger part occurs within the combustor (T2) because this has a positive effect on the mixing of fuel and air as well as on the combustion process [143].

Subsequently, the compressed air is split into a stoichiometric and an excess part. The stoichiometric air enters the throttling unit (T2) representing the pressure losses caused by the combustor swirler at the combustor inlet. Compared to the compressed air, the fuel gas enters the system at a higher pressure. It gets throttled to the lower pressure of the compressed air and is then mixed with the stoichiometric air flow. Hence, the combustor uses the pre-mixing configuration. The subsequent stoichiometric combustion results in the adiabatic combustion temperature at the combustor exit. The combustion gas is then mixed with the excess air flow which decreases the temperature. Prior to that, the excess air is throttled to the lower pressure of the combustion gas. The heat loss of the overall system caused by high temperatures is represented by the cooler HX. At the outlet of the combustion chamber, the combustion air is mixed with the throttled cooling air of the combustion chamber. The particular design of the combustion chamber is highly complex and strongly depends on the choice of the manufacturer.

The model of each turbine stage according to Kail [142] is presented in Fig. 4.3 within the dotted line in the upper right corner. Only within the last stage no cooling air is needed because the main gas temperature drops below the maximum acceptable temperature of the vanes and blades surface without TBC of 950 °C [144]. The pressure ratio (about 0.5) is assumed to stay constant among the turbine stages. Furthermore,

the pressure drop of the vane caused by profile and surface friction is represented by a throttling unit. The first three stages are cooled by convective heat transfer as well as an air film layer to protect the materials against the high temperature of the main gas stream. The amount of convective heat transfer within the vanes and blades is estimated by the temperature of the exiting cooling air, which is 600 °C in case of the first and second stage, and 480 °C in case of the third stage [142].

The sealing air prevents the main gas stream from passing the vane or blade through the clearance between tip and casing. The limited ability of the sealing air to generate mechanical power is represented by mixing the air into the main gas stream subsequent to the blades. Before the cooling or sealing air is mixed into the main gas stream, it is throttled to the lower pressure level of the main stream representing the mixing at different pressures. The cooling air of the blades is then mixed into the main stream. On the one hand, a part of this air produces work through the blades but on the other hand, a part of the vane cooling air does not produce work through the blades. Based on the assumptions presented by Kail [142], both effects compensate each other approximately. Finally, the sealing air of the blades is mixed into the main gas stream subsequent to the throttling unit representing the pressure loss of the next stage vane. Throttling within the secondary air system includes the pressure drop caused by transport as well as the mixing at different pressures. The determination of the losses associated with transport depends on the particular design considering the pipe diameter, pipe length and air velocity. The preparation of ambient air by filtering is not part of this work. The developed model potentially enables engineers to perform a sensitivity analysis, for example, on the stage pressure ratio or the working fluid. Changing the firing temperature will need further modeling enhancements.

4.4.3 Cases Running on Different Fuels

Gas turbine systems running on natural gas are widely used in the industry and major parameters are well published. Data of gas turbine systems running on H_2-rich syngas are not that much available, and some systems are still under research. Based on characteristic parameters identified by simulating a gas turbine running on natural gas, a gas turbine running on syngas was simulated. Both systems are further denoted as:

- NGGT - Gas Turbine running on Natural Gas,
- SGT - Gas Turbine running on Syngas.

First, the description of the NGGT case is presented and then the SGT case follows.

Table 4.4: Fixed and adjusted parameters from literature (case NGGT).

Parameter	Unit	Reference value	Adjusted value
Air compressor			
Number of stages [145]	-	13	
Pressure ratio [57]	-	19.2	
Polytropic efficiency [146]	%	91.5	
Combustion chamber			
Pressure loss overall (Δp_{cc}) [147]	%	6.5	
Pressure loss diffuser (average) [143]	% of Δp_{cc}	35	
Pressure loss swirler (average) [143]	% of Δp_{cc}	65	
Radiation loss [141]	% of H_i	0.5	
Cooling air [142]	% of inlet air	12.4	9.92
Gas turbine			
Number of stages [22]	-	4	
1st stage cooling/sealing air [142]	% of inlet air	9.68/2.25	8.71/2.03
2nd stage cooling/sealing air [142]	% of inlet air	2.95/2.25	2.66/2.03
3rd stage cooling/sealing air [142]	% of inlet air	1.97/1.69	1.77/1.52
4th stage sealing air [142]	% of inlet air	1.12	1.01
1st stage ratio vane/blade cooling and sealing [147]	%	52/48	
2nd stage ratio vane/blade cooling and sealing [147]	%	56/44	
3rd stage ratio vane/blade cooling and sealing [147]	%	44/56	
Pressure loss of a single vane [142]	% of p_{in}	3	
Exit temperature convective cooling of the 1st, 2nd/ 3rd turbine stage	°C	600/480	
Surface temperature vane/blade (TBC used) [144, 148]	°C	950/1040	
Exhaust temperature [57]	°C	625	612.9
Exhaust mass flow rate [57]	kg/s	820	815.4
Other			
Overall efficiency [57]	% of H_i	40	39.7
Mechanical efficiency shaft [147]	%	99.5	
Electrical efficiency generator [147]	%	99	

The Case with Natural Gas (NGGT)

Most of the parameters are based on data published by Siemens according to the state-of-the-art gas turbine Siemens SGT5-8000H, being the largest operating gas turbine in the world. In the stand-alone configuration, the electric power output is 375 MW and the overall net efficiency is 40 % based on the lower heating value [57]. In the combined cycle configuration, the turbine is only scaled and the plant has a world

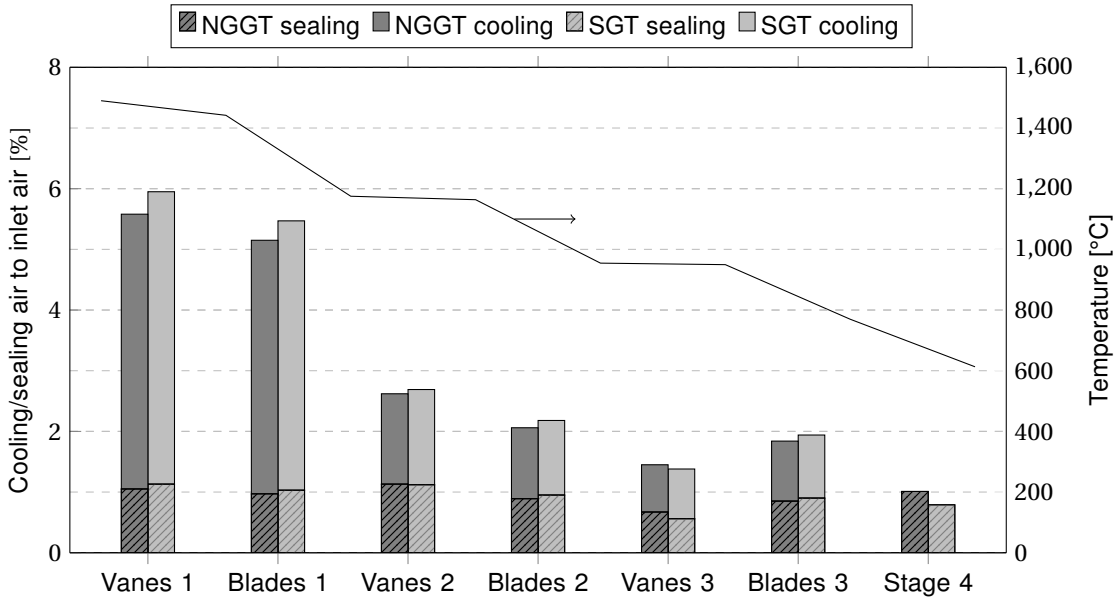

Figure 4.4: Temperature and cooling/ sealing air of the turbine stages.

record overall net efficiency of 60.7 % which was performed first at the German power station Ulrich Hartmann in 2011 [57, 145]. The high efficiency is mainly achieved by a high firing temperature. Thus, the first and second stages of the turbine use thermal barrier coating (TBC) to protect the materials from the high temperature of the combustion gas stream [57].

Table 4.4 presents the parameters assumed in the NGGT case and further basic assumptions are given in Section 4.2. Some values taken from the literature are adjusted to satisfy the better values published by the manufacturer. Natural gas enters the system at ambient temperature and 20 bar, having a mole composition of 93.1 % CH_4, 3.2 % C_2H_6, 1.6 % N_2, 1 % CO_2, 0.7 % C_3H_8 and 0.4 % C_4H_{10} [6]. The calculated lower heating value H_i is 47.19 MJ/kg. Among the turbine stages, the demand for cooling and sealing air is taken from the former, smaller gas turbine SGT5-4000F [142]. The particular demand is adjusted by using 90 % of the literature value, except the cooling demand of the combustion chamber which is adjusted to 80 %. Figure 4.4 shows the resulting amount of air entering the turbine related to the inlet air flow of the compressor for both cases. The lower bar represents the sealing air and the upper bar represents the cooling air used among the turbine stages. Only within stage four no cooling air is needed. Additionally, the temperature of the main gas stream is shown on the secondary axis. The temperatures result from the NGGT case and are also taken for the SGT case. For obvious reasons, the temperature mainly drops

through the blades during the expansion. The overall cooling and sealing demand amounts to 19.7 % in case of the turbine and 9.9 % in case of the combustion chamber.

The COT (Combustor Outlet Temperature) results to 1490 °C and the isentropic stage efficiencies of the blades, starting from the first stage, are 90.5 %, 91 %, 91.5 % and 92 %, respectively. According to the ISO 2314 standard, the Turbine Inlet Temperature TIT_{ISO} is calculated to 1309 °C, and the isentropic efficiency of the compressor and turbine are 88.2 % and 87.9 %, respectively. Furthermore, the air-fuel equivalence ratio amounts to 1.79 in the case of the combustion chamber, and 2.54 for the overall system.

The Case with Syngas (SGT)

Based on the characteristic parameters found by the simulation of the NGGT case, a gas turbine model firing syngas was developed. The syngas is produced by gasification of the coal type Illinois No.6 (see Section 4.2) within an IGCC plant with carbon capture described in Section 4.5.1 (case IGCC-1). The final mole composition of the prepared syngas amounts to 80.6 % H_2, 2.8 % CO, 12.5 % H_2O, 4.1 % N_2 and on the balance CH_4 and CO_2. The final temperature is 145.1 °C and the pressure is 34.1 bar.

The model design is similar to the NGGT case (see Fig 4.3). Identical assumptions are made for a) the air compressor pressure ratio, b) each isentropic efficiency and c) the combustion chamber. Compared to the NGGT case, the temperatures of the main gas flow within the turbine remain constant which corresponds to the same material limitations. Hence, it is feasible to keep the isentropic efficiencies of the rotor stages constant. The demand of cooling and sealing air gets adjusted by the constant outlet temperatures of each mixing process within the turbine. The exit temperature of the cooling air leaving the vanes and blades after convective heat transfer is assumed to remain constant at 600 °C in the case of the first and second stage and 480 °C in the case of the third stage.

The state changes are shown by the *T-s* diagram in Fig. 4.5. Thereby the presented entropy relates to the mass flow rate of air at the compressor inlet. On the left side, the overall system is presented including the convective heat transfer within the vanes and blades. The calculated adiabatic combustion temperature is presented at 2366 °C. On the right side, the state variables of the first turbine stage are presented in detail. The cooling and sealing demand of the whole turbine related to the compressor inlet air amounts to 20.4 % and in the case of the combustion chamber to 10.6 %. Compared to the NGGT case, the overall cooling demand increases due to a higher specific

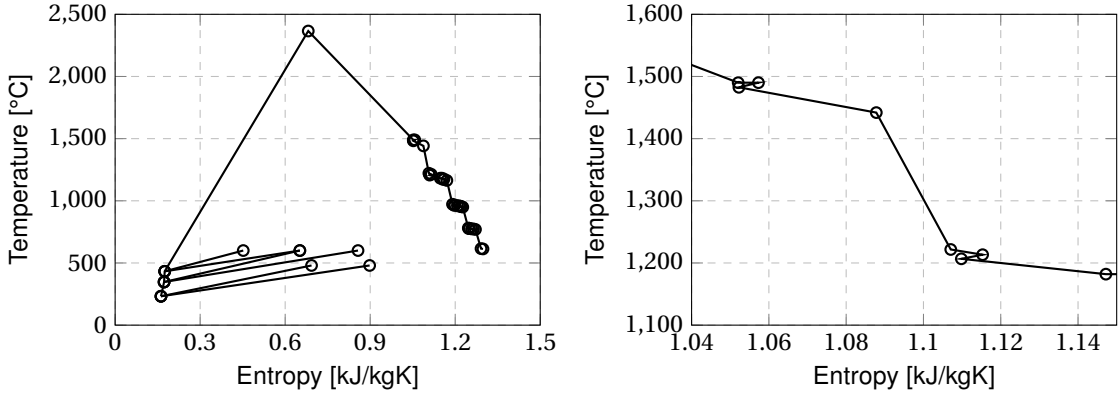

Figure 4.5: *T-s* diagram of the gas turbine system (SGT case): (left) overall, (right) first turbine stage.

heat capacity of the combustion gas determined by the combustion of syngas. The adiabatic combustion temperature increases slightly due to the higher mass-based heating value of hydrogen as well as the higher fuel gas temperature. The resulting air-fuel equivalence ratio is 2.1 in case of the combustion chamber and 2.9 for the overall system. Furthermore, the TIT_{ISO} results in 1313°C, and the isentropic efficiency of the compressor and turbine are 88.2 % and 89.1 %, respectively. The overall net efficiency increases by 2.1 % points to 41.8 %.

4.5 Reference IGCC with Pre-Combustion Decarbonisation

4.5.1 High-Efficiency IGCC Using a Shell Gasifier

The IGCC plants using CLC are benchmarked against a conventional, high-efficiency IGCC process serving as the reference case. The plant configuration was chosen according to plants discussed by the U.S. DOE [6] and others. A simplified flow diagram of case IGCC-1 is shown in Fig. 4.6, and a selection of flows from the simulation is presented in Table 4.5. The basic assumptions and type of coal are presented in Section 4.2, and further assumptions of this case are shown in Table 4.6. The major subsystems of the IGCC are the gasification island, Air Separation Unit (ASU), Acid Gas Removal (AGR) unit, gas turbine system, and steam cycle. A dry coal-fed Shell gasifier is used for gasification, this being a well-proven and efficient technology. The received bituminous coal containing 9.5 % moisture enters the dryer unit and is dried to a residual moisture of 5 %, using heated nitrogen within the dryer. The prepared coal is

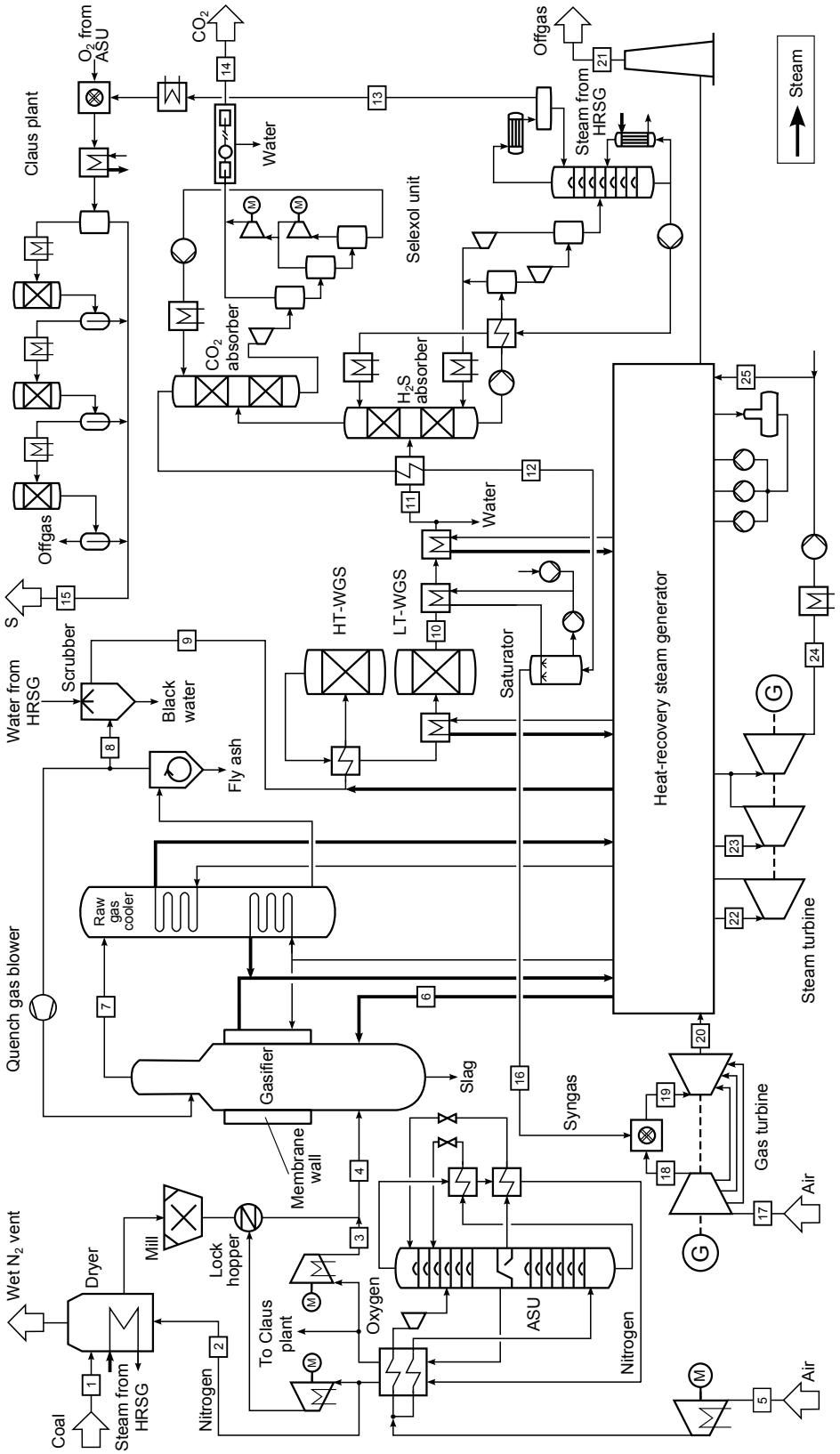

Figure 4.6: Flow diagram of the IGCC plant with carbon capture using a Shell gasifier (case IGCC-1).

Table 4.5: Simulation results for the selected flows of case IGCC-1.

Flow no.	Type	Temperature [°C]	Pressure [bar]	Mass flow [kg/s]	Exergy [MW]
1	Coal	15.0	1.0	80.0	2557.5
2	Nitrogen	18.0	1.1	175.0	5.7
3	Oxygen	120.6	45.0	60.3	24.9
4	Coal only	50.0	1.0	76.2	2557.5
5	Air	15.0	1.0	257.8	1.5
6	Steam	400.0	45.0	6.8	9.0
7	Raw gas	900.0	40.0	301.4	3888.7
8	Raw gas	280.0	39.3	139.9	1713.7
9	Raw gas	141.4	39.0	154.2	1711.6
10	Shift gas	281.0	38.8	249.2	1718.5
11	Shift gas	29.4	34.9	207.3	1648.8
12	Clean gas	20.0	34.6	25.7	1480.0
13	Acid gas	48.0	1.6	2.0	18.1
14	CO_2	45.0	110.0	170.3	163.6
15	Sulfur	150.0	1.1	0.6	11.8
16	Syngas	145.1	34.1	42.0	1493.7
17	Air	15.0	1.0	1230.0	7.3
18	Air	432.8	19.2	957.8	401.3
19	Combustion gas	1490.0	18.0	999.8	1555.0
20	Exhaust gas	612.9	1.1	1272.0	451.3
21	Offgas	133.0	1.1	1272.0	69.7
22	Steam	590.0	164.0	196.1	332.5
23	Steam	562.0	42.0	213.1	330.3
24	Condensate	26.7	0.035	245.8	32.9
25	Water	22.0	2.0	368.6	18.6

then crushed in a bowl mill. The ASU operates at cryogenic temperatures, primarily to provide 98 % pure oxygen for the gasification process and combustion within the Claus plant. Almost 90 % of the separated nitrogen is heated to 250 °C in order to dry the wet coal and about 3.3 % is used to transport the coal particles through the lock hopper into the gasifier.

The Shell gasifier is an oxygen-blown, entrained-flow gasifier characterized by high feed rates, low residual methane, high carbon conversion, and almost tar-free exhaust gas. The unit operates at 1550 °C and 40 bar [149]. This temperature is above the melting point of ash of 1430 °C when using the bituminous coal type Illionois No.6 [51]. In this way, a slag layer protects the membrane wall and the molten slag can be easily removed at the bottom. The steam demand for gasification is 0.09 kg/kg of coal at 400 °C and 45 bar and the oxygen demand is 0.78 kg/kg, according to Zheng and

Table 4.6: Assumptions of case IGCC-1.

System/Component	Unit	Value
Shell gasification island		
Coal dryer - residual moisture	%	5
Coal mill - electrical demand	kJ/kg	36
Steam/$coal_{ar}$ mass ratio [150]	-	0.09
Oxygen/$coal_{ar}$ mass ratio, according to [150]	-	0.78
Transport nitrogen/coal mass ratio	-	0.09
Steam gasification agent temperature	°C	400
O_2 gasification agent pressure	bar	45
N_2 gasification agent pressure	bar	56
Carbon conversion efficiency gasifier [149]	%	99.7
Heat loss gasifier ($H_{s,coal}$) [20]	%	0.5
Steam production gasifier ($H_{i,coal}$) [20]	%	1.5
Gasifier temperature [149]	°C	1550
Gasifier pressure [149]	bar	40
Gas quench temperature [149]	°C	900
Quench gas blower isentropic efficiency	%	78
Pressure loss cyclone and filter [6]	bar	0.69
Pressure loss scrubber [6]	bar	0.34
WGS unit		
HT-WGS reactor inlet temperature [20]	°C	275
LT-WGS reactor inlet temperature	°C	210
Steam demand by outlet mole fraction of CO [151]	%	1.9
Pressure loss [6]	bar	3.87
Selexol® unit		
Gas temperature at inlet	°C	30
Lean solvent temperature [38]	°C	-1
LP steam production per kg of H_2S [38]	MJ/kg	29.5
Solvent pumps isentropic efficiency	%	75-85
Solvent/gas mole ratio H_2S absorber	-	0.17
Solvent/gas mole ratio CO_2 absorber, based on [38]	-	1.05
Solution temperature within the reboiler [38]	°C	100
Refrigeration compressor isentropic efficiency [135]	%	78
Claus plant		
Combustion temperature	°C	1050
H_2S/SO_2 mole ratio [42]	-	2

Furinsky [150]. At the top of the gasifier, the raw product gas is cooled down to 900 °C by a gas quench [149]. Saturated steam is produced by cooling the raw gas down to 250 °C. Subsequently, fly ash gets captured by a cyclone and candle filter. A Venturi type scrubber removes the remaining particles [6].

A Water Gas Shift (WGS) reactor converts the CO of the raw syngas into H_2 and CO_2 by adding steam from the intermediate pressure level at 380 °C. Only a two-stage WGS reactor is capable of meeting carbon capture efficiencies above 75% [152]. The steam demand and temperature are selected to reduce the CO mole fraction to about 1.9 % [151]. The sour gas enters the High-Temperature Water Gas Shift reactor (HT-WGS) at 275 °C [20] and exits it at 520 °C. The Low-Temperature Water Gas Shift reactor (LT-WGS) increases the temperature from 210 to 289 °C. The gas is then cooled to 30 °C and sent to the dual-stage AGR unit introduced in Section 2.2.1.

The Selexol® solvent is used for physical absorption of H_2S and CO_2. In order to ensure proper absorption conditions, a refrigeration machine using CO_2 as the working fluid is required. The regeneration of the H_2S-rich solvent is realized by an acid gas stripper, which needs latent heat within the reboiler provided by steam from the HRSG. The mole composition of the acid gas is 35 % H_2S, 52.9 % CO_2, 0.2 % H_2O, 11 % H_2, and the remainder is N_2. Subsequently, the amount of H_2S is converted into elemental sulfur by using a three-stage Claus plant. In this process, pure oxygen provided by the ASU is required. The CO_2-rich solvent passes three flash stages in order to separate the CO_2, which is further pressurized by an intercooled three-stage compressor to ensure the transport conditions. Finally, the clean syngas exits the AGR unit at 20°C.

Due to the high mole fraction of hydrogen (92.1 %) of the clean syngas, it is reasonable to dilute the syngas before entering the gas turbine. Therefore, a saturator increases the mole fraction of water to about 12.5 %. Conditioned by hot water, the temperature of the gas stream increases from 20 °C to 145.1 °C. After conditioning, the syngas mole composition amounts to 80.6 % H_2, 2.8 % CO, 12.5 % H_2O, 4.1 % N_2 and on the balance CH_4 and CO_2. The syngas is fired in a gas turbine system which is described in Section 4.4. Especially the assumptions are presented in Table 4.4. According to the ISO 2314 standard, the resulting turbine inlet temperature TIT_{ISO} is calculated to 1313 °C. The exhaust gas enters the HRSG at 615 °C and is cooled to 132 °C. Details of the steam cycle are presented in Section 4.3.2.

4.5.2 Low-Cost IGCC Using a GEE Gasifier

The IGCC plant presented in this section was developed in order to analyze the potential for a flexible generation of electricity and hydrogen. In general, the plant configuration and major assumptions were mainly selected according to a plant discussed by the U.S. DOE [6]. Some units like the ASU, WGS reactor, AGR unit and

Table 4.7: Assumptions of case IGCC-2 (mainly taken from [6]).

System/component	Unit	Value
GEE gasification island		
Coal mill - electrical demand	kJ/kg	36
Slurry concentration to gasifier	%	44
Oxygen/$coal_{ar}$ mass ratio, according to [150]	-	0.8
O_2 gasification agent pressure	bar	38
isentropic efficiency recycle pump	%	85
Carbon conversion efficiency gasifier	%	98
Heat loss gasifier ($H_{s,coal}$)	%	0.5
Gasifier temperature [150]	°C	1250
Gasifier pressure	bar	36
Radiant cooler raw gas temperature	°C	667
Pressure loss scrubber	bar	0.3
WGS unit		
HT-WGS reactor inlet temperature	°C	225
LT-WGS reactor inlet temperature	°C	204
Steam demand by outlet mole fraction of CO	%	0.5
Pressure loss	bar	0.7
Gas turbine system		
Turbine inlet temperature TIT_{ISO}, according to [153]	°C	1253
Air compressor exit pressure [153]	bar	18.8
Air compressor isentropic efficiency	%	88.2
Gas turbine isentropic efficiency	%	87.9

the steam cycle are likely selected according to the high-efficiency case IGCC-1 (see Section 4.5.1). The basic assumptions are presented in Section 4.2 and further assumptions are presented in Table 4.7. In case of the AGR unit and Claus plant, the solvent to gas mole ratio within the absorbers remain almost constant compared to the case IGCC-1 presented in Table 4.6. The flow diagram is illustrated in Fig. 4.7 and the simulation results for some selected flows are presented in Table 4.8.

Compared to the case IGCC-1, the major difference is given by the gasifier type. The General Electric Energy (GEE) gasifier (former called Texaco gasifier) features a carbon conversion efficiency of 98 % including a recycle stream of fines. Based on the slurry-fed type of gasifier, the coal feed gets first crushed by a bowl mill and then mixed with water within a slurry tank resulting in a slurry concentration of 44 %. The type of coal as well as the oxygen-blown entrained-flow gasifier type are similar when compared to the case IGCC-1. The gasification temperature is set to 1250 °C which is the lower operating temperature limit [150]. The raw syngas is then further cooled by a radiant cooler to 667 °C at the gasifier bottom. As the temperature required for the

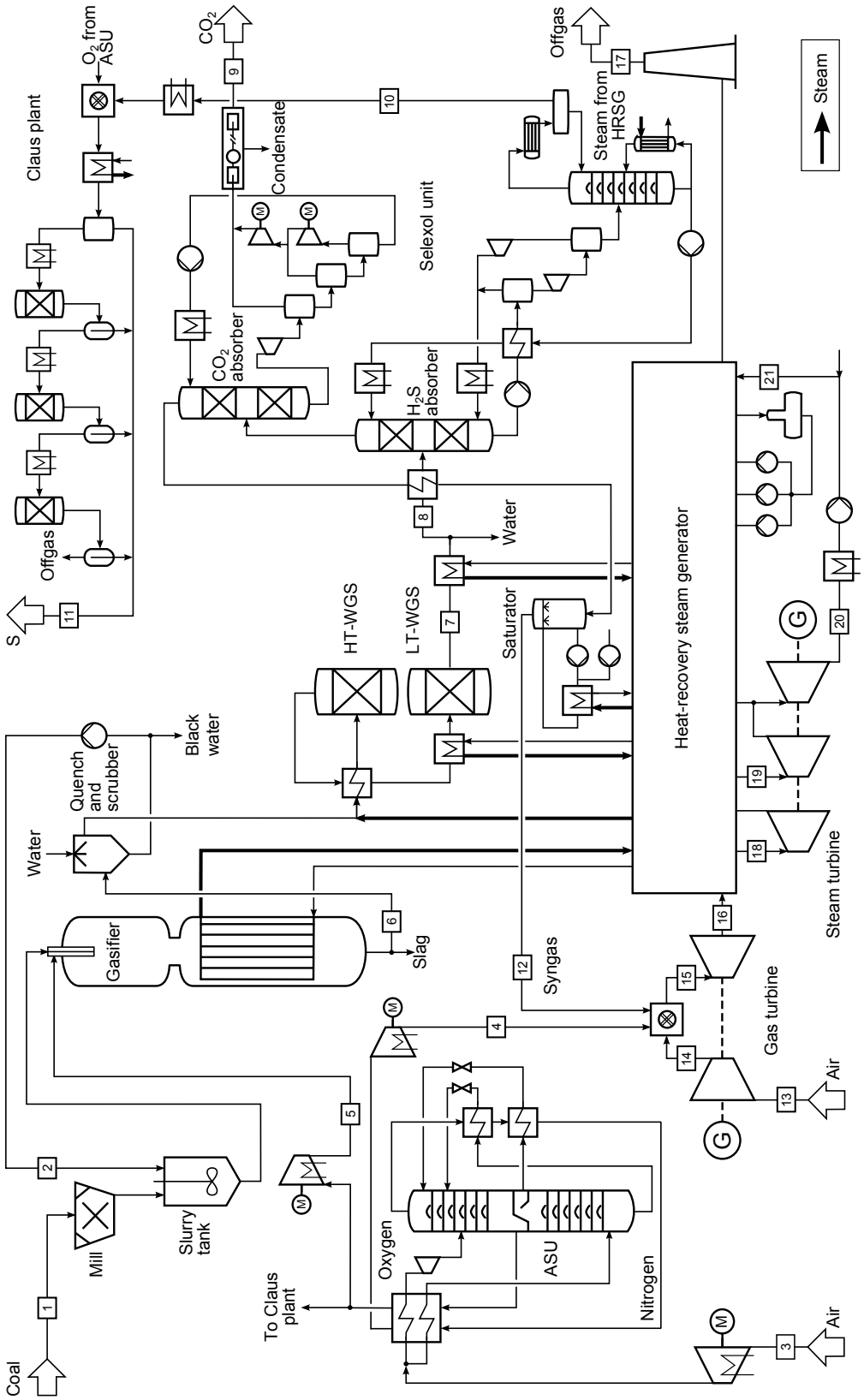

Figure 4.7: Flow diagram of the IGCC plant with carbon capture using a GEE gasifier (case IGCC-2).

Table 4.8: Simulation results for the selected flows of case IGCC-2.

Flow no.	Type	Temperature [°C]	Pressure [bar]	Mass flow [kg/s]
1	Coal	15.0	1.0	50.0
2	Water	177.3	35.7	22.0
3	Air	15.0	1.0	164.1
4	Nitrogen	127.6	26.8	124.1
5	Oxygen	93.6	38.0	40.0
6	Raw gas	677.0	35.6	87.8
7	Shift gas	243.7	34.4	165.1
8	Shift gas	29.8	34.1	125.6
9	CO_2	45.0	110.0	108.0
10	Acid gas	24.9	1.3	1.3
11	Sulfur	150.0	1.1	0.4
12	Syngas	130.9	33.3	16.7
13	Air	15.0	1.0	626.4
14	Air	426.1	18.8	626.4
15	Combustion gas	1253.0	18.3	767.2
16	Exhaust gas	588.6	1.1	767.2
17	Offgas	148.4	1.1	767.2
18	Steam	567.0	160.3	69.2
19	Steam	551.4	46.5	106.9
20	Condensate	26.7	0.0	148.8
21	Water	22.0	6.3	253.2

WGS reactor is 225 °C, the raw syngas gets further cooled. A water quench removes the particulates from the raw syngas and reduces the temperature. A purge stream separates the particle-loaded black water representing the function of a scrubber. The major part of the black water gets recycled to the slurry tank.

The WGS reactor and AGR unit act similar compared to the case IGCC-1. A saturator is used as well but the heat is supplied by the HRSG instead of the LT-WGS product gas because the temperature and mass flow rate is smaller and cannot satisfy the heat demand. Furthermore, the separated nitrogen from the ASU is used to dilute the combustion process within the gas turbine system. Therefore a boost compressor pressurizes the nitrogen to about 27 bar. The temperature and pressure ratio of the gas turbine system are taken from the gas turbine SGT5-4000F from Siemens running on natural gas [153]. However, the isentropic efficiencies are taken from the case IGCC-1 (see Table 4.7). The temperature profiles of the final heat exchanger network are presented in Fig. 4.8, whereat the hidden temperature of the raw syngas cooler

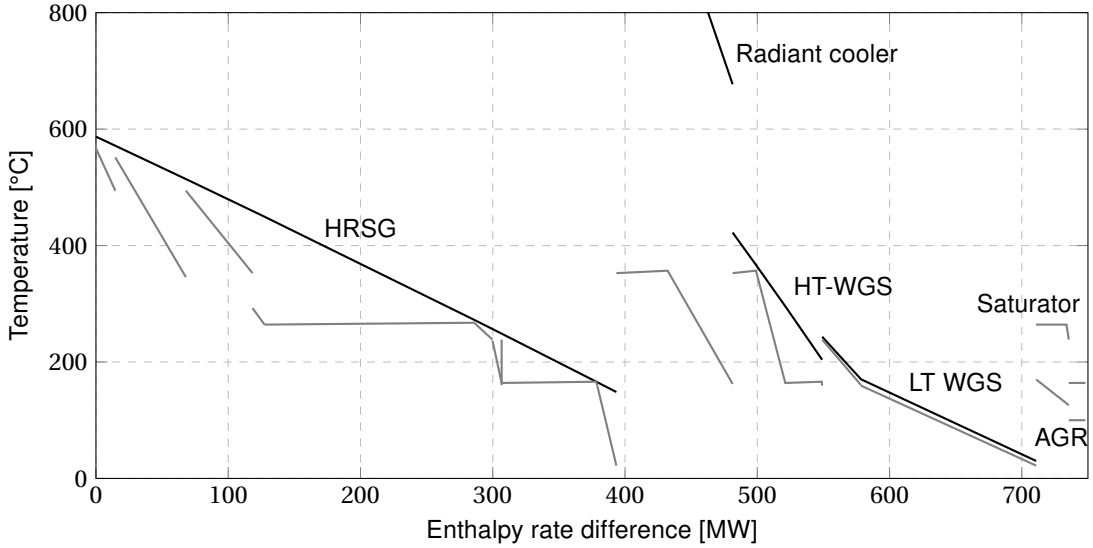

Figure 4.8: Temperature profiles of the heat transfer within case IGCC-2.

inlet is about 677 °C, see Table 4.8. The flow diagram of the steam cycle is given in Section 5.4.1 in context of the off-design analysis.

4.6 IGCC Using Chemical-Looping Combustion

This section presents the assumptions as well as the system and component modeling of the IGCC plants using CLC simulated in the scale of a conventional coal-fired power plant. All cases, including a CLC unit, use recycled CO_2 to transport the coal into the gasifier instead of using pressurized N_2 provided by the ASU to increase the purity of the captured CO_2 stream. Similar to the base cases, the air demand of the ASU is not provided by the gas turbine system compressor in order to ensure a good operational flexibility. The temperature profiles of the heat transfer that are not presented in this section are given in the Appendix A (cases CLC-Ni1,CLC-Ni2,CLC-Ni4,CLC-Fe2,CLC-Fe4,CLC-Fe5).

Among others, the author of this work already published the analysis of an IGCC using a two-reactor CLC system with nickel oxide as the oxygen carrier [89, 90] as well as the results of an IGCC using a three-reactor CLC system with iron oxide as the oxygen carrier [98–101]. In this work, some system configurations, like e.g. the cooling concept of the CLC reactors, are changed and a consistent set of assumptions was used to accomplish a convenient discussion of the results.

4.6.1 Modeling of the CLC System

The fundamentals of CLC are introduced in Section 2.4. The two-reactor system uses NiO and the three-reactor system uses Fe_2O_3 as the oxygen carrier circulating among the CLC reactors. The circulation rate of the oxygen carrier is determined by the reactions within the fuel reactor. Increasing the oxygen carrier circulation rate increases the fuel conversion. On the contrary, the demand of cooling air within the air reactor simultaneously increases, which causes a larger component size and therefore higher capital costs. Additionally, the exit temperature of the fuel reactor increases slightly as the characteristic of the net reaction is slightly endothermic and on that account heat is transferred from the oxygen carrier to the product gas. In general, higher temperatures are potentially useful to produce superheated steam within the subsequent HRSG but the costs of the HRSG potentially increase due to a higher thermal resistance required by the heat exchanger materials. However, additional support material within the CLC unit is not considered within the simulations because it merely acts as an inert catalyst.

The pressure drop of the CLC reactors is supposed to depend on the factual size and particular design. Kempkes and Kather [77] present a pressure drop of 200 mbar used in the air reactor and 300 mbar used in the fuel reactor. In this work, the pressure drop is higher in all cases.

4.6.2 IGCC Using a Two-Reactor CLC Unit

The CLC unit using a two-reactor system replaces the conventional combustion chamber of the gas turbine system. General assumptions are presented in Section 4.2 and Table 4.1 presents specifications of the analyzed cases. The complex model of the gas turbine presented in Section 4.4 is not suitable as the turbine inlet temperature changes. Instead, a simplified three-component model according to the ISO 2314 standard has been developed using the parameters presented in Table 4.7 similar to the base case IGCC-2. The turbine inlet temperature corresponds to the air reactor temperature varied among the analyzed cases.

IGCC Plant Using a Shell Gasifier

The cases CLC-Ni1 to CLC-Ni3 use almost the same system components as the base case IGCC-1 presented in Section 4.5.1. A simplified flow diagram is shown in Fig. 4.9, and selected flows of case CLC-Ni3 are presented in Table 4.9. Upward of the scrubber,

the characteristic parameters and the arrangement of components are identical to case IGCC-1 except the transport of coal into the gasifier uses recycled CO_2 instead of N_2. Physical absorption of CO_2 as well as a WGS unit are not required due to the inherent capture ability. The AGR unit only consists of the H_2S capture cycle. However, without a WGS unit an additional hydrolizer is needed to convert carbonyl sulfide (COS) into CO_2 and H_2S ba using steam. For IGCC plants using a high-temperature, entrained-flow gasifier in combination with a two-reactor CLC unit, applying a hot gas cleaning unit (HGCU) is not recommended. In respect to a high overall efficiency, an air reactor temperature should be desired which also causes a high fuel reactor exit temperature depending on the syngas composition. Temperatures above 1000 °C increase the costs of the flue gas piping system as well as the subsequent HRSG significantly. Furthermore, this effect is supported by a higher fuel gas temperature. Compared to the conventional low-temperature, absorption-based gas cleaning, the application of an HGCU increases the syngas temperature by about 500 °C.

The cleaned syngas exiting the AGR unit is fed to the fuel reactor of the CLC unit, introduced in Section 2.4, at 20 °C and 36 bar. The syngas mole composition amounts to 58.1 % CO, 34.3 % H_2, 6.3 % CO_2 and on the balance N_2. Within the fuel reactor, the oxygen carrier gets reduced and the gaseous product consists of H_2O and CO_2. The product gas is then fed to the HRSG 1. The reduced oxygen carrier gets re-oxidized in the air reactor at temperatures ranging from 1100 °C to 1300 °C, depending on the particular case. In the air reactor, pressurized air supplied by the compressor of the gas turbine system is used to fluidize the metal particles. After reactions took place, the depleted air is separated by a cyclone and then fed to the gas turbine. The expanded exhaust gas then enters HRSG 2 and finally exits the overall system through a stack. Like in the base case, the parameters of the steam cycle are determined by applying mathematical optimization presented in Section 4.3.2. The resulting temperature profiles of the overall heat transfer are shown in Fig. 4.10 and the Appendix A. To allow a clearly arranged view on the overall heat transfers, temperatures exceeding 700 °C are not indicated within the diagram. The hidden temperatures can be received from Table 4.9. In HRSG 1, mainly steam is superheated due to the higher temperature on the hot side compared to HRSG 2. However, HRSG 2 is mainly used for producing saturated steam. Other configurations were found to be worse. Further remarks on the heat exchanger network design are presented in Section 4.3.2 and 5.3.1.

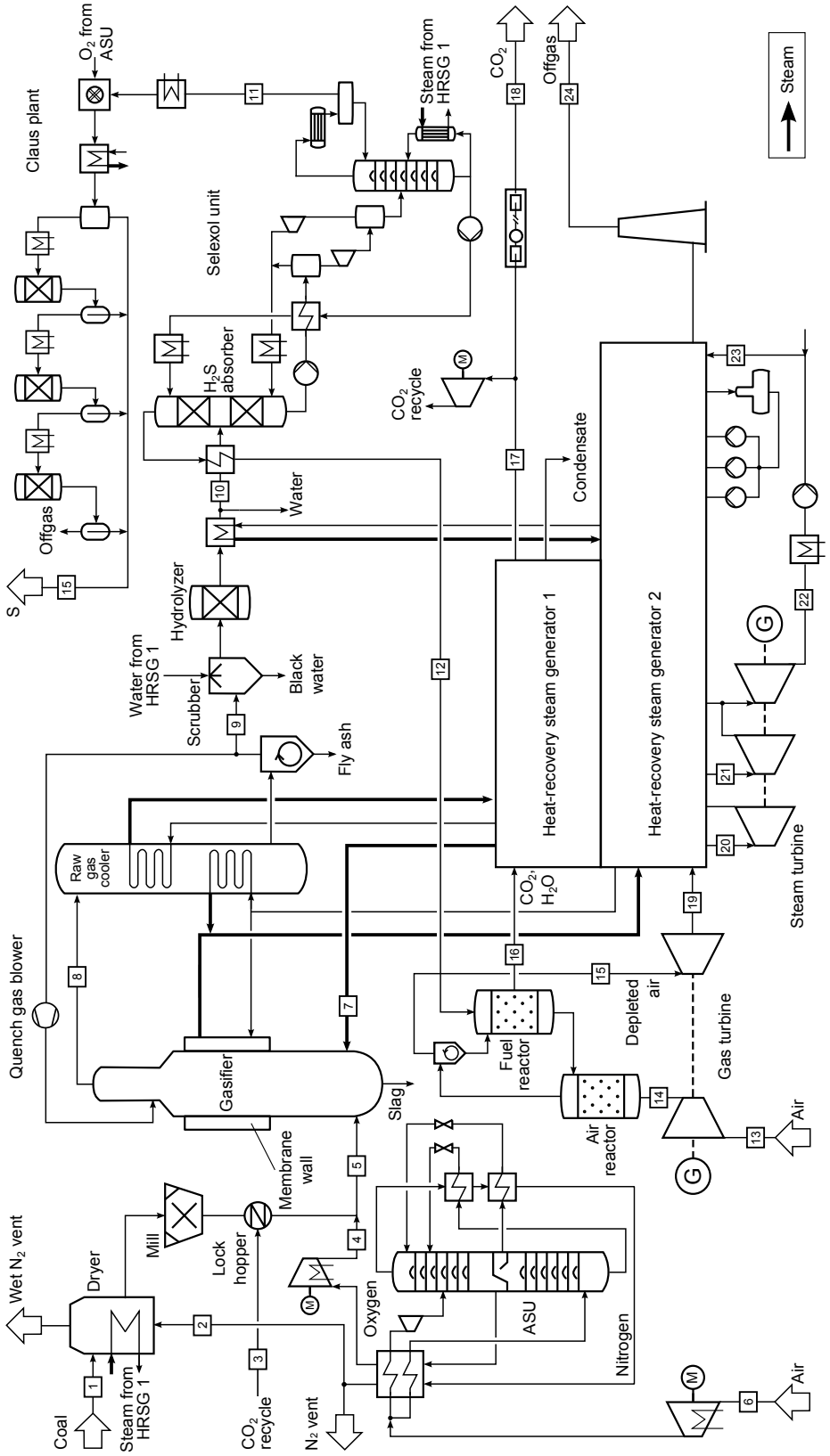

Figure 4.9: Flow diagram of the IGCC plant using a two-reactor CLC unit and a Shell gasifier.

Table 4.9: Simulation results for the selected flows of case CLC-Ni3.

Flow no.	Type	Temperature [°C]	Pressure [bar]	Mass flow [kg/s]	Exergy [MW]
1	Coal	15.0	1.0	80.0	2557.5
2	Nitrogen	17.0	1.1	175.0	5.7
3	CO_2	112.6	56.0	7.0	5.1
4	Oxygen	120.6	45.0	60.4	25.0
5	Coal only	50.0	1.0	76.2	2557.5
6	Air	15.0	1.0	257.3	1.5
7	Steam	400.0	45.0	6.8	9.0
8	Raw gas	900.1	40.0	302.7	3894.0
9	Raw gas	280.0	39.3	140.5	1715.4
10	Raw gas	30.0	38.6	154.9	1699.2
11	Acid gas	37.0	1.6	2.1	17.0
12	Clean gas	20.0	36.0	135.3	1674.6
13	Air	15.0	1.0	1443.1	8.5
14	Air	471.9	24.0	1443.1	671.2
15	Depleted air	1300.0	19.2	1345.3	1574.8
16	CO_2, H_2O	1190.8	34.3	233.1	417.3
17	CO_2	60.0	31.8	192.2	150.0
18	CO_2	45.0	110.0	184.7	151.0
19	Exhaust gas	594.0	1.1	1345.3	393.7
20	Steam	590.0	130.0	70.6	119.1
21	Steam	480.0	51.0	372.8	539.9
22	Condensate	26.7	0.035	428.1	56.3
23	Water	17.2	2.0	455.9	22.8
24	Offgas	131.5	1.1	1345.0	57.6

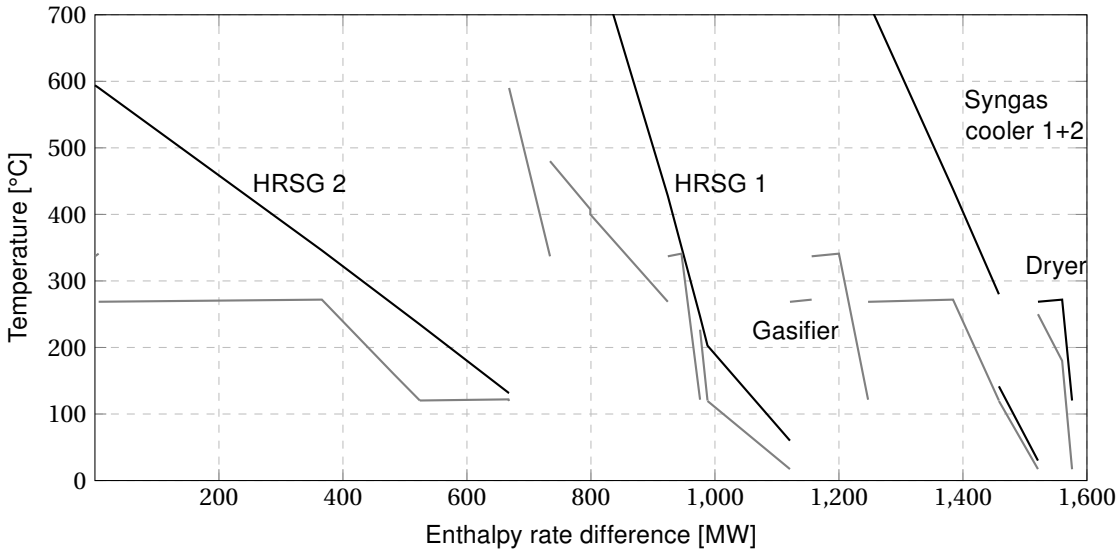

Figure 4.10: Temperature profiles of heat transfer (case CLC-Ni3).

IGCC Plant Using a BGL Gasifier

The cases CLC-Ni4 and CLC-Ni5 use the same system components compared to the cases CLC-Ni1 to CLC-Ni3 introduced above, except the gasification island and AGR unit differ (see Fig 4.11). Selected flows of case CLC-Ni5 are given in Table 4.10 and the major assumptions are shown in Table 4.11. The received coal is first crushed in a bowl mill and is then fed to the gasifier through a lock hopper. Similar to the cases in which a Shell gasifier is used, recycled CO_2 is used for the coal particle transport to increase the purity of the exiting CO_2 stream.

The gasification takes place in an oxygen-blown, moving-bed, slagging BGL gasifier. Due to the restricted equilibrium within a moving-bed gasifier, the temperature approach was used for the participating major gasification reactions. The temperatures were adapted to obtain the typical raw syngas composition of a BGL gasifier (see Table 4.11). The resulting mole composition amounts to 52.9 % CO, 31.1 % H_2, 7.7 % H_2O, 4.8 % CH_4, 2.4 % CO_2, 0.3 % H_2S and on the balance N_2, according to [51]. The oxygen demand is provided by a cryogenic ASU introduced in Section 4.5.1, and steam required for the gasification process is produced within HRSG 1. Fly ash is leaving the reactor through the raw syngas stream and is captured by a cyclone to ensure a high carbon conversion efficiency. Moreover, the molten ash gets separated by using a slag trap and water quenching at the bottom of the gasifier.

The conventional AGR unit and the WGS unit are replaced by a HGD unit. The gasifier exit temperature is significantly smaller compared to the cases in which a Shell gasifier is used. The fundamentals of the HGD process are introduced in Section 2.2.1. Within the desulfurization reactor, the temperature increases slightly by about three Kelvin. Pressurized air used within the regenerator is provided by a compressor and after the reaction the product gas is separated from the solid particles by a cyclone. The SO_2 contaminated product gas leaves the system through a turbine to recover some compression work. A Flue Gas Desulfurization (FGD) unit finally captures the sulfur entering the overall system as part of the coal by using, for example, limestone. The clean syngas then enters the fuel reactor of the CLC unit. Further descriptions are similar to the cases using a Shell gasifier. The temperature profiles of the heat exchanger network are shown in Fig. 4.12 for the case CLC-Ni5, whereas the temperature of the hot inlet air of the HRSG 1 is 1158 °C. The other cases temperature profiles are given in the Appendix A. Further remarks on the heat exchanger network design are presented in Section 4.3.2 and 5.3.1.

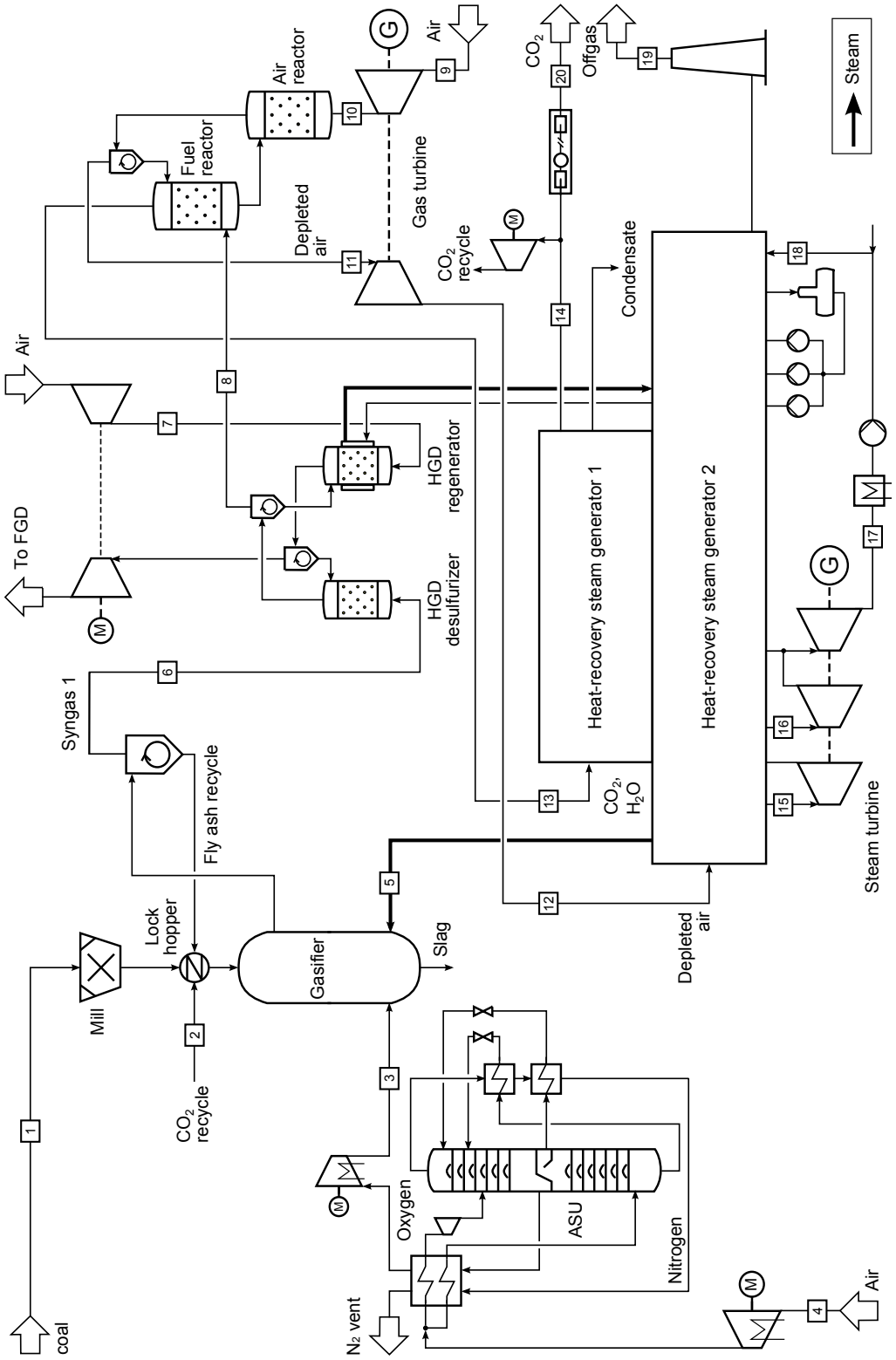

Figure 4.11: Flow diagram of the IGCC plant using a two-reactor CLC unit and a BGL gasifier.

Table 4.10: Simulation results for the selected flows of case CLC-Ni5.

Flow no.	Type	Temperature [°C]	Pressure [bar]	Mass flow [kg/s]]
1	Coal	15.0	1.0	80.0
2	CO_2	108.5	48.0	7.0
3	Oxygen	132.1	56.0	37.6
4	Air	15.0	1.0	158.6
5	Steam	400.0	40.0	25.4
6	Raw gas	552.0	31.0	129.5
7	Air	615.4	44.0	6.6
8	Syngas	555.1	30.4	129.7
9	Air	15.0	1.0	2414.6
10	Air	471.9	24.0	2414.6
11	Depleted air	477.6	19.2	2295.7
12	Exhaust gas	475.6	1.1	2295.7
13	CO_2, H_2O	1158.3	34.3	248.5
14	CO_2	60.0	32.0	195.1
15	Steam	590.0	137.0	27.0
16	Steam	590.0	74.0	312.6
17	Condensate	26.7	0.035	394.4
18	Water	22.0	2.0	401.2
19	Offgas	130.5	1.1	2296.0
20	CO_2	45.0	110.0	187.7

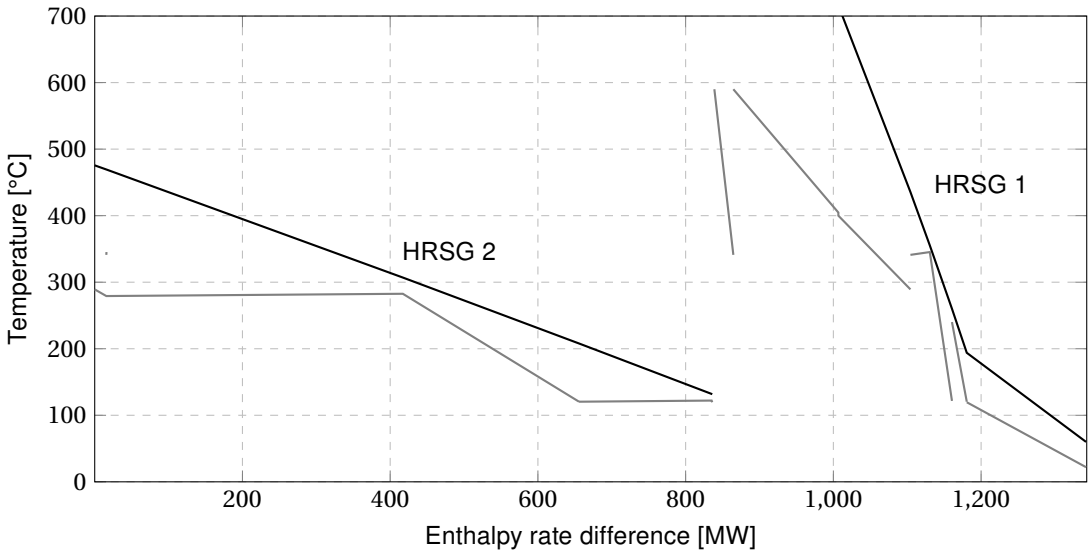

Figure 4.12: Temperature profiles of heat transfer (case CLC-Ni5).

Table 4.11: Assumptions of cases using a BGL gasifier or a HGD unit.

System/component	Unit	Value
BGL gasification island		
Coal mill - electrical demand	kJ/kg	36
Steam/$coal_{maf}$ mass ratio [51]	-	0.385
Oxygen/$coal_{maf}$ mass ratio, according to [51]	-	0.57
O_2 gasification agent temperature	°C	400
O_2 gasification agent pressure	bar	40
CO_2 gasification agent pressure	bar	48
Carbon conversion efficiency gasifier	%	99
Heat loss gasifier ($H_{s,coal}$)	%	1
Gasifier temperature	°C	~550
Gasifier pressure	bar	32 bar
HGD unit		
Regenerator reactor temperature	°C	650
Air compressor isentropic efficiency	%	88
Turbine isentropic efficiency	%	80
Mole ratio ZnS/ZnO in regenerated sorbent [154]	-	0.1
Gasifier temperature approach		
$C + H_2O \rightarrow CO + H_2$	K	461
$CO + H_2O \rightarrow CO2 + H_2$	K	1413
$C + CO_2 \rightarrow 2\,CO$	K	564
$C + 2\,H_2 \rightarrow CH_4$	K	346
$CO + 3\,H_2 \rightarrow CH_4 + H_2O$	K	408

4.6.3 IGCC Using a Three-Reactor CLC Unit

In this section, the modeling of five cases featuring a three-reactor CLC unit is discussed. Their specifications are presented above in Table 4.1. The assumptions for the cases using a Shell gasifier (CLC-Fe1 and CLC-Fe2) are presented in Section 4.5.1, Table 4.6. All other cases use a BGL gasifier and a HGD unit as described in Section 4.6.2. Basic assumptions are given in Section 4.2. All cases analyzed in this section consider the comprehensive gas turbine model presented in Section 4.4.2. The application of a CO_2 turbine is analyzed in case CLC-Fe5, where the air reactor temperature is 900 °C.

Within the three-reactor CLC system, the fuel reactor is represented by a five-stage, moving-bed, counter-current reactor. As the solid phase exits at the bottom and the gaseous phase at the top, the exit temperature of the product gas is higher, whereas the temperature difference ranges from 13 to 175 °C. The concentrations of H_2 and CO are too small to reduce the Fe_2O_3 particles to the state of Fe, while assuring complete fuel conversion. Thus, less H_2 can be produced in the subsequent steam reactor. Moreover,

due to the absence of Fe the undesirable carbon decomposition cannot take place. It has been suggested that Fe acts as a catalyst for the reverse Boudouard reaction [79].

Within the steam reactor, the reduced particles exiting the fuel reactor, which consists of almost pure FeO, are partially re-oxidized to the Fe_3O_4 state by using superheated steam at 300 °C and 40 bar. A cyclone separates the gas from the solid phase and the product gas is subsequently cooled to 600 °C. The Fe_3O_4 particles are then fully oxidized to the Fe_2O_3 state within the air reactor in order to close the redox cycle. Pressurized air is provided by an intercooled compressor. On the one hand, this compressor increases the internal power consumption. On the other hand, depleted air exiting the air reactor is used to dilute the combustion process within the gas turbine, which reduces compression work used by the gas turbine system air compressor.

IGCC Plant Using a Shell Gasifier

The plant design and assumptions of the cases incorporating a Shell gasifier (CLC-Fe1 and CLC-Fe2) are based on the process design of the reference case IGCC-1 (see Section 4.5.1). Figure 4.13 shows a simplified flow diagram, and Table 4.12 presents the corresponding simulation results of some selected flows of the case IGCC-Fe1. Compared to the base case, the WGS unit and AGR unit are replaced by a HGD unit. The fundamentals of the HGD process are introduced in Section 2.2.1 and some modeling details are presented in Section 5.3.1 in conjunction with the BGL gasifier. The cleaned syngas enters the CLC unit at about 550 °C and 38 bar having a mole composition of 67.2 % CO, 29 % H_2, 1.7 % CO_2, 1.2 % N_2 and on the balance H_2O.

Similar to the cases using a two-reactor system, the gaseous product of the fuel reactor is a mixture of H_2O and CO_2. General remarks concerning the CLC unit are presented above in Section 4.6.1. Applying an HGCU in combination with a three-reactor CLC system is reasonable, compared to the plant using a two-reactor system (cases CLC-Ni1 to CLC-Ni3) because the product gas exiting the fuel reactor is not heated that much by the hot oxygen carrier. As a result, a higher fuel gas temperature is tolerated to maintain an acceptable inlet temperature of the subsequent HRSG.

Although Fig. 4.13 shows only one stream entering the gas turbine, only the ultra-wet H_2 exiting the steam reactor is combusted directly. The depleted air is used as excess air to dilute the stoichiometric combustion gas. Under ultra-wet conditions, H_2 still remains ignitable and the NO_x emissions get significantly reduced, based on the high steam content [155]. Any alternative NO_x reduction option, like catalytic exhaust

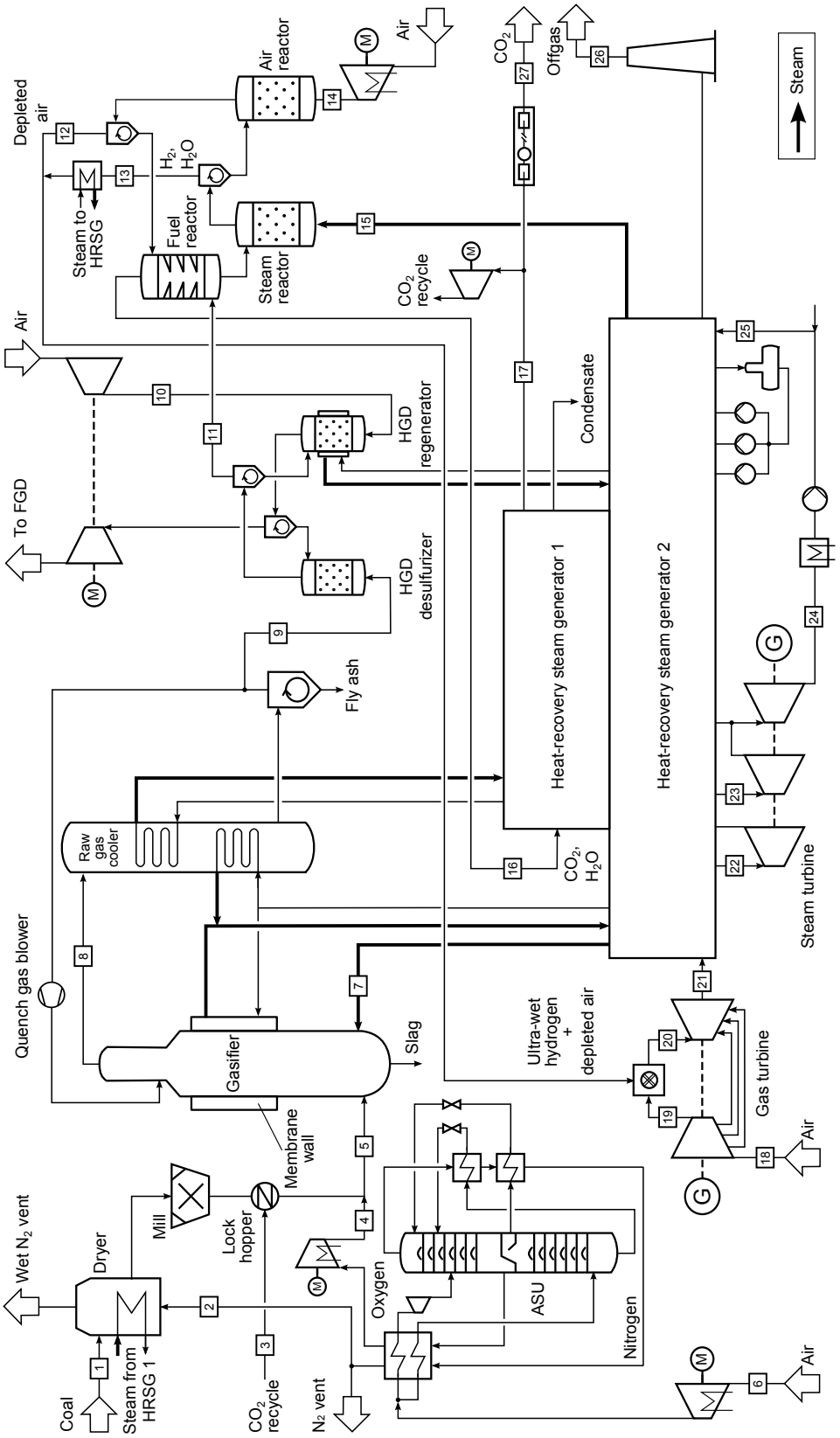

Figure 4.13: Flow diagram of the IGCC plant using a three-reactor CLC unit and a Shell gasifier.

Table 4.12: Simulation results for selected flows of the case CLC-Fe1.

Flow no.	Type	Temperature [°C]	Pressure [bar]	Mass flow [kg/s]	Exergy [MW]
1	Coal	15.0	1.0	80.0	2557.5
2	Nitrogen	12.3	1.1	175.0	5.7
3	CO_2	111.0	56.0	7.0	4.7
4	Oxygen	120.6	45.0	60.3	24.9
5	Coal only	50.0	1.0	76.2	2557.5
6	Air	25.0	1.0	257.6	1.6
7	Steam	400.0	45.0	6.8	9.0
8	Raw gas	899.9	40.0	409.3	5554.3
9	Raw gas	550.1	38.5	133.1	1753.4
10	Air	635.6	48.0	6.6	4.2
11	Clean gas	567.2	37.9	140.8	1734.1
12	Depleted air	900.0	22.0	454.5	364.6
13	H_2, H_2O	550.0	35.2	195.1	1277.7
14	Air	154.2	24.0	489.7	144.7
15	Steam	300.0	40.0	259.1	321.2
16	CO_2, H_2O	795.7	36.2	239.9	289.4
17	CO_2, H_2O	60.0	34.7	191.3	120.8
18	Air	15.0	1.0	406.9	2.4
19	Air	432.8	19.2	90.1	37.8
20	Combustion gas	1490.0	18.8	739.7	1464.9
21	Exhaust gas	612.9	1.1	1056.5	491.7
22	Steam	590.0	170.0	104.7	172.4
23	Steam	590.0	45.0	149.5	231.8
24	Condensate	26.7	0.035	161.9	13.7
25	Water	22.0	2.0	427.8	0.2
26	Offgas	97.4	1.1	1056.5	122.3
27	CO_2	45.0	110.0	190.9	125.9

treatment or separate steam production, would further reduce the overall efficiency. The exhaust gas of the gas turbine system only consists of humid, partially depleted air which is further used within the HRSG 2 for the production of steam. The temperature profiles of the heat exchanger network are presented in Fig. 4.14 and the Appendix A. The hidden temperatures can be received from Table 4.12. Further remarks on the heat exchanger network design are presented in Section 4.3.2 and 5.3.2.

IGCC Plant Using a BGL Gasifier

The cases CLC-Fe3 to CLC-Fe5 use the same system components compared to the cases CLC-Fe1 and CLC-Fe2 introduced above, except the gasification island and

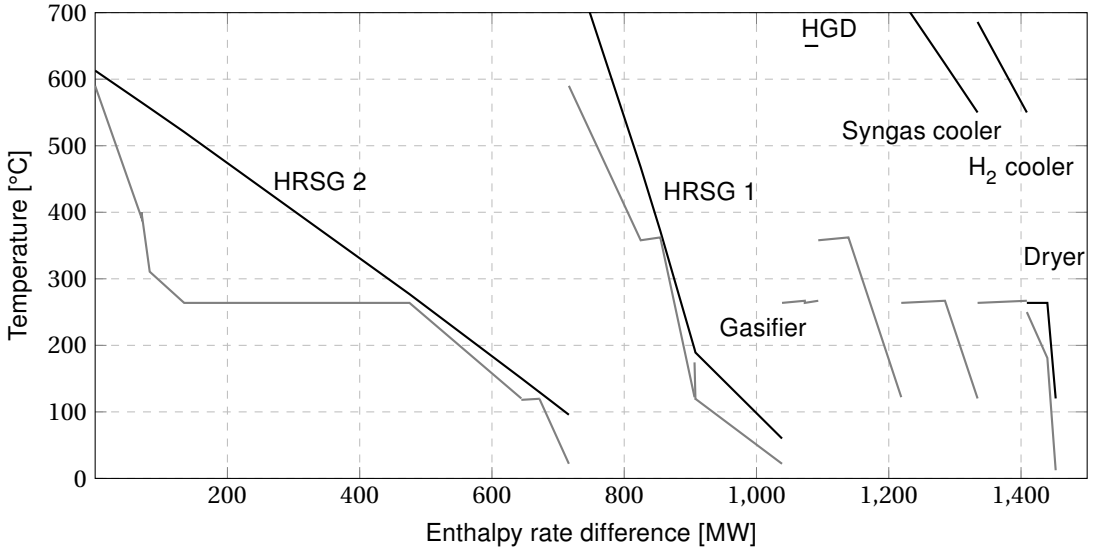

Figure 4.14: Temperature profiles of heat transfer (case CLC-Fe1).

syngas cooling section differ (see Fig. 4.15). Due to the relatively low gasification temperature, further cooling of the syngas is not required. The coal dryer is also obsolete because the BGL gasifier supports a wet feed. Selected flows of case CLC-Fe3 are given in Table 4.13.

The raw coal gets first crushed in a bowl mill and is then fed to the gasifier through a lock hopper. Moreover, the cryogenic ASU provides 98 % pure oxygen to the gasifier and steam is provided by the HRSG 2. After the syngas is cleaned by the HGD unit (see Section 2.2.1) the prepared syngas enters the CLC unit at the same conditions of the cases CLC-Ni1 to CLC-Ni3 (see Section 5.3.1). The principle of the CLC unit is described above in Section 4.6.1 and further remarks on the heat exchanger network design are presented in Section 4.3.2 and 5.3.2. The resulting temperature profiles of the heat exchanger network are shown in Fig. 4.16 and the Appendix A.

Case CLC-Fe5 exclusively considers a CO_2 turbine. Compared to case CLC-Fe3, the component configuration as well as the characteristic parameters are identical in order to evaluate the application of a CO_2 turbine. On the one hand, additional electric power is generated by the turbine and the pressure of the hot gas within HRSG 1 is reduced to an elevated pressure, which reduces the capital costs, too. On the other hand, the expanded gas has to be re-pressurized to meet the CO_2 transport conditions, and furthermore the hot gas temperature of HRSG 1 decreases significantly. Moreover, the capital costs of a CO_2 turbine are supposed to be higher than a charged HRSG.

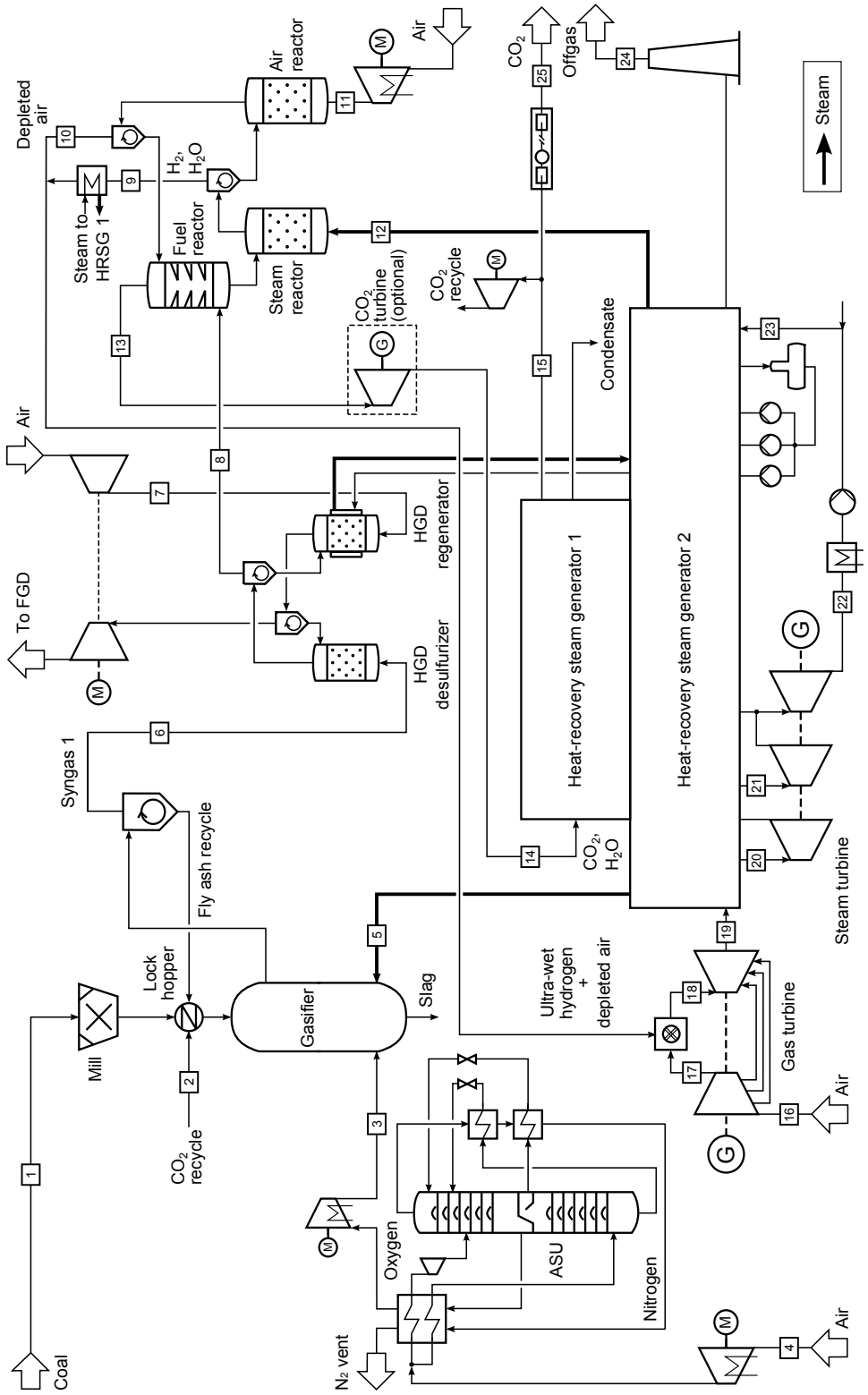

Figure 4.15: Flow diagram of the IGCC plant using a three-reactor CLC unit and a BGL gasifier.

Table 4.13: Simulation results for selected flows of the case CLC-Fe3.

Flow no.	Type	Temperature [°C]	Pressure [bar]	Mass flow [kg/s]
1	Coal	15.0	1.0	80.0
2	CO_2	108.5	48.0	7.0
3	Oxygen	132.1	56.0	37.6
4	Air	15.0	1.0	158.6
5	Steam	400.0	40.0	25.4
6	Raw gas	552.0	31.0	129.5
7	Air	615.4	44.0	6.6
8	Syngas	555.1	30.4	129.7
9	H_2, H_2O	647.6	29.0	185.5
10	Depleted air	900.1	22.0	528.5
11	Air	154.2	24.0	573.8
12	Steam	300.0	40.0	260.9
13	CO_2, H_2O	856.6	30.0	250.4
14	CO_2, H_2O	856.6	30.0	250.4
15	CO_2	60.0	28.5	196.6
16	Air	15.0	1.0	537.5
17	Air	432.8	19.2	195.2
18	Combustion gas	1490.0	18.8	909.2
19	Exhaust gas	612.9	1.1	1251.5
20	Steam	590.0	155.0	78.2
21	Steam	590.0	70.0	110.5
22	Condensate	26.7	0.035	149.4
23	Water	22.0	2.0	435.7
24	Exhaust gas	70.7	1.1	1252.0
25	CO_2	45.0	110.0	189.1

4.7 Operation Under Off-Design Conditions

In this section, the equations required to simulate the off-design performance are presented. The characteristics are described by using the following subscripts: 0 = design state, 1 = inlet, 2 = outlet. Correlations regarding heat transfer and pressure loss were also selected to ensure a good mathematical manageability.

From a thermodynamic point of view, modeling the off-design characteristic of a gas turbine system is very challenging as it is a highly complex machine and the control strategy strongly influences the performance. In this work, only the case IGCC-2, using a gas turbine model based on the Siemens SGT5-4000F, is analyzed under off-design conditions. Usually, the control strategy at first considers a constant turbine exhaust temperature, and below a load of 50 % the compressor inlet mass flow rate is kept constant. Another important fact is that the CO emissions significantly

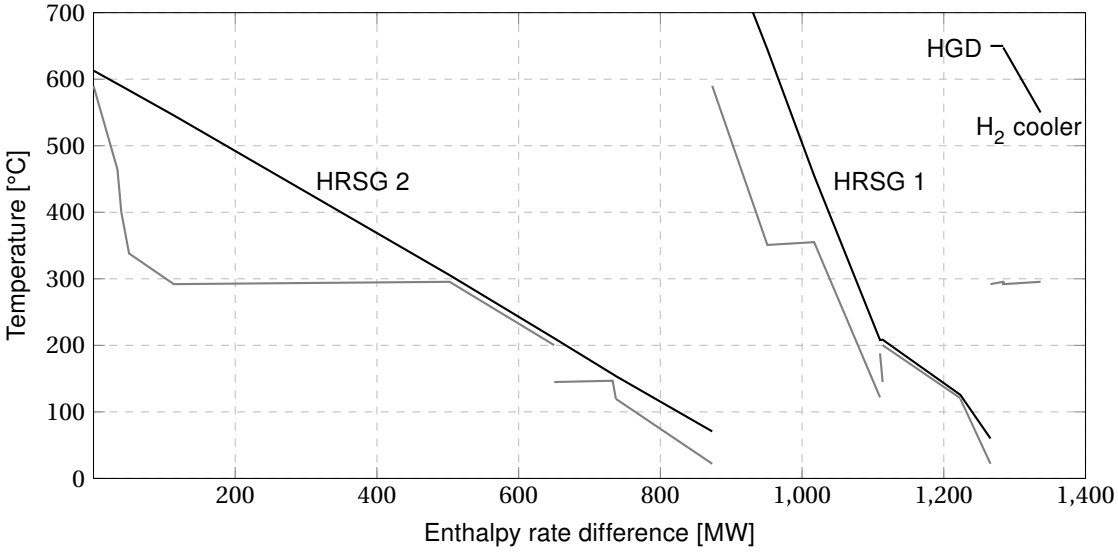

Figure 4.16: Temperature profiles of heat transfer (case CLC-Fe3).

increase below a load of 50 % [156]. A smaller relative load should not be considered. The dependency of the relative efficiency to the relative power is rarely published in literature. In this work, the characteristic of a smaller F-class gas turbine by Siemens, published by Jansen et al. [157], was selected. The characteristic is presented in Fig. 4.17. In the case IGCC-H2, the relative off-design efficiency of the N_2 and H_2 compressor was taken to be 90 %.

In the case when a steam turbine operates under off-design conditions, it acts as an additional throttling unit. This behavior is described by the Stodola law [158], depending on the mass flow rate $\dot{m}$, the inlet and outlet pressure p, as well as the inlet temperature T_1.

$$\left(\frac{\dot{m}}{\dot{m}_0}\right)^2 = \left(\frac{p_1^2 - p_2^2}{p_{1,0}^2 - p_{2,0}^2}\right) \cdot \left(\frac{T_{1,0}}{T_1}\right) \tag{4.5}$$

For the off-design correction of the steam turbines efficiency, several approaches are suitable. In practice, mostly a characteristic polynominal line is used which satisfies a particular fixed design. In general, a physical correlation is preferred. Ray [159] presents an equation which uses the difference in enthalpy at isentropic state change to determine the correction factor for the polytropic efficiency under off-design conditions $\eta_{\mathrm{pol},0}$.

$$\eta_{\mathrm{pol}} = \eta_{\mathrm{pol},0} - 2 \cdot \left(\left(\frac{h_1 - h_{2,s}}{h_{1,0} - h_{2,s,0}}\right)^{0.5} - 1\right)^2 \tag{4.6}$$

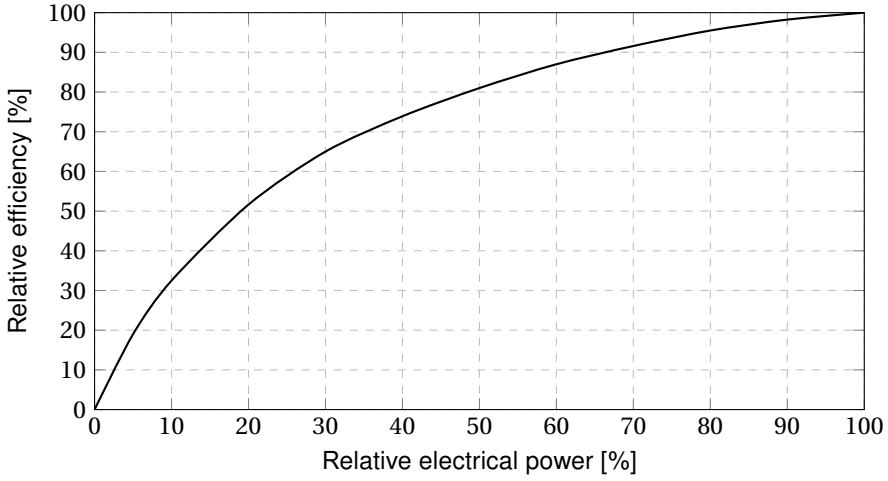

Figure 4.17: Off-design characteristic of the gas turbine used in the case IGCC-2 (acc. to [157]).

Another approach is needed for the correction of heat transfer under off-design conditions. The heat transfer area mostly remains constant and solely the heat transfer coefficient U has to be corrected. In literature, several approaches are presented. The correction is generally based on the Nusselt number as well as Reynolds number, depending on a certain type of heat exchanger . In this work, the heat transfer coefficient is corrected by the mass flow rate $\dot{m}$ and the exponent μ [160]. This exponent is determined by the configuration of the tubes within the HSRG. In this work, a staggered configuration is used in connection with the traverse pitch S_T (distance 90° off from the flow direction between the centers of two adjacent tubes), the longitudinal pitch S_L (the distance in flow direction between the centers of two adjacent tubes) and the tube diameter D.

$$\frac{U}{U_0} = \left(\frac{\dot{m}_\mathrm{gas}}{\dot{m}_\mathrm{gas,0}}\right)^{\mu} \tag{4.7}$$

$$\frac{S_\mathrm{T}}{D} = \frac{S_\mathrm{L}}{D} = 2.5 \Rightarrow \mu \simeq 0.57 \tag{4.8}$$

Within the heat exchanger, the pressure loss of the waterside changes. Several approaches use the Reynolds number to determine the pressure loss. The following correlation solely uses the mass flow rate $\dot{m}$ which is valid for a turbulent flow of a liquid within a plain tube with $5000 < Re < 10^5$ [161]. Other regimes have not been used in this work.

$$\left(\frac{p_2 - p_1}{p_{2,0} - p_{1,0}}\right) = \left(\frac{\dot{m}_1}{\dot{m}_{1,0}}\right)^{\frac{7}{8}} \tag{4.9}$$

As discussed in Section 4.3.1, the use of the Fourrier law or NTU-method to describe the heat transfer arises mathematical convergence problems. This becomes particularly important under off-design conditions.

Chapter 5

Results and Discussion

This chapter presents the results obtained from the thermodynamic and economic analysis introduced in Chapter 3. First, the reference IGCC (case IGCC-1) is analyzed in order to deeply understand the thermodynamic characteristics of the commercially operating IGCC technology. The inefficiencies associated with the gas turbine system using syngas are further analyzed since the gas turbine significantly affects the overall performance. Moreover, a comparison of the results obtained from the simulation of the IGCC plants using a CLC unit is conducted. Finally, the off-design performance and the product costs of the base case IGCC-2 are discussed for adressing a flexible operation mode.

5.1 Inefficiencies of the Reference IGCC

In this section, the energetic characteristics of the base cases are presented and the high-efficiency base case IGCC-1 is further analyzed from a thermodynamic point of view. Base case IGCC-1 is introduced in Section 4.5.1 and case IGCC-2 in Section 4.5.2 accordingly. The fundamentals of the energy and exergy analysis are given in Section 3.1.

The identification of thermodynamic improvement potentials is conducted based on a conventional and advanced exergy analyses. At first, the most important aggregated subsystems are identified rated by their exergy destruction. In the next step, a detailed conventional exergy analysis is undertaken in order to identify the top ten system components. Moreover, these components are analyzed employing the advanced exergy analysis approach for the identification of the subsystem's interdependencies and potential for improvement.

Table 5.1: Power distribution of the reference cases based on $H_{i,ar}$ in [%].

Subsystem	IGCC-1	IGCC-2
Gasification island	-1.0	-1.0
ASU	-2.6	-2.6
AGR unit	-1.7	-1.8
CO_2 compression	-2.9	-3.0
N_2 compression for GT	-	-3.7
Auxiliaries	-0.2	-0.4
Gas turbine (GT)	28.6	30.0
Steam cycle	17.7	14.5
Net power production	37.9	32.1

5.1.1 Energy Analysis

The results obtained from the simulation of both base cases are presented in the following. The resulting power distribution is given in Table 5.1. To ensure a comprehensible view, the values are presented in relation to the thermal input determined by the product of the as-received coal mass flow rate and the as-received lower heating value $H_{i,ar}$. Obviously, the high-efficiency base case exhibits a larger overall efficiency that is about 5.8 %-points higher. From an energetic point of view, the gross power production within the gas turbine system (including the N_2 compression) as well as the steam turbine is worse in case IGCC-2.

Regarding the gasifier efficiency, the cold gas efficiency of the Shell gasifier is 3.4 %-points higher, having an absolute value of 82.4 % based on the lower heating value which is a reasonable value [149, 162]. The resulting live steam parameters are already given in Table 4.5 and 4.8 in Section 4.5. In case IGCC-1, the corresponding parameters are 590 °C and 164 bar as well as 562 °C and 42 bar, compared to 567 °C and 160 bar as well as 551 °C and 47 bar in case IGCC-2. Especially the high-pressure live steam temperature is determined by the flue gas temperature at the gas turbine system outlet which is about 25 °C smaller in case IGCC-2. However, the condensation pressure and the condenser inlet vapor fraction are similar.

In the case IGCC-1, the temperature of the offgas exiting through the stack is calculated to be about 132 °C. Further heat recovery is not possible because a lot of low-temperature heat is already transferred to the steam cycle by the LT-WGS unit cooler. In the case IGCC-2, the offgas temperature is slightly higher.

Table 5.2: Results obtained from the conventional exergy analysis for the aggregated subsystems (case IGCC-1.)

Subsystem	$\dot{E}_D$ [MW]	y_D [%]	$\dot{E}_L$ [MW]
Gasification island	857.1	34.35	26.8
Gas turbine system	446.4	17.70	9.0
Steam cycle	88.1	8.35	126.9
AGR unit	75.9	2.95	0.0
ASU	34.9	1.38	0.5
CO_2 compressor	19.2	0.75	163.6
Total	1521.7	65.47	326.8

5.1.2 Conventional Exergy Analysis IGCC-1

The distribution of exergy destructions among the major subsystems of case IGCC-1 is presented in Table 5.2. The gasification island includes the gasifier, compressors for the gasification agents, coal dryer, quenching and cooling units, particulate removal, WGS reactors, as well as the saturator. However, the steam cycle includes only heat transfer within the HRSG and condenser, several pumps, as well as the steam turbine.

Based on high shares in exergy destruction, a dominant role of the gasification island and the gas turbine system is clearly indicated. Usually, chemical reactions, like the gasification and combustion process, are highly irreversible, and furthermore the gasification island also includes a lot of additional components for preparation. The steam cycle and the AGR unit also show a significant share in exergy destruction.

In order to obtain more detailed information about the components causing thermodynamic inefficiencies, the subsystems are further disaggregated. However, the ASU and the CO_2 compressor are not further discussed. The largest exergy loss is represented by the conditioned CO_2 stream exiting the overall system due to its high absolute chemical exergy. Another large exergy loss is represented by the offgas exiting the HRSG.

Based on a more detailed exergy analysis, the ten components with the highest exergy destruction among all system components are presented in Fig. 5.1. The corresponding absolute values are given in Table 2.1 in the Appendix B. The HRSG is split into its separate heat exchangers. Similar to the initial evaluation, the gasifier and the GT combustion chamber have the highest shares in exergy destruction. Another significant share in exergy destruction is caused by heat transfer within the WGS unit which includes the injection of steam, too. Within the GT turbine, irreversibilities are

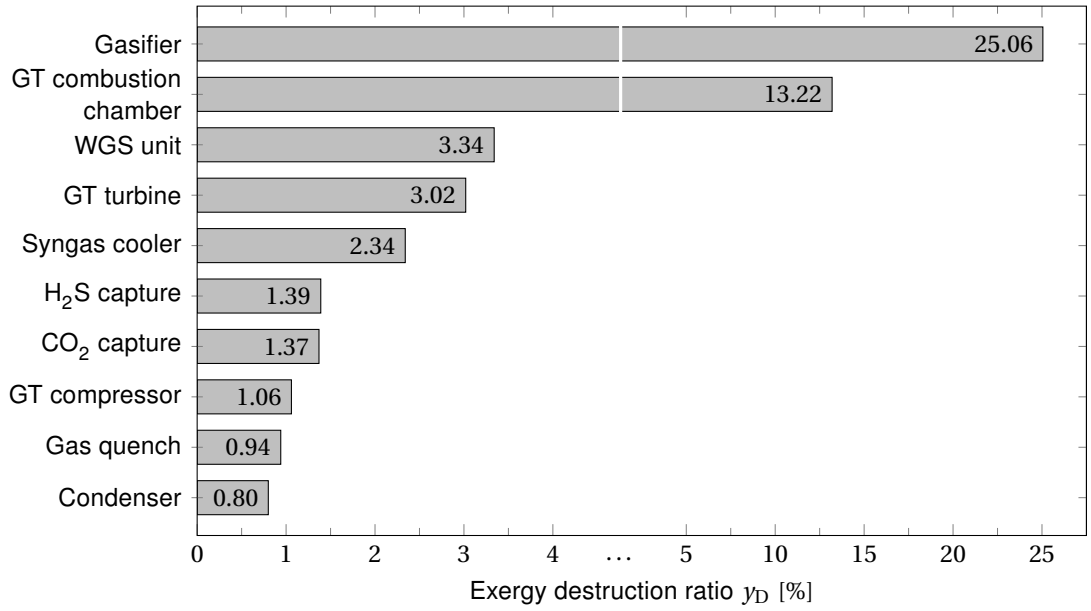

Figure 5.1: Detailed results of the conventional exergy analysis (case IGCC-1).

caused by the mixing of the cooling and sealing air into the main gas stream, blade and vane cooling, as well as surface friction caused by the main gas stream. The syngas cooler has a significant share in exergy destruction due to a large rate of heat transfer and big temperature differences. The H_2S and CO_2 capture cycles are subsystems of the AGR unit and exhibit almost the same share in exergy destruction.

The H_2S capture cycle has a significant demand for electrical power and cooling capacity due to the low absorption temperature. The recycle compressor of the H_2S concentrator requires more specific work compared to one of the recycle solvent pumps. However, the CO_2 capture cycle does not require a compressor but some electric power is needed by the solvent pump. Furthermore, the CO_2 desorption from the rich solvent through a flash process causes a large amount of exergy destruction. The GT compressor is associated with high exergy destruction due to the large amount of air required to dilute the syngas within the GT combustion chamber. The gas quench is calculated to position nine since the temperature difference is in fact about 1260 K, while the gas composition does not change.

Splitting the steam cycle into its components reveals that approximately half of its exergy destruction is caused by the heat transfer within the HRSG. The steam turbine, which generates 38 % of the gross electric power, causes approximately a quarter of this exergy destruction, although the polytropic efficiencies are relatively high representing the current technology status. Another quarter is represented by the

condenser which strongly depends on the ambient temperature and the constraints given by the particular cooling system.

The results obtained from the calculation of the exergetic efficiencies show an interesting characteristic (see Table 2.1 in the Appendix B). Most of the units exhibit a high exergetic efficiency because the case IGCC-1 was designed to be efficient. However, smaller efficiencies of the gasifier and the combustion chamber result from the highly irreversible chemical reactions. The efficiency of the syngas cooler is limited by the minimum temperature differences of the two high and intermediate pressures and the fact that only saturated steam can be produced for economic reasons. For the AGR capture units, the gas quench and the condenser, no attempt was made to define an exergetic efficiency as these units are merely dissipative units.

The results obtained from the conventional analysis suggest that the high exergy destructions within the gasifier, GT combustion chamber, WGS unit, GT turbine, and syngas cooler make them the most important units for further improvement of the overall system.

5.1.3 Advanced Exergy Analysis IGCC-1

A first overview on the inefficiencies of case IGCC-1 was obtained from the conventional exergy analysis. In the next step, an advanced exergy analyses is conducted to provide a deeper understanding of the IGCC technology. Beside others, the results have already been published by the author [163].

Unavoidable and Avoidable Exergy Destruction

The unavoidable exergy destruction is determined by the best parameters under consideration of the current technical and economic constraints. Even though the assumptions made are subjective, general trends can be identified. In this work, a conservative approach was used.

The gasifier was identified to cause the highest share in exergy destruction based on the conventional exergy analysis. The parameters for the unavoidable case consider a temperature decrease of 100 K, induced by a reduced oxygen and steam demand as well as a higher temperature and lower pressure of the gasification agents. In addition, the nitrogen flow entering the gasifier through the lock hopper is slightly reduced.

Within the enhanced combustion chamber of the gas turbine system, the TIT is increased by 200 K, based on a smaller air-fuel equivalence ratio. Moreover, the

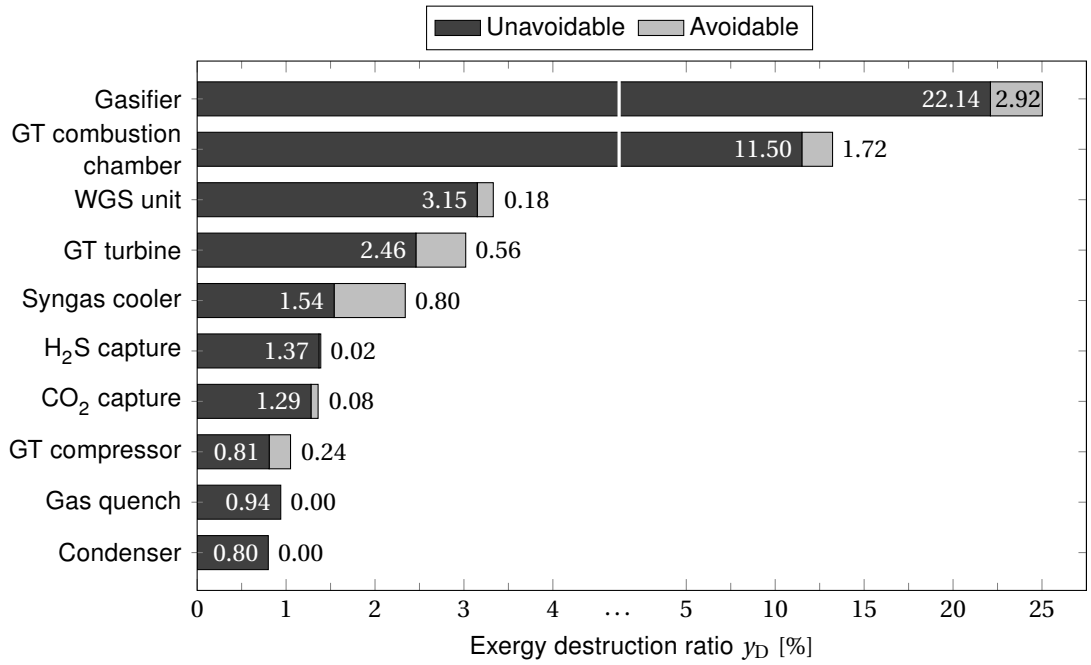

Figure 5.2: Unavoidable and avoidable exergy destruction (case IGCC-1).

radiation heat loss is neglected and the pressure drop is slightly reduced. The WGS unit and the syngas cooler are assumed to produce superheated steam instead of saturated steam. The units produce as much HP steam as possible and the pressure drop is reduced. Furthermore, the minimum temperature difference between the raw gas and water is further reduced and the evaporation pressure of water increases accordingly.

The enhanced gas turbine considers slightly higher isentropic stage efficiencies. In this context, the demand for cooling air is reduced by considerung a constant main gas stream temperature subsequent to the mixing units. It is further assumed that the exhaust temperature remains constant. In case of the enhanced capture cycles, the isentropic efficiencies for compression and expansion increase. Additionally, the pressure drop within the columns is reduced and a smaller temperature difference for cooling is assumed. The air compressor of the enhanced gas turbine system is assumed to operate at higher isentropic stage efficiencies. Finally, for the gas quench and the condenser no changes were taken into account, as these units are subject to technological or external constraints, respectively.

The modifications effect is illustrated in Fig. 5.2 and the corresponding values are given in Table 2.1 in the Appendix B. In general, the amount of avoidable exergy destruction is small and it is apparent that only some components show a considerable avoidable exergy destruction. This applies to the gasifier, gas turbine system, and

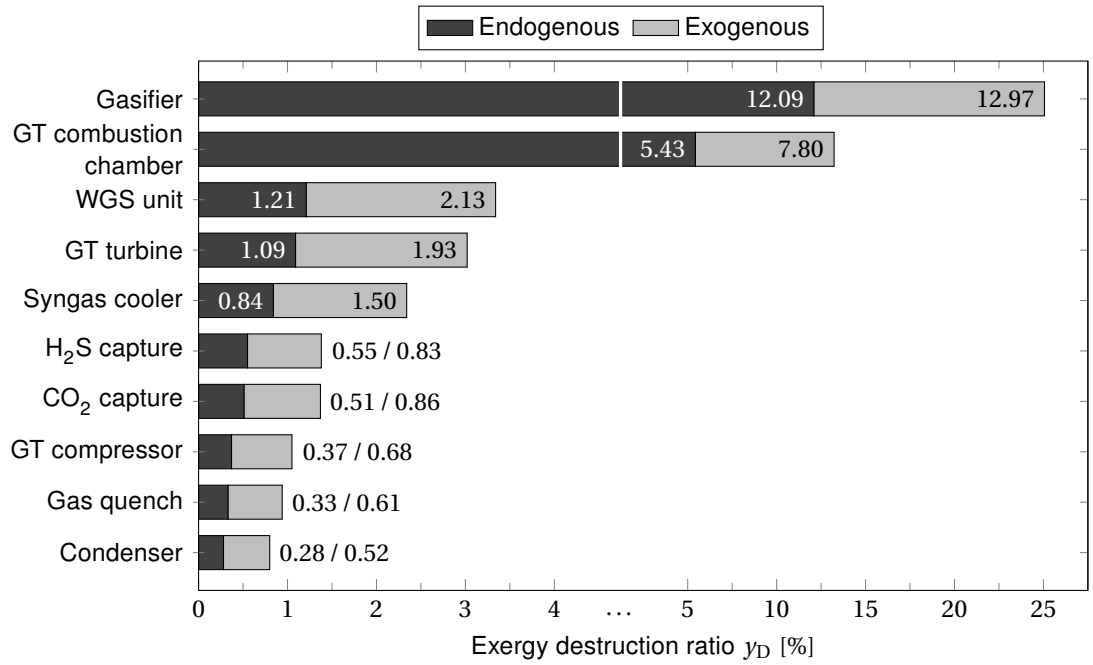

Figure 5.3: Endogenous and exogenous exergy destruction (case IGCC-1).

syngas cooler. However, for the WGS unit, both capture cycles, as well as the gas quench and condenser only a marginal or no potential is identified, respectively.

The largest potentials are available for the GT combustion chamber and the gasifier. Here small improvements in terms of thermodynamic efficiency are sufficient as the absolute exergy destruction is already large. The production of superheated HP steam within the syngas cooler is advantageous over a production within the WGS unit, due to the larger absolute cooling demand of the syngas cooler. The potential of the GT turbine, which is the most complex component for simulation, is calculated to position four. The absolute potential of the GT compressor is almost exhausted. In summary, it is apparent that only some components have a potential for further improvement in the future.

Endogenous and Exogenous Exergy Destruction

The exergy destructions related to the component interactions are plotted in Fig. 5.3 and values are presented in Table 2.1 in the Appendix B. The definitions of the exergetic efficiencies required by the calculation of the endogenous exergy destruction is given in the Appendix B, Eq. 2.1 to 2.12. Generally, the exogenous part of the exergy destruction of all incorporated components is significantly large. This characteristic results from the highly integrated IGCC system design. Moreover, for this set of

Table 5.3: Results of the advanced exergy analysis for gasifier and the GT combustion chamber concerning the interactions on subsystem level in [MW] (case IGCC-1).

		Component k	
	Subsystem r	Gasifier	GT comb. chamber
EN		311.2	139.7
EX		333.7	200.6
total		644.9	340.3
EX	ASU	7.0	2.7
	Gasification island	55.5	119.6
	- only gasifier	–	70.0
	AGR	17.3	6.5
	Gas turbine system	122.0	9.0
	- only comb. chamber	82.9	–
	Steam turbine	4.0	1.5
	HRSG	12.9	4.9
	CO_2 compressor	3.8	1.5
mexo		111.2	54.9

components, the exogenous exergy destructions is always positive, meaning that the improvement of other components decreases the exergy destruction within the component in regard.

The gasifier and the GT combustion chamber exhibit the highest endogenous exergy destruction, due to the highly irreversible chemical reactions that are taking place, and having a endogenous share of 48.3 and 41.1 % on the exergy destruction of the component, respectively. Other components have shares below 40 % which shows a relatively strong dependence on other components.

The H_2S and CO_2 capture cycles have the third and fourth largest endogenous amount. One reason for this is that the separation of pollutants with existing technologies exhibits inherent limitations due to a high energy demand. However, the endogenous amount of the following components is almost the same.

As shown above, the gasifier and GT combustion chamber cause the highest exergy destruction among all system components. Hence, further investigations on the influence of both units on other components are highly interesting. The resulting binary interactions are collected in Table 5.3. Whereby in case the k-th component is part of the subsystem r itself, this component is naturally excluded from the subsystem. In case of the steam cycle, only major subunits, being the HRSG and the steam turbine, were considered.

From Table 5.3 it is apparent that the gasifier and the GT combustion chamber are highly interconnected. Particularly the gasifier strongly influences the combustion chamber (35 % of $\dot{E}_{\mathrm{D}}^{\mathrm{EX}}$) because the GT fuel gas is produced by gasification. Overall, the impact on the component in regard correlates to the ranking of exergy destructions derived from the conventional exergy analysis. In case of the gasifier, a large share of exergy destruction is caused by the other units of the gasification island. On the contrary, the interactions of the GT combustion chamber with the remaining components of the GT system are small.

The high mexogenous part of the gasifier and the GT combustion chamber reveals the generally high interdependencies within the IGCC technology. The mexogenous part of the gasifier and GT combustion chamber is calculated to about one third of the exogenous exergy destruction. Thus, interdependencies between other subsystems or units cause about one third additional exergy destruction to the exogenous amount in both components. In case of the GT combustion chamber, the values are marginally smaller. A descriptive explanation in the case of the gasifier is the larger syngas stream required to compensate the irreversibilities within other subsystems.

The values deriving from this splitting are further useful to compare this IGCC design with other processes that employ the same fuel and product.

Combined Splittings of Exergy Destruction

Based on the combined splittings, the most promising components are identified to determine the priorities in a potential improvement strategy. The avoidable endogenous and exogenous exergy destructions are illustrated in Fig. 5.4 and Table 2.1 in the Appendix B present the corresponding values in detail. The previously derived findings presented above do not change much within this analysis.

Basically, the gasifier and the GT combustion chamber should be improved first, as both components exhibit the highest potential in independent improvements indicated by the relatively large avoidable endogenous exergy destruction. If modifications in the operating range of both components can be practically realized, positive effects on other components likely occur. To a minor extent, the GT turbine and the syngas cooler should be considered for stand-alone improvement attempts, too. Taking into account the constraints identified by the previous analyses, improvements are likely to be realized here. On the contrary, relevant improvements of the WGS unit as well as in the H_2S and CO_2 capture cycles can only be realized if technological modifications are considered.

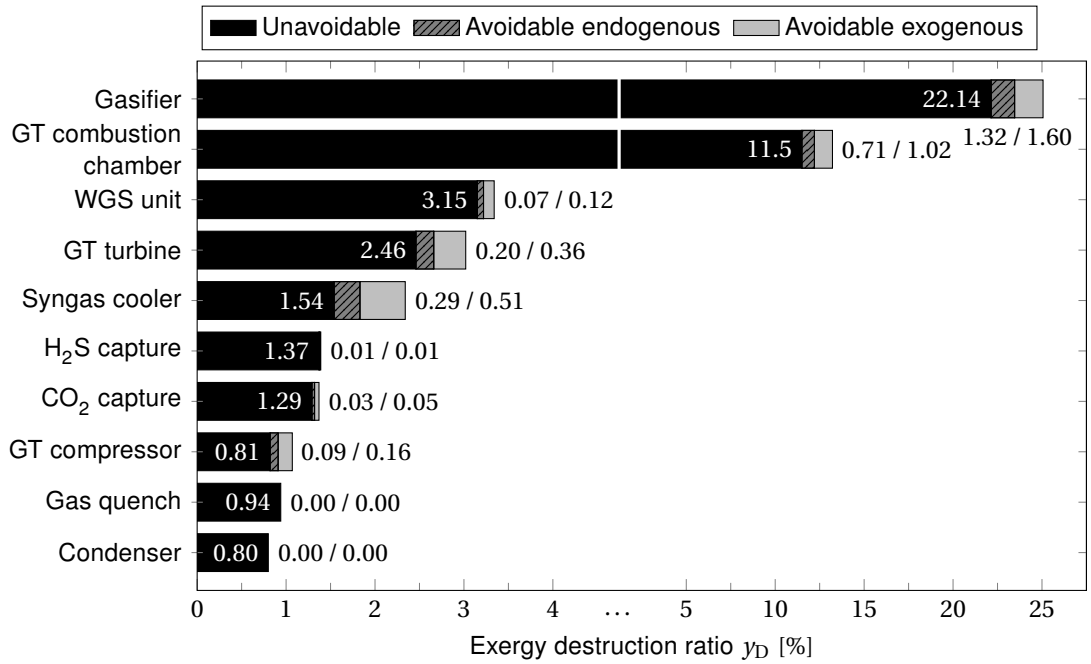

Figure 5.4: Unavoidable, avoidable endogenous and avoidable exogenous exergy destruction (case IGCC-1).

Based on the highly integrated IGCC technology, the suggested modifications have to be examined carefully in order to improve the system's overall efficiency. In general, the large amount of exogenous and mexogenous exergy destruction implies a great potential for improvement if components or subsystems can be replaced by systems featuring a highly efficient technology.

Finally, the results of the advanced exergy analysis are collected and illustrated in Fig. 5.5 for the gasifier and GT combustion chamber, which are the two most important system components. In Fig. 5.5 the area of each splitting of exergy destruction is scaled to one common standard.

5.2 Inefficiencies of the Gas Turbine System

In this section, the results obtained from the simulation of a gas turbine, using the model presented in Section 4.4.2, as well as conditions taken from case IGCC-1 are discussed. Twelve processes are incorporated that are associated with characteristic inefficiencies in a heavy-duty gas turbine system. The impact of each inefficiency is rated by a conventional exergy analysis, which is introduced in Section 3.1. The assessment is based on exergy destruction ratios of the components, respectively. Each value is given in the Appendix B. The exergy loss of the overall system is represented

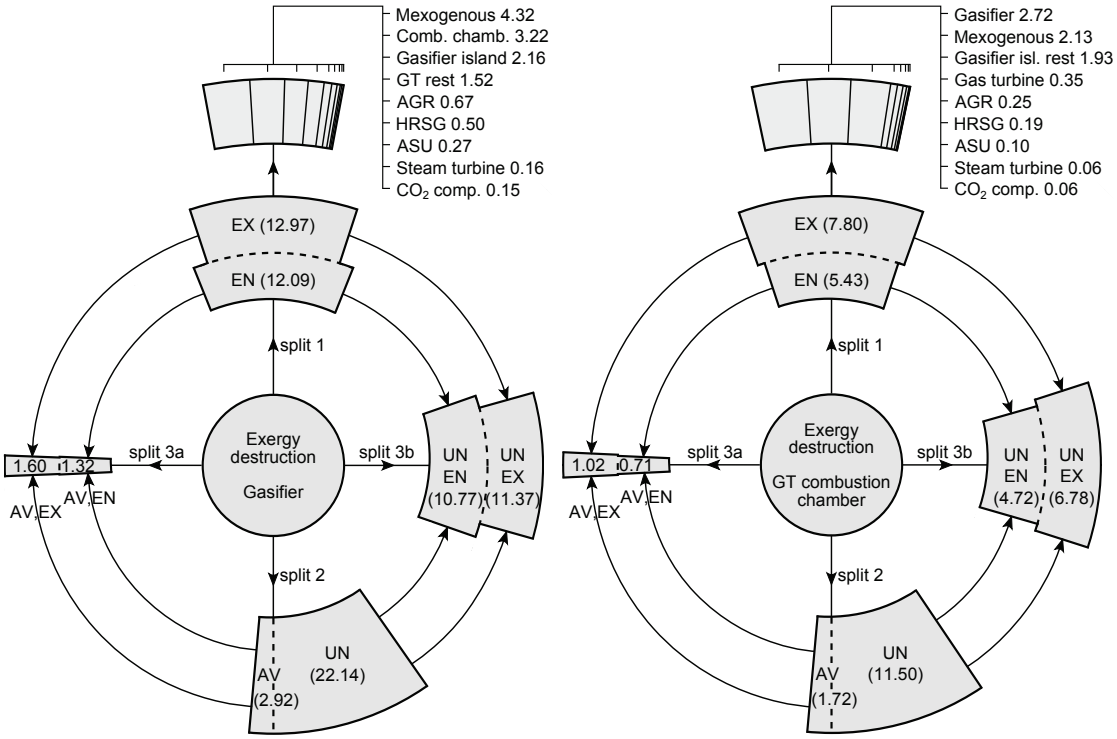

Figure 5.5: Results of the advanced exergy analysis for the gasifier and GT combustion chamber presented by the exergy destruction ratio y_D in [%] (case IGCC-1).

by the exhaust gas which is not discussed further. Among others, the results of an analysis performed on a gas turbine system running on natural gas were published by the author [164, 165].

The resulting hierarchy of inefficiencies divided by the system components is illustrated in Fig. 5.6. Apparently, the largest exergy destruction is associated with the stoichiometric combustion since chemical reactions are highly irreversible. This exergy destruction only depends on the composition of fuel gas and oxidant. The compilation of expansion and mixing at different temperatures and pressures is calculated to the second position. Based on the developed model, it is not possible to subdivide these inefficiencies because the real expansion is determined by the reaction level of the stages, respectively. In this work, the results claim to be valid for a universal gas turbine system without setting the reaction level. Usually, the reaction level depends on the particular way the design was manufactured, as the secondary air system is affected, too. Using the isentropic efficiency as a surrogate model does not acceptably satisfy this real behavior. However, the energetic analysis is not affected when using isentropic efficiencies.

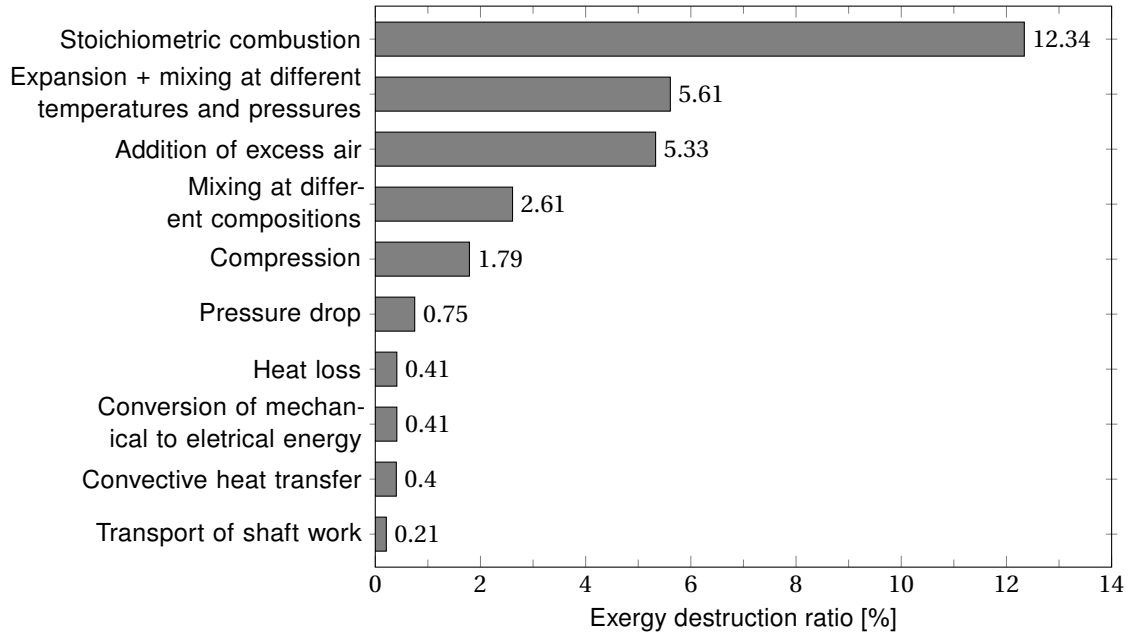

Figure 5.6: Hierarchy of inefficiencies ordered by their exergy destruction (case IGCC-1).

The addition of excess air is calculated to the third position, due to a temperature drop of about 746 °C. The corresponding exergy destruction is determined by the thermal resistance of the first stage vane material as well as the cooling design. The mixing at different compositions was calculated to the next position, resulting from the composition of the fuel gas and oxidant as well as the mass flow rates of the mixed fluids. Only using enhanced TBC materials is useful for further improvements as the cooling demand decreases. The inefficiency associated with compression (1.8 %) is in the fifth position of importance, whereas the exergy destruction caused by pressure drop from fluid transport only has a small share. In this work, the pressure drop caused by fluid transport is generated by surface friction within the combustor and vanes.

The inefficiencies associated with heat loss, conversion of mechanical to eletric energy, and convective heat transfer within the vanes and blades are rated to almost have the same small share in exergy destruction. The major cooling part is provided by the film layer which reduces the exergy destruction associated with convective heat transfer. The potential of applying hybrid steam cooling seems to be relatively low, in the case when the absolute convective heat remains constant and a film layer is still used. Compared to others, the effect of shaft work transport can be neglected. The overall exergetic efficiency results to 40.8 %.

Figure 5.7 presents the distribution of some inefficiencies within the combustion chamber and gas turbine. The largest exergy destruction is caused by mixing fuel

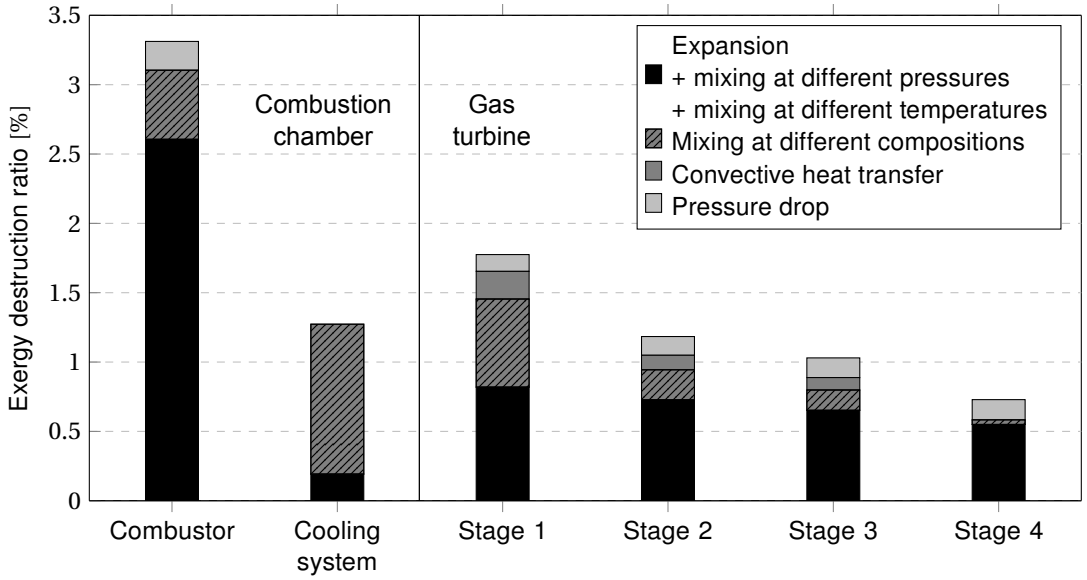

Figure 5.7: Exergy destruction of some inefficiencies within the combustion chamber and gas turbine (case IGCC-1).

gas and stoichiometric air within the combustor at different temperatures and pressures. Although the fuel gas is heated by hot water within a saturator, the temperature difference between the mixed flows is about 288 °C. In general, further preheating improves the exergetic efficiency of the combustion process because the amount of fuel decreases when a constant combustion outlet temperature is considered. The autoignition temperature of H_2 is well above the fuel gas temperature. As presented in Fig. 5.6, the combustion gas temperature is significantly reduced when adding excess air which causes high exergy destruction. Subsequently, the cooling air of the combustion chamber is mixed into the main combustion gas. In this process, the major amount of exergy destruction is associated with a mixing at different compositions because the temperature difference accounts to only 124 °C, compared to 746 °C involved by the addition of excess air.

Within a single gas turbine stage, the exergy destruction has a relatively small share. Towards lower pressures, the effect of mixing at different compositions decreases because the combustion gas composition approaches the composition of air. This slightly corresponds with the behavior of the group of expansion and mixing at different pressures and temperatures as the temperature difference of the mixed gases decreases towards lower pressures. Since the effect of friction increases towards lower temperatures, the exergy destruction associated with a pressure drop caused by fluid transfer through the vanes increases within the low-pressure stages.

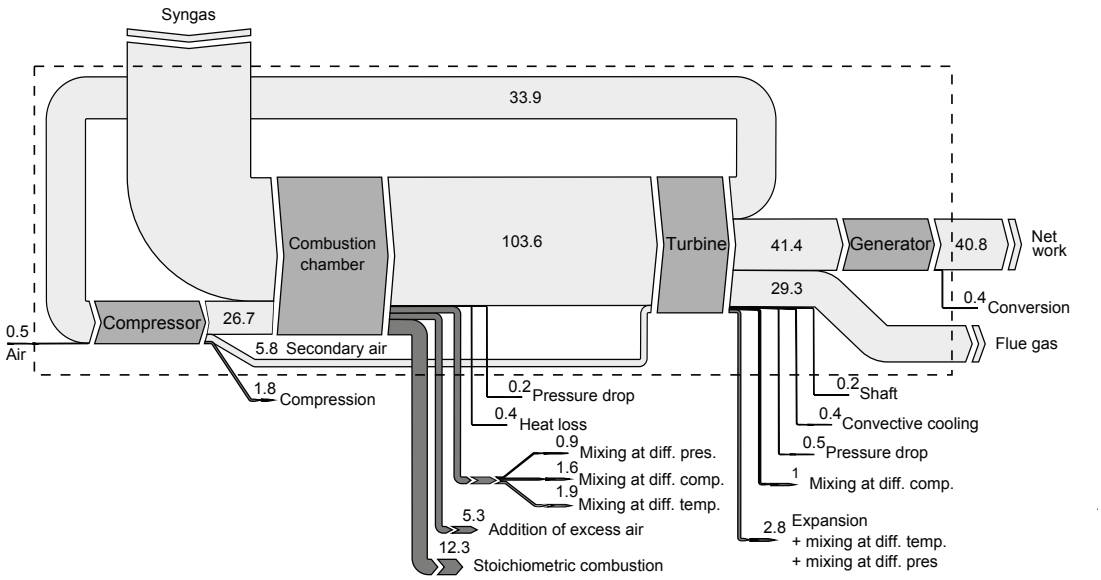

Figure 5.8: Exergy flow diagram of the gas turbine system running on syngas (case IGCC-1).

Improvements can be realized by (a) optimizing the vane and blade shape which improves the isentropic efficiency and pressure drop of the vane, (b) reducing the convective heat transfer within the vanes and blades by using enhanced TBC materials, and (c) improving the extraction points position of the compressor in order to reduce the pressure difference of the mixing agents as well as compression work. An overview of the overall gas turbine system is given in the exergy flow diagram presented in Fig 5.8. Compared to this detailed model, the exergy destruction shifts from the gas turbine to the combustion chamber when applying the three-component model according to ISO conditions.

A comparison with other conventional exergy analysis considering cooling flows and separate turbine stages is not satisfiable. Generally, other studies use natural gas for combustion. The results presented by El-Masri [67] are based on a lower firing temperature as well as a lower pressure ratio of the compressor (127 7°C/14 compared to 1490 °C/19.2), and the final conclusions are not presented in detail. Staudacher and Zeller [69] calculated the so-called *irreversible combustion*, *nozzle heat* and *chemical losses* to share the largest amount of exergy destruction of an aircraft engine. A comparison is not possible because the underlying assumptions are not presented.

An advanced exergy analysis for a gas turbine system running on natural gas was performed by the author of this work and Tsatsaronis et al. [166, 167]. Splitting the exergy destruction into an avoidable and an unavoidable part, reveals that about 95 %

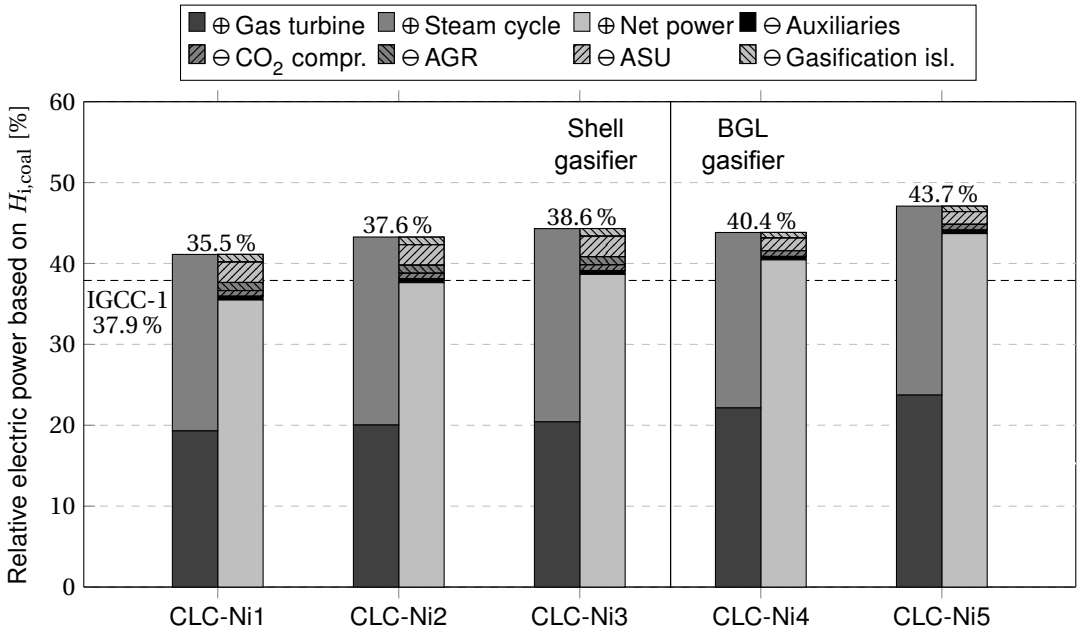

Figure 5.9: Power distribution and overall net efficiency of the analyzed cases using a two-reactor CLC system.

of the exergy destruction associated with combustion and about 76 % of the exergy destruction associated with mixing are unavoidable.

5.3 Improvement of the Overall Net Efficiency

The modeling and assumptions of the IGCC plant using a CLC unit is presented in Section 4.6 and the case declarations are introduced in Section 4.1. In this section, characteristic parameters and results are discussed. The exergetic evaluation then follows in Section 5.3.3.

5.3.1 IGCC Using a Two-Reactor CLC Unit

The resulting power distribution as well as the overall net efficiency is given in Fig. 5.9 and Table 5.4 shows the resulting key parameters. The final overall net efficiency varies from 35.5 to 43.7 % (based on $H_{i,ar}$). From the diagram it is evident that only some of the analyzed cases have a higher efficiency than the reference case IGCC-1. In case of using a Shell gasifier similar to the reference case, an air reactor temperature above 1200 °C is necessary to outperform the reference case. Changing the air reactor temperature from 1100 to 1200 °C (case CLC-Ni1 to CLC-Ni2) increases the overall efficiency to a greater extend than from 1200 to 1300 °C (case CLC-Ni2 to CLC-Ni3).

Table 5.4: Selected results of the analyzed cases using a two-reactor CLC system.

Case CLC-...		Ni1	Ni2	Ni3	Ni4	Ni5
H_i syngas to CLC	MJ/kg	12.8	12.8	12.8	15.0	15.0
Air reactor conversion efficiency	%	98.6	98.3	98.1	98.3	98.1
Gas turbine exhaust temperature	°C	458	535	594	417	476
Fuel reactor mole ratio NiO/syngas	%	91	91	91	110	110
Fuel reactor exit temperature	°C	1068	1129	1191	1095	1158
HP live steam pressure	bar	136	136	130	140	137
IP live steam pressure	bar	60	54.7	51	60	74
LP live steam pressure	bar	1.9	1.9	1.9	2.8	1.9
HP live steam temperature	°C	590	590	590	590	590
IP live steam temperature	°C	470	480	480	590	590
LP live steam temperature	°C	278.6	261.1	226.7	310.7	240.1
Ratio IP/LP steam production	-	2.7	4.1	5.5	2.6	4.5
Exit temperature offgas HRSG 1	°C	131.4	131.4	131.5	141.4	130.5

This behavior results from the increasing IP live steam temperature from case CLC-Ni1 to CLC-Ni2 (see Table 5.4). In general, when varying the air reactor temperature, the internal consumption of the overall plant remains almost constant. However, the conversion efficiency of the fuel reactor slightly decreases and also the mass flow rate of the gas turbine decreases due to a reduced cooling demand of the air reactor at higher temperatures. Contrawise, the turbine inlet temperature simultaneously increases, having a stronger effect on the overall efficiency. Moreover, the gas turbine and fuel reactor exit temperature increases which causes a shift from the LP to the IP steam production at the underlying conditions.

The cases featuring a BGL gasifier outperform the cases featuring a Shell gasifier. Firstly, the internal consumption by the gasifier island, ASU and AGR unit are smaller compared to cases using the Shell gasifier. Similar to the discussion above, an increasing air reactor temperature positively affects the overall efficiency. However, this effect is even stronger when the air reactor temperature is being raised from 1000 to 1100 °C, then the efficiency increases by about 3 %-points.

Generally, the air reactor temperature is limited upwards and downwards. The upper limit is determined by the temperature within the CLC reactors and the HRSG entry at the hot side due to material costs. Otherwise, the lower limit is determined by several issues. This could be the exit temperature of HRSG 1 resulting from the constrains of the integrated heat management. In order to satisfy the condensation of water from the mixture of CO_2 and H_2O, indirect external cooling could be necessary causing additional costs. Another limiting issue might be the vapor fraction at the

steam turbine outlet which is influenced by the design and constrains of the heat management system.

Moreover, different options regarding the design of the CLC system are possible. One option is represented by an atmospheric operation of the air reactor. Thus, an air compressor is not needed and the hot depleted air can be fed directly to the HRSG for steam production. However, from a thermodynamic point of view the bottoming steam cycle affects the overall efficiency less, when compared to the case in which a topping Joule cycle is included. Furthermore, ensuring good sealing conditions among the high-pressure fuel reactor and the atmospheric air reactor may cause technical barriers that have to be overcome.

Another option is represented by applying an intercooled air compressor. This reduces the air reactor size as the cooling air inlet temperature drops and therefore the cooling air mass flow rate can be reduced. On the contrary, the mass flow rate of the Joule cycle simultaneously decreases disproportionately too, which consequently affects the overall efficiency negatively. In this work, the air reactor pressure is determined by the desired inlet pressure of the GT combustion chamber which is favorable over the other options presented above.

In comparison to other studies using a two-reactor CLC system introduced in Section 2.4, the overall efficiencies obtained from this work result in higher values in all analyzed cases. Cormos [28] as well as Rezvani [27] analyzed IGCC plants using a Shell gasifier and a gas quench using the same air reactor temperature range. In this work, results from simulations that also feature both components showed slightly higher efficiencies. Furthermore, the results obtained from this work analysis outperform the IGCC featuring a dual-stage CLC unit analyzed by Rezvani, too. Applying a BGL gasifier in combination with an HGCU significantly outperforms all other cases analyzed in this work as well as other convenient literature data.

5.3.2 IGCC Using a Three-Reactor CLC Unit

The dimensionless subsystem performance as well as the overall efficiency of the five analyzed cases is given in Fig. 5.10 and Table 5.5 shows the resulting key parameters. The resulting overall net efficiency varies from 36.9 to 41.4 % (based on $H_{\mathrm{i,ar}}$), which are higher than the reference case IGCC-1 in almost every case. In general, cases featuring a BGL gasifier outperform the cases featuring a Shell gasifier by about 3 %-points at the same air reactor temperature. Through the comparison of cases CLC-Fe3

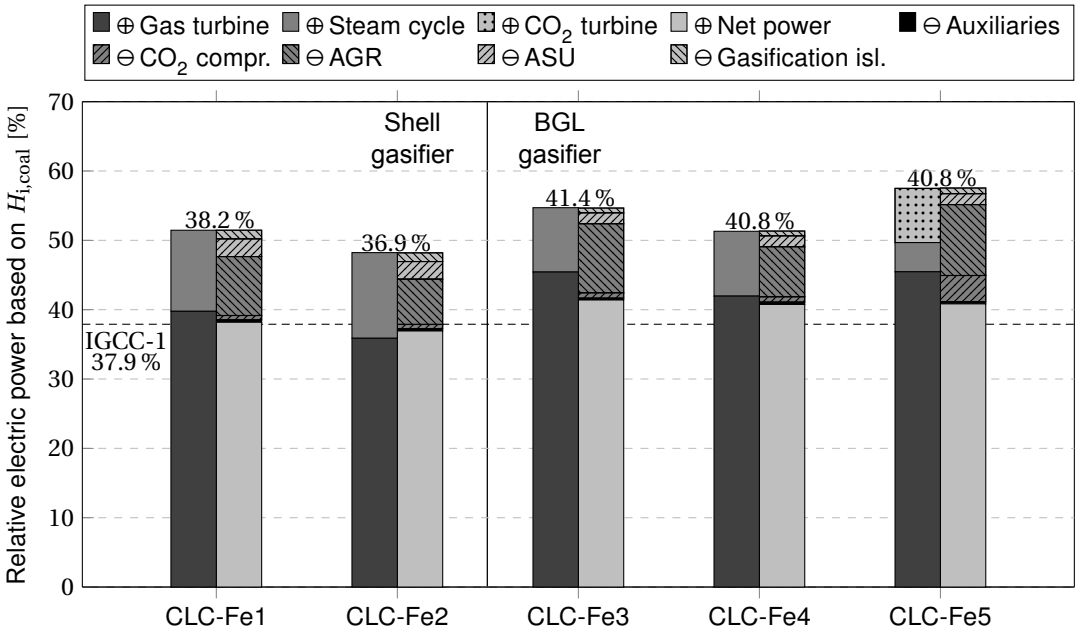

Figure 5.10: Power distribution and overall net efficiency of the analyzed cases using a three-reactor CLC design.

and CLC-Fe5, the application of a CO_2 turbine is not recommended as the efficiency drops by about 0.6 %-points.

Furthermore, an increasing air reactor temperature negatively effects the overall net efficiency which shows an opposing trend compared to the cases using a two-reactor CLC design. This results from the lower reduction state of the oxygen carrier exiting the fuel reactor at higher temperatures, represented by the ratio of Fe_3O_4 to FeO presented in Table 5.5. Within the subsequent steam reactor, the absolute production of ultra-wet hydrogen decreases. The absence of steam fed to the combustion chamber of the gas turbine causes additional compression of air to ensure a constant combustor outlet temperature. Thus, the power consumption of the air compressor increases and the TIT_{ISO} (according to ISO 2314) decreases. Moreover, at higher air reactor temperatures also the fuel reactor exit gas temperature increases which favors the production of HP steam instead of IP steam, and additionally the HP level increases (see Table 5.5). The fuel reactor conversion efficiency is constantly high at 99.9 % due to the multi-stage moving-bed reactor design.

In general, the internal consumption of the cases in which a BGL gasifier is used change, compared to the cases using a Shell gasifier. The electric power demand of the ASU is reduced due to the smaller oxygen demand for gasification. However, the consumption of the CLC system rises because more oxygen carrier is needed,

Table 5.5: Selected results of the analysed cases using a three-reactor CLC system.

Case CLC-...		Fe1	Fe2	Fe3	Fe4	Fe5
H_i syngas to CLC	MJ/kg	12.76	12.76	15.02	15.02	15.02
H_i syngas to GT	MJ/kg	4.95	4.47	6.14	5.34	6.12
TIT_{ISO} gas turbine	°C	1400	1441	1201	1229	1192
Fuel reactor mole ratio Fe_2O_3/syngas	%	96	108	125	126	128
Fuel reactor mole ratio Fe_3O_4/FeO	%	0.00	0.02	0.03	0.33	1.24
Fuel reactor gas exit temperature	°C	796	998	857	998	420
Steam reactor H2 mole fraction	%	39.4	25.7	32.5	29.4	32.5
HP live steam pressure	bar	170	130	155	145.4	185
IP live steam pressure	bar	45	45	70	77	117
LP live steam pressure	bar	1.83	3	4.1	4	1.9
HP live steam temperature	°C	590	590	590	590	590
IP live steam temperature	°C	590	590	590	590	590
LP live steam temperature	°C	174.4	163.5	188	207.3	280.3
Ratio IP/HP steam production	-	2.6	2.2	3.5	3.2	9.0
Exit temperature offgas HRSG 2	°C	99.6	92.7	70.7	67.1	95.2

to ensure a total conversion of the fuel gas within the fuel reactor (see Table 5.5). Thus, the demand for pressurized cooling air within the air reactor increases. Another advantage of the cases using a BGL gasifier is represented by a less complex design which is favorable for operation.

The simulation results of case CLC-Fe3 as well as CLC-Fe5 show that the application of a CO_2 turbine is not advantageous. On the one hand, only 48 % of the electric power generated by the CO_2 turbine is additionally needed for the recompression of CO_2 to meet the transport condition. On the other hand, the steam turbine output is disproportionately reduced.

Similar to the discussion presented for the two-reactor CLC system, the upper limit of the air reactor temperature is determined by the costs of the fuel reactor and HRSG materials. For the cases analyzed in this section, the utilization of common carbon steel is suitable. With increasing hydrogen content of the syngas generated by gasification, the production of solid particles switches from FeO to Fe_3O_4 which negatively affects the production of hydrogen within the subsequent steam reactor.

In comparison to other studies using a three-reactor CLC system introduced in Section 2.4, the results obtained in this work seem to be more realistic. The study performed by Fan [30] showed a much higher overall efficiency but this result derives from a very rough simulation without considering auxiliaries. Compared to the results presented by Cormos [28, 29], the IGCC plant using a three-reactor CLC unit

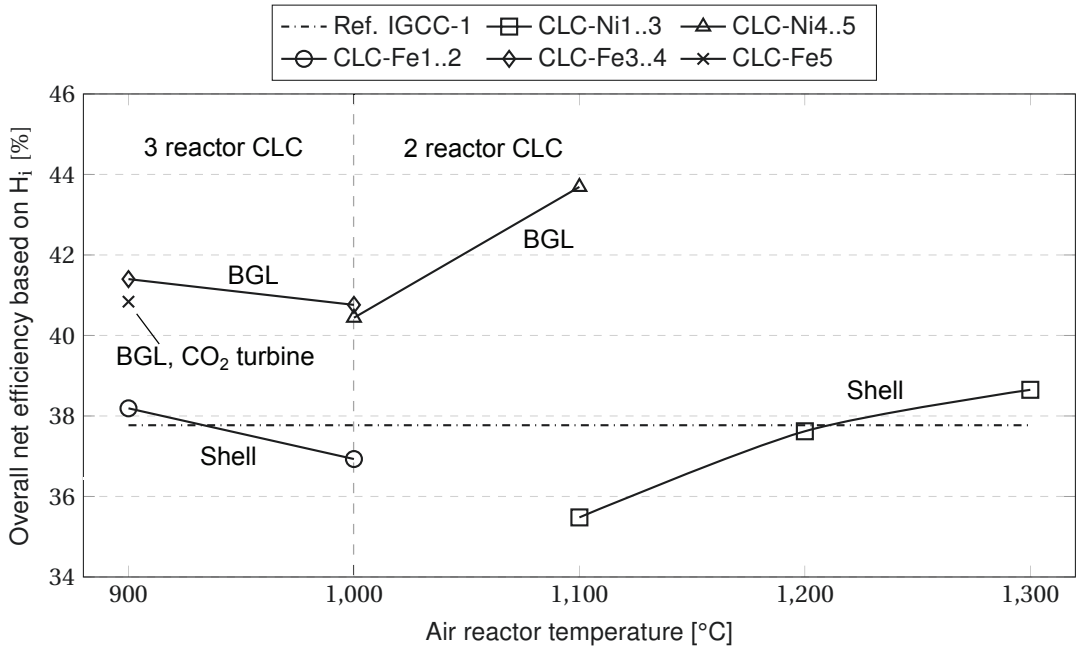

Figure 5.11: Overall net efficiencies of the analyzed cases.

outperforms a CLC system featuring only a fuel and a steam reactor. The air reactor temperature was about 920 °C, which corresponds to the best cases analyzed in this work. Additionally, only in this work a HGD unit, a state-of-the-art gas turbine, and an optimization algorithm was used.

5.3.3 Comparison of the Analyzed Cases

The comparison of the analyzed cases is carried out mainly based on the results obtained from the exergy analysis. The detailed discussion of the base case IGCC-1 is presented in Section 5.1 and the exergy destruction ratios of the underlying cases are given in Table 2.3 in the Appendix B. Information about characteristic parameters are presented above in Section 5.3.1 and 5.3.2.

The collection of the overall net efficiencies is presented in Fig. 5.11 as a function of the air reactor temperature. The general trend shows higher efficiencies for the IGCC plant using a BGL gasifier of up to 5.8 %-points when using a two-reactor CLC system. Considering an advantage of 2.5 %-points in case of using an HGCU [44], the potential in efficiency results to about 3.3 %-points. In case of practical problems concerning the operation of the HGCU, the cases using a Shell gasifier show merely slightly higher overall efficiencies only for air reactor temperatures above 1200 °C.

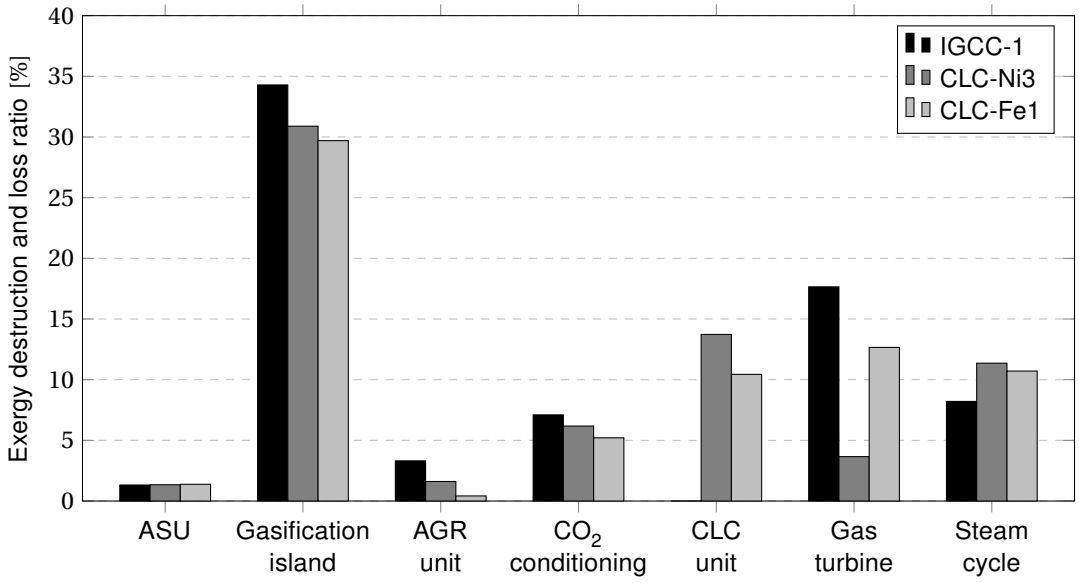

Figure 5.12: Exergy destruction and loss ratios at the subsystem level of selected cases.

In the following, a comparison based on the exergy analysis is presented. For a better understanding of the changes generated by the integration of a CLC unit, only cases using the same type of gasifier are compared. In comparison to the base case IGCC-1, the most efficient cases using a Shell gasifier (CLC-Ni3, CLC-Fe1) are considered. Simulation results for selected flows are presented in the modeling Section 4.6.

Regarding the exergy destruction and exergy loss of the major subsystems presented in Fig. 5.12, a shift can be observed although the overall efficiency only marginally changes when a CLC unit is used. Generally, the irreversibilities of the reference case shift from the syngas production and gas turbine system to the CLC unit and steam cycle. The ASU provides almost the same amount of oxygen and nitrogen in all cases, and therefore the exergy destruction remains almost constant.

The exergy destruction associated with the gasification island is mainly smaller in the cases using a CLC unit, due to the absence of a WGS unit. Replacing the N_2 stream that transports the coal particles into the gasifier by recycled CO_2 does not significantly influence the exergy destruction. The exergy destruction associated with the syngas cooler strongly depends on the evaporation temperature on the cold side. In the case CLC-Ni3, the amount of HP steam production results in the smallest which generates the largest exergy destruction.

In the reference case IGCC-1, the raw syngas is cleaned by physical absorption for capturing CO_2 and H_2S in the AGR unit. When using CLC, CO_2 is captured inherently

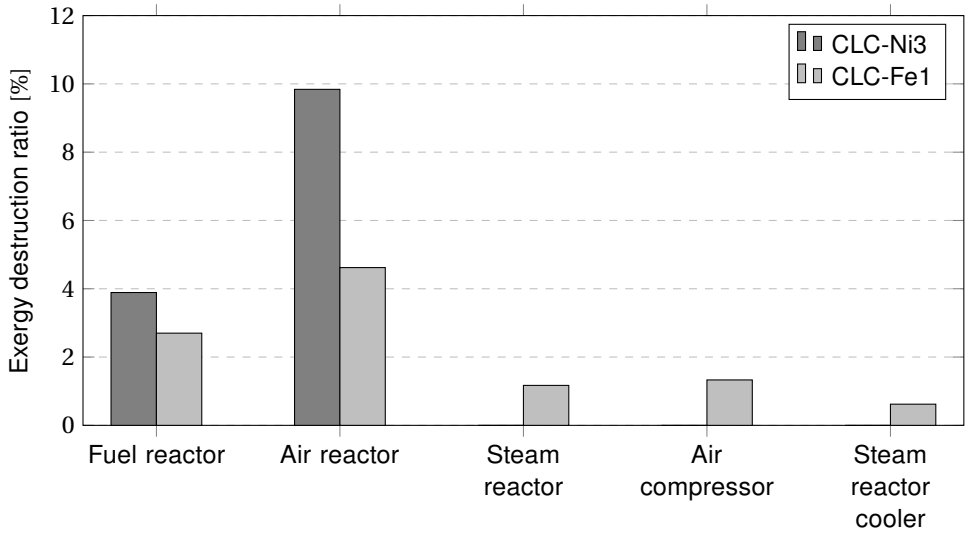

Figure 5.13: Exergy destruction ratios within the CLC unit of case CLC-Ni3 and CLC-Fe1.

and only H_2S must be captured separately. This reduces the exergy destruction by more than 50 % when physical absorption is still applied for H_2S removal. Using an HGCU further reduces the irreversibilities of the H_2S capture by about 70 %. The CO_2 conditioning unit includes exergy destruction caused by the compression and cooling of CO_2 to meet the transport conditions as well as the exergy loss associated with the exiting stream. Here it is advantageous for the cases using CLC unit that the inlet pressure determined by the gasification process and additional pressure losses is higher compared to the pressure of the base case. In the base case, the inlet pressure varies depending on the flash stage of the Selexol® process, respectively.

In case of the CLC unit, the total exergy destruction of case CLC-Ni3 is higher, even though the reactor temperatures are higher and the system includes less components. The distribution of the exergy destruction among the components of the CLC unit is illustrated in Fig. 5.13. In general, the air reactor generates more exergy destruction because it has a highly exothermic characteristic and the outlet temperature is determined by a large amount of excess air. However, the design of the fuel reactor is determined by the fuel conversion. In the case CLC-Fe1, the reduced oxygen carriers are partially oxidized within the steam reactor which leads to a reduction of the exergy destruction in the air reactor. Moreover, the cooling demand of the air reactor is reduced because the temperature difference of the oxygen carriers passing the air reactor is about three times higher compared to the case CLC-Ni3. In the case CLC-Ni3, the exergy destruction of the steam reactor and the air compressor are calculated to share almost the same amount.

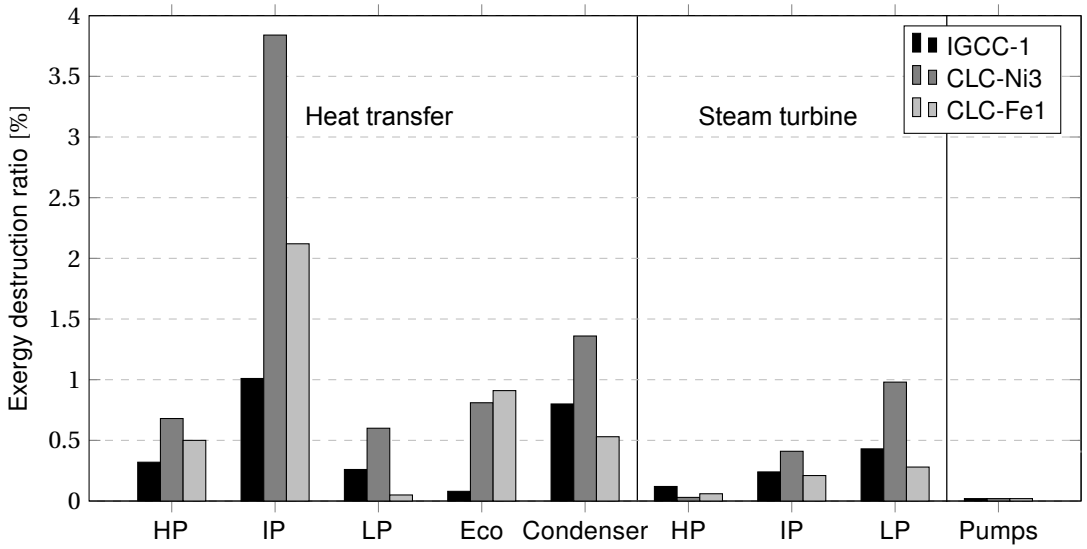

Figure 5.14: Exergy destruction ratios of the steam cycle (case IGCC-1, CLC-Ni3 and CLC-Fe1).

In comparison of the case CLC-Fe1 to the base case IGCC-1, the exergy destruction associated with the gas turbine system decreases due to the different fuel gas composition. In the case CLC-Fe1, pressurized steam enters the combustion chamber which substitutes excess air to some extend used to dilute the combustion gas. The depleted air produced by the air reactor also replaces the pressurized air provided by the air compressor. The difference in composition is marginal but the temperature is much higher (900 °C instead of 433 °C) which has a positive effect on the joule cylce efficiency. Moreover, the efficiency of the combustion process increases due to the higher fuel gas temperature (550 °C instead of 145 °C). Considering the case CLC-Ni3, the CLC unit completely replaces the GT combustion chamber. On that account, the exergy destruction of the gas turbine system decreases by far significantly because the combustion process generates the largest amount of irreversibilities. In comparison of the CLC unit and the conventional combustion chamber, it is interesting that the exergy destruction of the CLC unit is slightly higher. However, the gross generation of electricity by the steam turbine increases significantly because the product stream of the fuel reactor is further used to generate steam. In the reference case, the mass flow rate passing through the turbine is larger compared to the mass flow rate of the air compressor. This relation switches in the case CLC-Ni3 because the pressurized air gets depleted and the product of the combustion process enters the HRSG 1 directly without passing the turbine. Both effects decrease the exergy destruction of the GT turbine.

Taking the steam cycle into consideration, the exergy destruction of the cases, including a CLC unit, increases. A detailed overview is given in Fig. 5.14. The heat transfer within the HRSGs significantly increases by about 57 % in the case CLC-Ni3 and by 45% in the case CLC-Fe1. However, the enthalpy rate difference associated with the overall heat transfer only marginally increases due to the absence of a WGS unit in the cases using CLC.

Another important factor is represented by the average temperature difference between the hot and cold side. For the cases using CLC, this difference increases mainly based on IP evaporation. In the case CLC-Fe1, a large demand of IP steam is required by the steam reactor. In the case CLC-Ni3, the production of IP steam is preferred over the HP production carried out by mathematical optimization. In comparison of both cases in which CLC is used, a larger part of the evaporation takes place outside of the HRSG in the case CLC-Fe1 which decreases the exergy destruction associated with the IP and HP section within the HRSGs (see Fig. 5.14).

The exergy destruction of the economizer, which preheats the feedwater, is very small in the base case compared to the others because the large low-temperature cooling demand by the LT-WGS unit has to be satisfied by the lowest temperatures within the steam cycle.

With respect to the steam turbine, the different mass flow rates and pressure ratios cause different exergy destructions. The HP steam turbine was identified to have no significant impact. In the case CLC-Ni3, the exergy destruction of the IP and LP steam turbine is larger, due to larger mass flow rates. Moreover, the pressure ratio is shifted from the IP to the LP steam turbine which additionally raises the exergy destruction within the LP steam turbine. The exergy destruction associated with the condenser directly corresponds to the circulating mass flow rate as the inlet steam quality remains almost constant in the underlying cases.

5.4 Operation with High Electricity Price Volatility

5.4.1 Flexible Operation of the Reference IGCC

In this section, the thermodynamic results of the base case IGCC-2, introduced in Section 4.5.2, operating under off-design conditions, are discussed. The results of the steam cycle are identical for both of the off-design cases IGCC-H2 and IGCC-H2i. Only the electric power of the gas turbine varies. Further results from the economic analysis are presented below in Section 5.4.2. The application of a syngas storage is not part of

Table 5.6: Power distribution of the IGCC plant using a GEE gasifier based on $H_{i,ar}$ in [%].

Subsystem	IGCC-2	IGCC-H2i	IGCC-H2
Gasification island	-1.0	-1.0	-1.0
ASU	-2.6	-2.6	-2.6
AGR unit	-1.8	-1.8	-1.8
CO_2 compressor	-3.0	-3.0	-3.0
N_2 compressor for GT	-3.7	0.0	-1.4
H_2 compressor	0.0	-0.7	-0.5
Auxiliaries	-0.4	-0.3	-0.3
Gas turbine (GT)	30.0	0.0	9.8
Steam cycle	14.5	0.6	0.6
Net power production	32.1	-8.7	0.0

this work. Compared to the analysis presented in this work, the capital costs further increase and suitable economic advantages strongly depend on the peak and average electricity prices. Moreover, the commercial-ready storage options feature a poor H_2 density.

The simulation of the HRSG operating under off-design conditions involves several challenges. A realistic characteristic can be obtained only when the control strategy is clearly indicated. In this work, the HRSG is bypassed by the gas turbine flue gas in order to ensure a fast load-change ability. In the case IGCC-H2, the external electrical power demand of the case IGCC-H2i must be generated internally. In general, the operation of the gas turbine system also induces the N_2 compressor working under off-design conditions, as well as a smaller H_2 compressor used to finally pressurize the generated H_2 stream. Regarding the gas turbine system in the case IGCC-H2, one option is given by the operation of one of the two gas turbines as well as the steam cycle under off-design conditions. Assuming a constant distribution of the gross power production when compared to the design case IGCC-2, the output of the one gas turbine is almost identical to the output of the steam turbine. On that account, the gas turbine load drops to about 29 % of the design power which is well below the lower limit determined by the strongly increasing CO emissions (see Section 4.7). However, another option is represented by operating one gas turbine only. In this case, the gas turbine load results in about 65 % which is well above the minimum load. Thus, the relative efficiency of the gas turbine results in 88.8 % (see Section 4.7). Finally, the produced H_2 stream decreases by about 35 % due to the demand of the gas turbine. In the case IGCC-H2i, the syngas demand of the steam cycle boiler reduces the final H_2 stream by about 3 %. The resulting power distribution of the three analyzed cases is presented in Table 5.6.

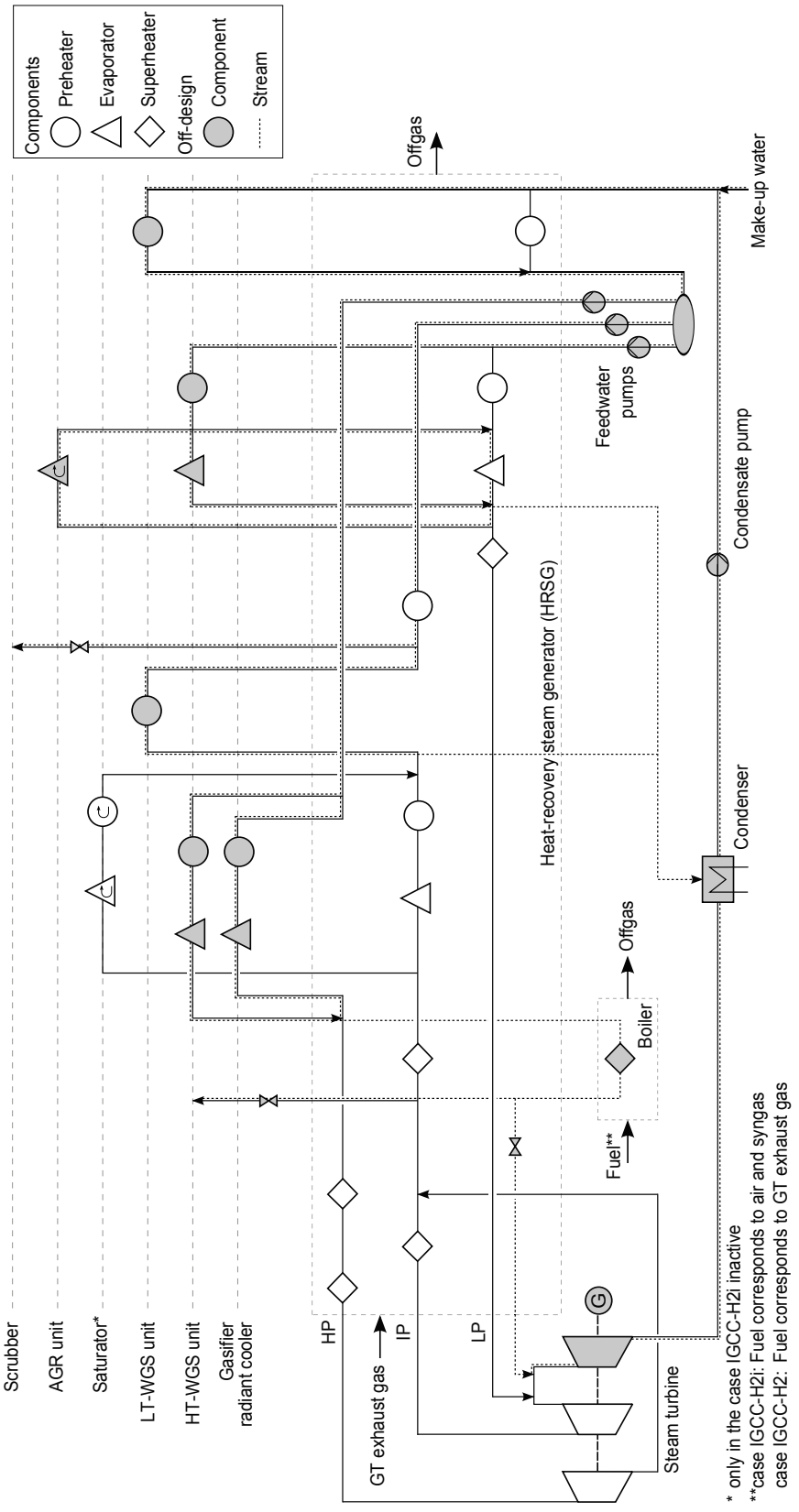

Figure 5.15: Flow diagram of the steam cycle of case IGCC-2 under design and off-design conditions.

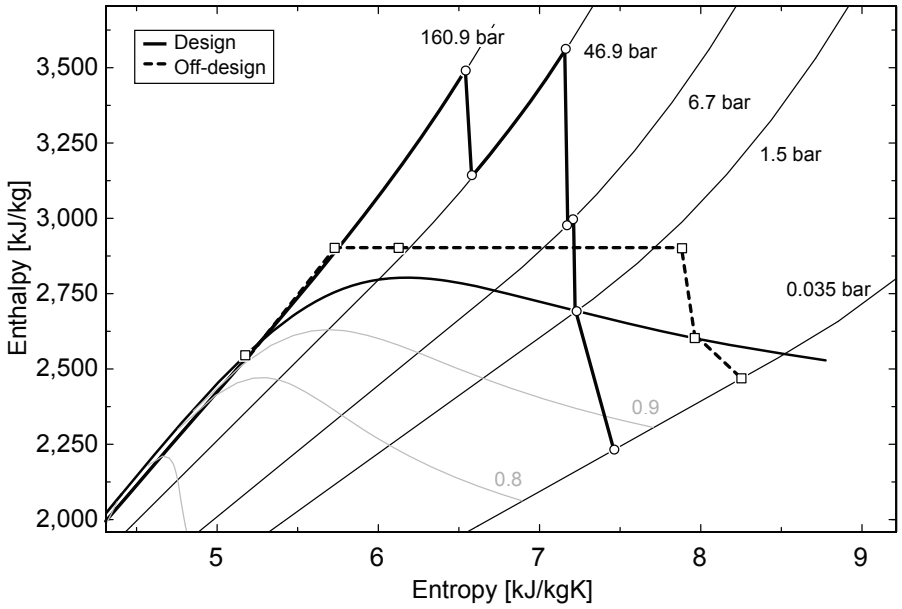

Figure 5.16: *T-s* diagram of the steam turbine under design and off-design conditions.

Figure 5.16 shows the *T-s* diagram according to the flow diagram presented in Fig. 5.15 and the state variables given in Table 3.1 in the Appendix C of the steam cycle. Under design conditions, the heat exchanger network design was found by applying mathematical optimization. The major optimization restriction is represented by the fact that steam is not superheated except within the HRSG. Thus, an additional boiler fired by cleaned syngas is used to superheat the HP saturated steam generated by the gasifier radiant cooler as well as the HT-WGS unit cooler. The HP and IP steam turbine are completely bypassed because the mass flow rate is reduced below the lower limit determined by a positive generation of electric power. Furthermore, the steam quality within the LP steam turbine decreases significantly after expansion through the HP or IP steam turbine. Under off-design conditions, the saturated HP steam is superheated as soon as the IP steam temperature used for the WGS reactors has been reached, subsequent to an additional throttling process (see flow diagram Fig. 5.15). The rest is throttled to a pressure lower than the design case pressure because the LP turbine operates at a lower mass flow rate while the outlet pressure remains constant.

5.4.2 Costs of Hydrogen

In this section, the results of a cost estimation analysis are presented. Assumptions are presented in Section 3.2 and the modeling of the off-design characteristics is shown in Section 4.7.

Table 5.7: Total capital investment (TCI) of the analyzed cases.

Subsystem/unit	Costs €^{2010}/kW
Bare erected costs IGCC-2	
Coal transport	43.3
Gasifier	0.0
Gasifier system incl. syngas cooler	267.2
ASU and oxidant compression	280.2
Other equipment	49.0
Gas cleanup and transport	
Dual-stage Selexol® unit	209.2
Claus plant	15.7
Mercury removal	3.8
WGS unit	23.1
Other	4.8
CO_2 compression	45.6
Gas turbine system	
Gas turbine incl. generator	150.5
Piping and foundation	12.3
HRSG incl. DeNOx, ductwork, stack, foundations	53.6
Steam cycle	
Steam turbine and auxiliaries	45.2
Condenser and auxiliaries	9.0
Piping and foundations	18.3
Cooling water system	54.8
Ash and spent handling	58.7
Accessors electrics	123.8
Instrumentation and control	38.4
Improvements on site	28.0
Buildings and structure	25.9
Sum	1560
TCI case IGCC-2	2060
TCI case IGCC-H2i	2112
TCI case IGCC-H2	2097

Based on the thermodynamic results obtained from the simulation of the base case IGCC-2 (see Section 4.5.2), the bare erected costs are calculated. Table 5.7 presents the cost distributions among the major subsystems as well as the final total capital investment (TCI) of the analyzed cases required for a full-cost accounting. In the cases producing H_2, the clean syngas from case IGCC-2 must be further purified and the final exit pressure is 75 atm to meet the pipeline requirements which are assumed for the competing SMR plant, too. However, the calculated capital costs are 0.88 €/kg_{H_2} in the case IGCC-H2i and 1.33 €/kg_{H_2} in the case IGCC-H2. In the case IGCC-H2, the

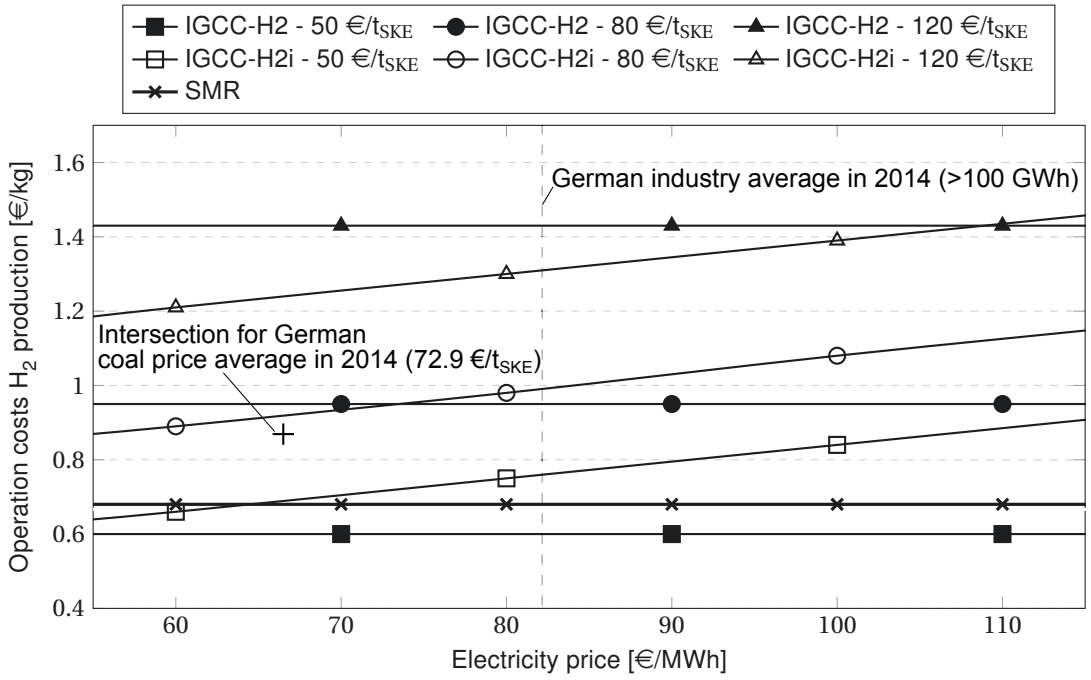

Figure 5.17: Hydrogen operation costs for the analyzed cases.

capital costs are much higher due to the smaller H_2 stream. In this work, the results are mainly based on operation costs because the reference IGCC case is only enhanced by an additional H_2 compression.

The operation costs essentially depend on the coal price. In the case IGCC-H2i, the price of the required external electric power additionally affects the operation costs. Figure 5.17 presents the operation costs for the production of H_2. While the costs for the case IGCC-H2 are independent of the electricity price, the costs in the case IGCC-H2i vary. For a particular coal price, the intersection of both cases curves shows to the left side an electricity price that favors an import of electricity (case IGCC-H2i) and to the right side a stand-alone operation (case IGCC-H2). With increasing coal prices this intersection shifts to higher electricity prices. Thus, importing electric power is recommended by trend at lower coal prices.

In case of the German market, characteristic values for the year 2014 are presented in Fig. 5.17. The derivation of the average electricity and coal price is given in Section 3.2. Considering the average coal price, the intersection of both cases is marked by a cross on the lower left side of the diagram associated with an operation cost of $0.87\,€/kg_{H_2}$. Moreover, the intersection is located left to the average electricity price. Thus, the stand-alone operating case IGCC-H2 is preferred over the import of electric power for Germany in the year 2014.

In Fig. 5.17 the costs for a natural gas-based H_2 production via steam methane reforming (SMR) are given, too, in order to estimate the potential for a hydrogen market entry. The corresponding operation costs include the process equipment published by Simbeck and Chang [120], as well as an additional CO_2 compression from 30 atm to 110 bar. The calculated costs are 0.68 €/kg_{H_2}. With regard to case IGCC-H2, the equivalent coal price is about 57 €/t_{SKE}. On that account, the coal price must be lower in order to prefer the case IGCC-H2 over the operation of a conventional SMR plant.

Chapter 6

Conclusions and Outlook

In this work, several analyses of conventional and enhanced IGCC plants with carbon capture using bituminous coal were performed. On the one hand, integrating novel technologies such as Chemical-Looping Combustion (CLC) or Hot Gas Desulfurization (HGD) into a conventional IGCC plant can promote higher overall efficiencies for steady-state operations. However, increasing the flexibility is one of the major future challenges since the electric power generation by renewable energies will increase the energy market's volatility. For both fields, the gas turbine system (GT) has a strong impact which favors a detailed model for simulation as well as an exhaustive analysis to improve the understanding of the process.

At first, a conventional and advanced exergy analysis of a commercial high-efficiency IGCC plant using a Shell gasifier was conducted in order to generate detailed informations about thermodynamic inefficiencies. The results of the conventional exergy analysis showed that the gasifier followed by the GT combustion chamber and the WGS unit cause the highest inefficiencies, primary due to chemical reactions. Subsequently, the gas turbine, syngas cooler, and AGR unit follow. The captured and conditioned CO_2 stream represents the largest exergy loss.

Using the advanced exergy analysis, the exergy destruction is further split into characteristic parts. The largest avoidable parts were calculated for the gasifier, GT combustion chamber, GT turbine, as well as the syngas cooler. The absolute potential of the GT compressor is almost exhausted. Representing the component's interaction, the exogenous exergy destruction of all incorporated components is significantly large which results from the highly integrated system design of the IGCC plant. Thus, the overall process design significantly affects the overall efficiency. The largest endogenous exergy destruction is generated in the gasifier and the GT combustion chamber deriving from the highly irreversible chemical reactions. When splitting the exogenous exergy destruction into further parts, the binary interactions of components can be

revealed. Particularly, the gasifier strongly influences the GT combustion chamber as the GT fuel gas is produced by gasification. Moreover, a large part of the inefficiencies associated with the gasifier are caused by other components of the gasification island. Additionally, it was found that about one third of the exogenous exergy destruction within the gasifier and the GT combustion chamber is produced by other component interdependencies. In the case of the gasifer, a larger syngas stream is required to compensate irreversibilities within other components.

Considering the combined splitting of avoidable endogenous exergy destruction, the gasifier and the GT combustion chamber should be improved first, and positive effects on other components will likely occur. Furthermore, only technological modifications of the WGS unit and the AGR unit can enable relevant improvements.

A detailed model for the gas turbine system running on syngas was developed, based on a state-of-the-art gas turbine running on natural gas. The model was further enhanced to account for twelve identified characteristic inefficiencies based on an exergy analysis. In case of using isentropic efficiencies, the effect of mixing at different temperatures and pressures as well as expansion cannot be further subdivided. Thus, this grouping was calculated to the second position directly subsequent to the stoichiometric combustion. The addition of excess air results to the third position, followed by mixing at different compositions which is mainly affected by the fuel gas composition. Subsequently, the compression process then follows. The major cooling part within the turbine is realized by the film layer and the rest by convective cooling, and therefore the heat transfer was calculated to represent a smaller inefficiency. Finally, some inefficiencies among the turbine as well as an exergy flow diagram are presented.

In general, the integration of a CLC unit into an IGCC plant has the potential to improve the overall efficiency. In this work, the two most promising systems in combination with the two most suitable gasifier types were analyzed. Based on the conventional high-efficiency IGCC plant, a two-reactor, as well as a three-reactor CLC unit was integrated. The plant featuring a two-reactor CLC unit uses NiO as the oxygen carrier which satisfies the most desired properties when an additional inert support material is used. This CLC unit replaces the conventional combustion chamber of the gas turbine whereat two hot, high-pressure streams exit the system instead of only one. Depleted air exits the air reactor and is recycled to the gas turbine expander. A mixture of H_2O and CO_2 exits the fuel reactor and is further used to produce steam within a HRSG. The CO_2 is then captured inherently by simply condensing the major amount of water.

The air reactor temperature was found to be one of the major parameters which has a significant impact on the overall efficiency. The thermal resistance of materials limits the air reactor temperature. Based on several simulations, a positive trend for higher air reactor temperatures was observed for the cases using a two-reactor CLC system as the higher outlet temperatures promote an efficient steam production. In general, the design of the heat exchanger network, which combines the cooling and heating sources, has a significant impact on the overall performance since the steam turbine performance is directly affected. In the cases using an entrained-flow Shell gasifier, the air reactor temperature was found to be at least 1200 °C to outperform the conventional reference case. The general trend showed a preference of the moving bed BGL gasifier in combination with a HGD unit. However, a satisfying practical application of a Hot Gas Cleanup Unit (HGCU), especially for removing mercury, ammonia and COS, has not been demonstrated yet. In the cases when a BGL gasifier was used, a significant rise in the overall efficiency was observed for an air reactor temperature of 1100 °C using the two-reactor CLC design. The maximum efficiency was calculated to be 43.7 %, based on the lower heating value which represents an increase of 5.8 %-points when compared to the conventional case. Without an HGCU, the efficiency potential is estimated to be about 3.3 %-points.

The other promising CLC system using three reactors and the oxygen carrier magnetite (Fe_2O_3) was found to be less efficient. In comparison to the two-reactor CLC system, the oxidation of the oxygen carrier occurs within an additional steam reactor prior to the air reactor. Thus, a third stream consisting of ultra-wet hydrogen exits the CLC unit and is further combusted within the gas turbine. It was found that the overall efficiency increases with lower air reactor temperatures which shows an opposing trend when compared to the two-reactor CLC system. This mainly results from the reduction state of the oxygen carrier exiting the fuel reactor which negatively affects the gas turbine performance. The application of an additional CO_2 turbine between the CLC unit and the HRSG is not recommended due to a lower overall efficiency. In summary, the results of this work only show an advantage in the performance for the integration of CLC into an IGCC plant when using a moving-bed gasifier in combination with an HGCU. The general trend shows a preference of the two-reactor CLC system.

Concerning a flexible operation, another conventional IGCC plant which is less efficient but also less cost-intensive, was simulated. The total capital investment was determined by a cost estimation. As a new product, the coal-derived syngas is further prepared to produce almost pure hydrogen. This hydrogen can be sold in

periods where the electricity spot price undercuts the operation costs of the IGCC plant. In this process, the internal electricity demand can be satisfied by either buying external electric power or by operating the gas turbine under off-design conditions. In the first case the capital costs were calculated to 0.88 €/kg_{H_2} and in the second case to 1.33 €/kg_{H_2}. In this work, the HRSG as well as the HP and IP steam turbine are bypassed and the LP steam turbine operates under off-design conditions, too. Regarding the operation costs for the production of hydrogen, a sensitivity analysis was performed depending on the price of coal ranging from 50 to 120 €/t_{SKE} and the price of electricity ranging from 60 to 110 €/MWh. Apparently, the import of electricity is only advantageous for low electricity prices. This effect increases with lower coal prices.

Depending on average prices from the year 2014, it was found that in Germany internal electricity production should be preferred because the electricity price for industrial consumers was relatively high. On that account, the operation costs for producing hydrogen were calculated to 0.87 €/kg_{H_2}. Based on this scenario, the operation costs of the competing SMR technology were calculated to only about 77 %, which represents a disadvantage to access the hydrogen market. The price of coal should be below 57 €/t_{SKE} in order to outperform a SMR plant.

For future work, more experimental investigations on the CLC system regarding sealing, heat losses, and operation characteristics have to be conducted in order to calculate the overall system performance more accurately, and to estimate the actual costs. The economic results can be combined with the exergetic results presented in this work in the so-called exergoeconomic analysis [168], which rates the cost of the exergy destructions to further improve the overall system. The actual limitations of a mathematical opimization applied for the highly non-linear and integrated IGCC plant have to be overcome by using more powerful solvers and computers to improve the system. Further analysis on a syngas storage might be useful, especially for markets involving high average or peak electricity prices.

Generally, in the last years the worldwide price of natural gas has decreased which promotes investments in gas-fired combined cycle power plants. Considering a future scenario with higher prices for natural gas, the IGCC technology has the potential to increase its market share. Additionally, the co-production of hydrogen for markets involving an electricity pricing with high volatility may present a suitable option. Furthermore, inventing large-scale technologies that reuse CO_2 has a significant impact on the industrial and public acceptance of efficient power plants with carbon capture.

Bibliography

[1] CO_2 emissions from fuel combustion. International Energy Agency, 2014. (Cit. on p. 1).

[2] Bp statistical review of world energy. BP, 2011. (Cit. on p. 1).

[3] T. Bruckner, I. A. Bashmakov, Y. Mulugetta, H. Chum, A. d. l. Vega Navarro, J. Edmonds, A. Faaij, B. Fungtammasan, A. Garg, E. Hertwich, D. Honnery, D. Infield, M. Kainuma, S. Khennas, S. Kim, H. B. Nimir, K. Riahi, N. Strachan, R. Wiser, and X. Zhang. *Climate change 2014: mitigation of climate change. contribution of working group iii to the fifth assessment report of the intergovernmental panel on climate change*. In. J. S. Kirit Parikh, editor. Cambridge University Press, Cambridge, United Kingdom and New York, NY, USA, 2014. part Energy Systems, pp. 518–570 (cit. on p. 1).

[4] World energy outlook. Paris: International Energy Agency, 2013. (Cit. on p. 1).

[5] International energy outlook. U.S. Energy Information Administration, 2011. (Cit. on p. 2).

[6] J. Black. Cost and performance baseline for fossil energy plants volume 1: bituminous coal and natural gas to electricity. National Energy Technology Laboratory, DOE/NETL-2010/1397, 2013. (Cit. on pp. 2, 7, 8, 11, 13, 33, 42, 53, 55, 58–60).

[7] T. Fout, A. Zoelle, D. Keairns, M. Turner, M. Woods, N. Kuehn, V. Shah, V. Chou, and L. Pinkerton. Cost and performance baseline for fossil energy plants volume 1b: bituminous coal (igcc) to electricity revision 2b - year dollar update. National Energy Technology Laboratory, DOE/NETL-2015/1727, 2015. (Cit. on p. 2).

[8] H. Spliethoff. *Power generation from solid fuels*. Springer-Verlag Berlin Heidelberg, 2010 (cit. on pp. 7, 8, 10–12, 14, 15).

[9] J. McJannett. Using physical solvent in multiple applications. *Gas - petroleum technology quarterly*:29–37, 2012 (cit. on pp. 8, 13, 14).

[10] I. Barnes. Recent operating experience and improvement of commercial igcc. IEA Clean Coal Centre, 2013. (Cit. on pp. 8, 11, 17, 18).

[11] R. Schlögl. Fossile energieträger werden genutzt, solange es eben geht (in german). *Vdi nachrichten*, 38:2, 2014 (cit. on p. 8).

[12] B. Metz, O. Davidson, H. d. Coninck, M. Loos, and L. Meyer. Ipcc special report on carbon dioxide capture and storage. Cambridge University Press, New York, 2005. (Cit. on pp. 9, 11).

[13] T. Tawfik, G. Tsatsaronis, and D. Price. Exergetic comparison of various igcc power plant designs. *Proceedings of the international conference on energy systems and ecology, july 5-9, 1993, cracow, poland*, 1:585–593, 1993 (cit. on p. 10).

[14] G. Tsatsaronis, T. Tawfik, and L. Lin. Exergetic comparison of two krw-based igcc power plants. *Journal of engineering for gas turbines and power*, 116:291–299, 1994 (cit. on p. 10).

[15] C. Kunze, K. Riedl, and H. Spliethoff. Structured exergy analysis of an integrated gasification combined cycle (igcc) plant with carbon capture. *Energy*, 36:1480–1487, 2011 (cit. on pp. 10, 11).

[16] N. S. Siefert and S. Litster. Exergy and economic analyses of advanced igcc-ccs and igfc-ccs power plants. *Applied energy*, 107:315–328, 2013 (cit. on p. 10).

[17] D. Jones, D. Bhattacharyya, R. Turton, and S. E. Zitney. Optimal design and integration of an air separation unit (asu) for an integrated gasification combined cycle (igcc) power plant with CO_2 capture. *Fuel processing technology*, 92:1685–1695, 2011 (cit. on p. 11).

[18] M. Liszka and J. Tuka. Parametric study of gt and asu integration in case of igcc with CO_2 removal. *Energy*, 45:151–159, 2012 (cit. on p. 11).

[19] C.-C. Cormos. Integrated assessment of igcc power generation technology with carbon capture and storage (ccs). *Energy*, 42:434–445, 2012 (cit. on p. 11).

[20] E. Martelli, T. Kreutz, and S. Consonni. Comparison of coal igcc with and without CO_2 capture and storage: shell gasification with standard vs. partial water quench. *Energy procedia*, 1(1):607–614, 2009 (cit. on pp. 11, 58, 59).

[21] J. Katzer. The future of coal. MIT - Massachusetts Institute of Technology, 2007. (Cit. on p. 11).

[22] Spallina, M. Romano, P. Chiesa, F. Gallucci, M. v. Sint Annaland, and G. Lozza. Integration of coal gasification and packed bed clc for high efficiency and near-zero emission power generation. *International journal of greenhouse gas control*, 27:28–41, 2014 (cit. on pp. 11, 23).

[23] C. Chen and E. S. Rubin. CO_2 control technology effects on igcc plant performance and cost. *Energy policy*, 37:915–924, 2009 (cit. on pp. 11, 12).

[24] V. A. R. Ibarra and M. Schmidt. Exergoeconomic analysis of an igcc power plant with a texaco gasifier and pre-combustion carbon capture. MA thesis. Technische Universität Berlin, Germany, 2011 (cit. on p. 11).

[25] C.-C. Cormos. Evaluation of energy integration aspects for igcc-based hydrogen and elextricity co-production with carbon capture and storage. *International journal of hydrogen energy*, 35:7485–7497, 2010 (cit. on p. 11).

[26] J. M. Klara. Cost and performance baseline for fossil energy plants - volume 1: bituminous coal and natural gas to electricity. National Energy Technology Laboratory, DOE/NETL-2007/1281, 2007. (Cit. on p. 11).

[27] S. Rezvani, Y. Huang, D. McIlveen-Wright, N. Hewitt, and J. D. Mondol. Comparative assessment of coal fired igcc systems with CO_2 capture using physical absorption, membrane reactors and chemical looping. *Fuel*, 88:2463–2472, 2009 (cit. on pp. 11, 12, 23, 24, 97).

[28] C.-C. Cormos. Evaluation of syngas-based chemical looping applications for hydrogen and power co-generation with ccs. *International journal of hydrogen energy*, 37:13371–13386, 2012 (cit. on pp. 11, 23, 24, 97, 99).

[29] C.-C. Cormos. Evaluation of iron based chemical looping for hydrogen and electricity co-production by gasification process with carbon capture and storage. *International journal of hydrogen energy*, 35:2278–2289, 2010 (cit. on pp. 11, 23, 24, 99).

[30] L.-S. Fan. *Chemical looping systems for fossil energy conversions*. John Wiley & Sons, Inc., Hoboken, New Jersey, 2010 (cit. on pp. 11, 22, 24, 99).

[31] M. Bracht, P. T. Alderliesten, R. Kloster, R. Pruschek, G. Haupt, E. Xue, J. R. H. Ross, M. K. Koukou, and N. Papayannakos. Water gas shift membrane reactor for CO_2 control in igcc systems: techno-economic feasibility study. *Energy conversion and management*, 38(1):5159–5164, 1997 (cit. on pp. 11, 12).

[32] C. Kunze. Simulation und bewertung zuünftiger igcc-kraftwerkskonzepte mit CO_2-abtrennung (in german). PhD thesis. Technische Universität München, 2012 (cit. on pp. 11, 12).

[33] G. Krishnan, D. Steele, K. O'Brien, R. Callahan, K. Berchtold, and J. Figueroa. Simulation of a process to capture CO_2 from igcc syngas using a high temperature pbi membrane. *Energy procedia*, 1(1):4079–4088, 2009 (cit. on pp. 11, 12).

[34] E. Grol and J. Wimer. Systems analysis of an integrated gasification fuel cell combined cycle. National Energy Technology Laboratory (NETL), DOE/NETL-40/080609, 2009. (Cit. on pp. 11, 12).

[35] A. Lanzini, T. Kreutz, E. Martelli, and M. Santarelli. Energy and economic performance of novel integrated gasifier fuel cell (igfc) cycles with carbon capture. *International journal of greenhouse gas control*, 26:169–184, 2014 (cit. on pp. 11, 12).

[36] J. J. Marano and J. P. Ciferino. Integration of gas separation membranes with igcc identifying the right membrane for the right job. *Energy procedia*, 1(1):361–368, 2009 (cit. on p. 12).

[37] Korea plans 360 mw fuel cell power facility with posco, doosan. *Fuel cells bulletin*, 10:4, 2014 (cit. on p. 12).

[38] R. Doctor, J. Molburg, and P. Thimmapuram. Krw oxygen-blown gasification combined cycle: carbon dioxide recovery, transport, and disposal. Energy Systems Division, Argonne National Laboratory, 1996. (Cit. on pp. 13, 14, 58).

[39] J. B. Tennant. Gasification technologies program - overview. National Energy Technology Laboratory (NETL), 2011. (Cit. on pp. 13, 14).

[40] B. Burr and L. Lyddon. A comparison of physical solvents for acid gas removal. *Bryan research & engineering, inc.*, 2008 (cit. on p. 14).

[41] S. AG. Neue verdichter für den ccs-markt (in german). *Bwk, das energie-fachmagazin*, 9:49–50, 2015 (cit. on p. 14).

[42] G. R. Schoofs. Sulfur condensation in claus catalyst. *Hydrocarbon processings*, 1985 (cit. on pp. 14, 58).

[43] G. Hochgesand. Rectisol and purisol. *Industrial engineering chemistry*, 62(7):37–43, 1970 (cit. on p. 14).

[44] A. Giuffrida, M. C. Romano, and G. Lozza. Efficiency enhancement in igcc power plants with air-blown gasification and hot gas clean-up. *Energy*, 53:221–229, 2013 (cit. on pp. 15, 100).

[45] D. Vamvuka, C. Arvanitidis, and D. Zachariadis. Flue gas desulfurization at high temperatures: a review. *Environmental engineering science*, 21(4):525–547, 2004 (cit. on p. 15).

[46] A. T. Atimtay. Cleaner energy production with integrated gasification combined cycle systems and use of metal oxide sorbents for H_2S cleanup from coal gas. *Clean products and processes*, 2:197–208, 2001 (cit. on p. 15).

[47] Warm-syngas cleanup technology. URL: `http://www.rti.org` (cit. on p. 15).

[48] R. Gupta, B. Turk, and M. Lesemann. Rti/eastman warm syngas clean-up technology: integration with carbon capture. In *Gasification technologies conference*. Colorado, USA, 2009 (cit. on p. 15).

[49] N. Korens, D. R. Simbeck, and D. J. Wilhelm. Process screening analysis of alternative gas treating and sulfur removal for gasification. SFA Pacific, Inc., 2002. (Cit. on p. 15).

[50] O. Turna. Sasol-lurgi fixed bed dry bottom gasification for fuels and chemicals. In *2nd international freiberg conference on igcc & xtl technologies*. Freiberg, Germany, 2007 (cit. on p. 16).

[51] C. Higman and M. v. d. Burgt. *Gasification*. Gulf Professional Publishing, Amsterdam, 2007 (cit. on pp. 16, 57, 68, 71).

[52] T. Blumberg, M. Sorgenfrei, and G. Tsatsaronis. Modelling and evaluation of an igcc concept with carbon capture for the co-production of sng and electricity. In *28th international conference on efficiency, costs, optimization, simulation and environmental impact of energy systems - ecos*. Pau, France, 2015 (cit. on p. 17).

[53] T. Blumberg, M. Sorgenfrei, and G. Tsatsaronis. Modelling and evaluation of an igcc concept with carbon capture for the co-production of sng and electricity. *Sustainablility*, 7:16213–16225, 2015 (cit. on p. 17).

[54] From solid fuels to substitute natural gas (sng) using tremp. Denmark: Haldor Topsøe, 2009. (Cit. on p. 17).

[55] World gasification database. URL: `http://www.gasification.org/what-is-gasification/world-database/` (cit. on pp. 17, 18).

[56] Gasification plant databases. U.S. Department of Energy (DOE). URL: `http://www.netl.doe.gov/research/coal/energy-systems/gasification/gasification-plant-databases` (cit. on p. 17).

[57] The sgt5-8000h - proven in commercial operation. Siemens AG - Energy Sector, 2012. (Cit. on pp. 18, 52, 53).

[58] R. Taud, J. Karg, and D. O'Leary. Gas turbine based power plants: technology and market status. *Energy issues*, 20:1–8, 1999 (cit. on p. 18).

[59] Energy technology perspectives - scenarios & strategies to 2050. IEA, 2006. (Cit. on p. 18).

[60] W. Renzenbrink and M. Scholz. H_2 gas turbine - a stepping stone to ccs. In *18th world hydrogen energy conference (whec) 2010*. Essen, Germany, 2010 (cit. on p. 18).

[61] I. S. Ertesvag, H. M. Kvamsdal, and O. Bolland. Exergy analysis of a gas-turbine combined-cycle power plant with precombustion CO_2 capture. *Energy*, 30:5–39, 2005. DOI: doi:10.1016/j.energy.2004.05.029 (cit. on p. 19).

[62] G. Cassetti, M. Rocco, and E. Colombo. Exergy based methods for economic and risk design optimization of energy systems - application to a gas turbine. *Energy*, 74:269–279, 2014. DOI: doi:10.1016/j.energy.2014.07.043 (cit. on p. 19).

[63] E. Acikkalp, H. Aras, and A. Hepbasli. Advanced exergy analysis of an electricity-generating facility using natural gas. *Energy conversion and management*, 82:146–153, 2014. DOI: doi:10.1016/j.enconman.2014.03.006 (cit. on p. 19).

[64] S. Soltani, M. Yari, S. Mahmoudi, and M. R. T. Morosuk. Advanced exergy analysis applied to an externally-fired combined-cycle power plant integrated with a biomass gasification unit. *Energy*, 59:775–780, 2013. DOI: http://dx.doi.org/10.1016/j.energy.2013.07.038 (cit. on p. 19).

[65] P. Ahmadi, I. Dincer, and M. A. Rosen. Exergy, exergoeconomic and environmental analyses and evolutionary algorithm based multi-objective optimization of combined cycle power plants. *Energy*, 36:5886–5898, 2011. DOI: doi:10.1016/j.energy.2011.08.034 (cit. on p. 19).

[66] Iso 2314:2009(e). Gas turbines - Acceptance tests (cit. on p. 19).

[67] M. A. EI-Masri. Exergy analysis of combined cycles: part 1 - air-cooled brayton-cycle gas turbines. *Journal of engineering for gas turbines and power*, 109:228–236, 1987 (cit. on pp. 19, 94).

[68] E. A. Khodak and G. A. Romakhova. Thermodynamic analysis of air - cooled gas turbine plants. *Journal of engineering for gas turbines and power*, 123:265–270, 2001. DOI: DOI:10.1115/1.1341204 (cit. on p. 19).

[69] S. Staudacher and P. W. Zeller. Exergy analysis for the performance evaluation of different setups of the secondary air system of aircraft gas turbines. In *Asme turbo expo: power for land, sea and air*. Montreal, Canada, 2007 (cit. on pp. 19, 94).

[70] K. F. Knoche and H. Richter. Verbesserung der reversibilität von verbrennungsprozessen (in german). *Brennstoff-wärme-kraft (bwk)*, 20(5):205–210, 1968 (cit. on p. 19).

[71] S. Hurst. Production of hydrogen by the steam-iron method. *Journal of the american oil chemists' society*, 16:29–36, 1939 (cit. on p. 20).

[72] E. R. G. Warren K. Lewis. Production of pure carbon dioxide. (US000002665971A). 1954 (cit. on p. 20).

[73] M. Ishida, D. Zheng, and T. Akehata. Evaluation of a chemical-looping-combustion power-generation system by graphic exergy analysis. *Energy*, 12(2):147–154, 1987 (cit. on p. 20).

[74] P. Markewitz, W. Kuckshinrichs, W. Leitner, J. Linssen, P. Zapp, R. Bongartz, A. Schreiber, and T. E. Müller. Worldwide innovations in the development of carbon capture technologies and the utilization of CO_2. *Energy and environmental science*, 5:7281–7305, 2012 (cit. on p. 20).

[75] J. Adanez, A. Abad, F. Garcia-Labiano, P. Gayan, and L. F. d. Diego. Progress in chemical-looping combustion and reforming technologies. *Progress in energy and combustion science*, 38:215–282, 2012 (cit. on p. 20).

[76] A. Lyngfelt. Chemical-looping combustion of solid fuels - status of development. *Applied energy*, 113:1869–1873, 2014 (cit. on p. 20).

[77] V. Kempkes and A. Kather. Chemical looping combustion: comparative analysis of two different overall process configurations for removing unburnt gaseous components. In *2nd international conference on chemical looping, 26-28 september 2012*. Darmstadt, Germany, 2012 (cit. on pp. 21, 64).

[78] C. F. Blazek, N. R. Baker, and R. R. Tison. High-btu coal gasification processes. Institute of Gas Technology, 1979. (Cit. on p. 21).

[79] P. Gupta, L. G. Velazquez-Vargas, and L.-S. Fan. Syngas redox (sgr) process to produce hydrogen from coal derived syngas. *Energy & fuels*, 21:2900–2908, 2007 (cit. on pp. 21, 72).

[80] N. A. Lange. *Lange's handbook of chemistry*. J. A. Dean, editor. McGraw-Hill, Inc., 1999 (cit. on p. 22).

[81] T. Mattisson, F. Garcia-Labiano, B. Kronberger, A. Lyngfelt, J. Adanez, and H. Hofbauer. Chemical-looping combustion using syngas as fuel. *International journal of greenhouse gas control*, 1:158–169, 2007 (cit. on p. 22).

[82] D. Jing, T. Mattisson, M. Ryden, P. Hallberg, A. Hedayati, J. V. Noyen, F. Snijkers, and A. Lyngfelt. Innovative oxygen carrier materials for chemical-looping combustion. *Energy prodecia*, 37:645–653, 2013 (cit. on p. 22).

[83] S. Bhavsar, B. Tackett, and G. Veser. Evaluation of iron- and manganese-based mono- and mixed-metallic oxygen carriers for chemical looping combustion. *Fuel*, 136:268–279, 2014 (cit. on p. 22).

[84] L.-G. Velazquez-Vargas, P. P. T. Thomas, and L.-S. Fan. Hydrogen production via redox reaction of syngas with metal oxide composite particles. In *Aiche annual meeting*. Austin, Texas, USA, 2004 (cit. on p. 22).

[85] R.-H. Perry and D.-W. Green. *Perrys chemical engineers handbook*. Vol. 8th edition. McGraw-Hill, Columbus, 2008 (cit. on p. 22).

[86] E. Johansson, T. Mattisson, A. Lyngfelt, and H. Thuman. Combustion of syngas and natural gas in a 300w chemical-looping combustor. *Chemcial engineering research and design*, 84:819–827, 2006 (cit. on p. 22).

[87] M. Anheden and G. Svedberg. Chemical looping combustion in combination with integrated coal gasification. In *31st intersociety energy conversion engineering conference (iecec 96)*. Washington DC, USA, 1996 (cit. on p. 23).

[88] M. Anheden and G. Svedber. Exergy analysis of chemical-looping combustion systems. *Energy conversion and management*, 39(16):1967–1998, 1998 (cit. on p. 23).

[89] M. Schmidt, B. Erlach, and G. Tsatsaronis. Comparison of an igcc with pre-combustion carbon capture and an igcc design with chemical-looping combustion. In *22nd international conference on efficiency, costs, optimization, simulation and environmental impact of energy systems - ecos*. Foz do Iguacu, Parana, Brazil, 2009 (cit. on pp. 23, 63).

[90] B. Erlach, M. Schmidt, and G. Tsatsaronis. Comparison of carbon capture igcc with pre-combustion decarbonisation and with chemical-looping combustion. *Energy*, 36(6):3804–3815, 2011. DOI: doi:10.1016/j.energy.2010.08.038 (cit. on pp. 23, 63).

[91] H. C. Mantripragada and E. S. Rubin. Chemical looping for pre-combustion CO_2 capture performance and cost analysis. *Energy procedia*, 37:618–625, 2013 (cit. on p. 23).

[92] K. Svoboda, G. Slowinski, J. Rogut, and D. Baxter. Thermodynamic possibilities and constraints for pure hydrogen production by iron based chemical looping process at lower temperatures. *Energy conversion and management*, 48:3063–3073, 2007 (cit. on p. 24).

[93] W. Xiang, S. Chen, Z. Xue, and X. Sun. Investigation of coal gasification hydrogen and electricity co-production plant with three-reactors chemical looping process. *International journal of hydrogen energy*, 35:8580–8591, 2010 (cit. on p. 24).

[94] S. Chen, Z. Xue, D. Wang, and W. Xiang. Hydrogen and electricity co-production plant integrating steam-iron process and chemical looping combustion. *International journal of hydrogen energy*, 37:8204–8216, 2012 (cit. on p. 24).

[95] P. Chiesa, G. Lozza, A. Malandrino, M. Romano, and V. Piccolo. Three-reactors chemical looping process for hydrogen production. *International journal of hydrogen energy*, 33:2233–2245, 2008 (cit. on p. 24).

[96] J. Wolf and J. Yan. Parametric study of chemical looping combustion for trigeneration of hydrogen, heat, and electrical power with CO_2 capture. *International journal of energy research*, 29:739–753, 2005 (cit. on p. 25).

[97] N. Gnanapragasam, B. Reddy, and M. Rosen. Hydrogen production from coal using coal direct chemical looping and syngas chemical looping combustion systems: assessment of system operation and resource requirements. *International journal of hydrogen energy*, 34:2606–2615, 2009 (cit. on p. 25).

[98] M. Sorgenfrei and G. Tsatsaronis. Exergetic assessment of a syngas-redox (sgr)-based igcc plant for generating electricity. In *Asme 2012 international mechanical engineering congress and exposition*. Houston, Texas, USA, 2012 (cit. on pp. 25, 63).

[99] M. Sorgenfrei and G. Tsatsaronis. Exergetic assessment of a syngas-redox-based igcc plant for generating electricity. *Journal of engineering for gas turbines and power*, 136(3), 2013. DOI: 10.1115/1.4025885 (cit. on pp. 25, 63).

[100] M. Sorgenfrei and G. Tsatsaronis. Design and evaluation of an igcc power plant using iron-based syngas chemical looping (scl) combustion. In *2nd international conference on chemical looping*. Darmstadt, Germany, 2012 (cit. on pp. 25, 63).

[101] M. Sorgenfrei and G. Tsatsaronis. Design and evaluation of an igcc power plant using iron-based syngas chemical looping (scl) combustion. *Applied energy*, 113:1958–1964, 2014 (cit. on pp. 25, 63).

[102] T. Herdan, G.-D. Krieger, and M. Zelinger. Fähigkeiten von stromerzeugungsanlagen im energiemix (in german). VDMA Power Systems, 2013. (Cit. on p. 25).

[103] U. Tomschi. Aufgaben thermischer kraftwerke im zuge der energiewende (in german). Siemens AG, 2014. (Cit. on p. 25).

[104] D. Cocco, F. Serra, and V. Tola. Assessment of energy and economic benefits arising from syngas storage in igcc power plants. *Energy*, 58:635–643, 2013 (cit. on p. 25).

[105] S. M. Douglas and L. M. Dunn. Improving the economic viability of igcc power plants using syngas storage and fuel-switching. West Virginia University, Washington & Jefferson College, 2008. (Cit. on p. 25).

[106] J. Apt, A. Newcomer, L. B. Lave, S. Douglas, and L. M. Dunn. An engineering-economic analysis of syngas storage. National Energy Technology Laboratory (NETL), DOE/NETL-2008/1331, 2008. (Cit. on p. 26).

[107] T.-P. Chen. Hydrogen delivery infrastructure options analysis. Nexant, Inc., Air Liquide, Argonne National Laboratory, Chevron Technology Venture, Gas Technology Institute, National Renewable Energy Laboratory (NREL), Pacific Northwest National Laboratory, and TIAX LLC, 2008. (Cit. on pp. 26, 34).

[108] J. Szargut, D. R. Morris, and F. R. Steward. *Exergy analysis of thermal, chemical and metallurgical processes*. New York: Hemisphere Publishing Corporation, 1988 (cit. on pp. 28, 29).

[109] A. Bejan, G. Tsatsaronis, and M. Moran. *Thermal design and optimization*. New York: JohnWiley & Sons, Inc., 1996 (cit. on pp. 28, 33).

[110] G. Tsatsaronis. Definitions and nomenclature in exergy analysis and exergoeconomics. *Energy*, 32:249–253, 2007 (cit. on p. 28).

[111] A. Lazzaretto and G. Tsatsaronis. Speco: a systematic and general methodology for calculating efficiencies and costs in thermal systems. *Energy*, 31, Issue 8-9:1257–1289, 2006 (cit. on p. 29).

[112] G. Tsatsaronis. *Thermodynamic optimization of complex energy systems*. In. A. Bejan and E. Mamut, editors. Kluwer Academic Publishers, 1999. part Strengths and Limitations of Exergy Analysis, pp. 93–100 (cit. on p. 30).

[113] T. Morosuk and G. Tsatsaronis. Strengths and limitations of advanced exergetic analyses. In *Asme 2013 international mechanical engineering congress and exposition*, 2013 (cit. on pp. 30, 33).

[114] T. Morosuk and G. Tsatsaronis. A new approach to the exergy analysis of absorption refrigeration machines. *Energy*, 33(6):890–907, 2008 (cit. on p. 31).

[115] T. Morosuk and G. Tsatsaronis. Advanced exergy analysis for chemically reacting systems - application to a simple open gas-turbine system. *International journal of thermodynamics*, 12(3)(3):105–111, 2009 (cit. on pp. 31, 32).

[116] S. Kelly, G. Tsatsaronis, and T. Morosuk. Advanced exergetic analysis: approaches for splitting the exergy destruction into endogenous and exogenous parts. *Energy*, 34(3):284–391, 2009 (cit. on p. 31).

[117] M. Penkuhn and G. Tsatsaronis. Calculation of thermodynamic system component interactions for advanced exergy analysis, status: manuscript in preparation, 2015 (cit. on p. 31).

[118] J. M. Douglas. *Conceptual design of chemical processes*. McGraw Hill, 1988 (cit. on p. 31).

[119] G. Tsatsaronis and M. Park. On avoidable and unavoidable exergy destructions and investment costs in thermal systems. *Energy conversion and management*, 43:1259–1270, 2002 (cit. on p. 31).

[120] D. Simbeck and E. Chang. Hydrogen supply: cost estimate for hydrogen pathways - scoping analysis. National Renewable Energy Laboratory (NREL), 2002. (Cit. on pp. 33, 34, 110).

[121] Chemical engineering plant cost index. URL: http://www.chemengonline.com (cit. on p. 34).

[122] Average exchange rate euro-dollar. URL: http://www.x-rates.com (cit. on p. 34).

[123] Price of bituminous coal. 2015. URL: http://www.bafa.de/bafa/de/energie/steinkohle/drittlandskohlepreis/ (cit. on p. 33).

[124] Industriestrompreise (in german). BDEW Bundesverband der Energie- und Wasserwirtschaft e.V., 2014. (Cit. on p. 34).

[125] Aspen plus®. URL: http://www.aspentech.com (cit. on p. 34).

[126] Engineering equation solver - professional version. URL: http://www.fchart.com/ees/ (cit. on p. 34).

[127] Matlab®. URL: http://www.mathworks.com/products/matlab/ (cit. on p. 35).

[128] I. Rumyantseva and S. Watanasiri. Acid gas cleaning using depg physical solvent: validation with experimental and plant data. Aspen Technology, Inc., 2014. (Cit. on p. 35).

[129] I. Barin. *Thermochemical data of pure substances*. VCH, Weinheim, 1989 (cit. on p. 35).

[130] M.-W. Chase. *Nist-janaf thermochemical tables*. 4. Edition, editor. American Chemical Society, Washington DC, USA, 1998 (cit. on p. 35).

[131] O. Knacke, O. Kubaschewski, and K. Hesselmann. *Thermochemical properties of inorganic substances (2nd edition)*. Springer, New York (NY), 1991 (cit. on p. 35).

[132] National institute of standards and technology (nist). URL: http://www.nist.gov/ (cit. on p. 35).

[133] The international association for the properties of water and steam (iapws). URL: http://www.iapws.org/ (cit. on p. 35).

[134] Iso 2533. Standard Atmosphere (cit. on p. 41).

[135] E. Ludwig. *Applied process design iii*. Gulf Professional Publishing, 2001 (cit. on pp. 41, 58).

[136] K. Baumann. Some recent developments in large steam turbine practice. *Journal of the institution of electrical engineers*, 59(302):565–623, 1921. DOI: 10.1049/jiee-1.1921.0040 (cit. on p. 42).

[137] A. Smith. The influence of moisture on the efficicency of a one-third scale model low pressure steam turbine. *Proceedings of the institution of mechanical engineers, part 30: symposium on wet steam*, 180:39–49, 1965 (cit. on p. 42).

[138] W. R. Paterson. A replacement for the logarithmic mean temperature. *Chemical engineering science*, 39:1635–1636, 1984 (cit. on p. 43).

[139] K. Kugeler and P.-W. Philippen. *Energietechnik (in german)*. Springer-Verlag Berlin Heidelberg, 1990 (cit. on p. 47).

[140] K. Menny. *Strömungsmaschine - hydraulische und thermische kraft- und arbeitsmaschinen (in german)*. Teubner B.G. GmbH, 2003 (cit. on p. 47).

[141] M. Boyce. *Gas turbine engineering handbook*. Gulf Professional Publishing, 3rd edition, 2006 (cit. on pp. 49, 52).

[142] C. Kail. Analyse von kraftwerksprozessen mit gasturbinen unter energetischen, exergetischen und ökonomischen aspekten (in german). PhD thesis. Technischen Universität München, 1998 (cit. on pp. 49–53).

[143] W. Bräunling. *Flugzeugtriebwerke (in german)*. Springer, 2009. DOI: http://dx.doi.org/10.1007/978-3-540-76370-3 (cit. on pp. 50, 52).

[144] C. Lechner and J. Seume. *Stationäre gasturbinen (in german)*. Springer, Berlin, Heidelberg, 2010 (cit. on pp. 50, 52).

[145] W. J. Fischer and P. Nag. H-class high performance siemens gas turbine sgt-8000h series. In *Power-gen international*. Las Vegas, USA, 2011 (cit. on pp. 52, 53).

[146] M. Jonsson, O. Bolland, D. Bücker, and M. Rost. Gas turbine cooling model for evaluation of novel cycles. In *18th international conference on efficiency, cost, optimization, simulation and environmental impact of energy systems - ecos*. Trondheim, Norway, 2005 (cit. on p. 52).

[147] G. Cerri, F. Botta, L. Chennaoui, A. Giovannelli, C. Salvini, M. Miglioli, C. Basilicata, S. Mazzoni, and E. Archilei. Description of the models adapted or devel-

oped ad hoc for the igcc&ccs plants. Low Emission Gas Turbine Technology for Hydrogen-rich Syngas (H2-IGCC), 2011. (Cit. on p. 52).

[148] R. Dennis. *The gas tubrine handbook*. National Energy Technology Laboratory (NETL), U.S. Department of Energy (DOE), 2006 (cit. on p. 52).

[149] Technologien der feststoffvergasung im hause uhde (in german). In *Dvv-fach-ausschuss grundlagen und anwendungen*. Uhde (ThyssenKrupp Technologies). Oberhausen, Germany, 2007 (cit. on pp. 57, 58, 82).

[150] L. Zheng and E. Furinsky. Comparison of shell, texaco bgl and krwgasifiers as part of igcc plant computer simulations. *Energy conversion and management*, 46:1767–1779, 2005 (cit. on pp. 58, 60).

[151] F. Ullmann. *Ullmann's encyclopedia of industrial chemistry*. Wiley-VCH, Weinheim , Germany, 1998 (cit. on pp. 58, 59).

[152] E. Grol. Evaluation of alternate water gas shift configurations for igcc systems. National Energy Technology Laboratory (NETL), DOE/NETL-401/080509, 2009. (Cit. on p. 59).

[153] Gas-turbine sgt5-4000f. Siemens AG, 06.2015. URL: http://www.energy.siemens.com/hq/en/fossil-power-generation/gas-turbines/sgt5-4000f.htm#content=Technical%20data (cit. on pp. 60, 62).

[154] A. Giuffrida, M. C. Romano, and G. G. Lozza. Thermodynamic assessment of igcc power plants with hot fuel gas desulfurization. *Applied energy*, 87:3374–3383, 2010 (cit. on p. 71).

[155] S. Göke, S. Terhaar, S. Schimek, K. Göckeler, and C. O. Paschereit. Combustion of natural gas, hydrogen and bio-fuels at ultra-wet conditions. In *Asme turbo expo 2011: power for land, sea and air*. Vancouver, Canada, 2011 (cit. on p. 72).

[156] E. Deuker, M. H. König, M. Möller, J. Slad, and H. Streb. Sgt5-4000f gas turbine and combined cycle power plant evolution reflecting the changing market requirements. Siemens AG - Energy Sector, 2013. (Cit. on p. 78).

[157] M. Jansen, T. Schulenberg, and D. Waldinger. Shop test result of the v64.3 gas turbine. *Journal of engineering for gas turbines and power*, 114:676–581, 1992 (cit. on pp. 78, 79).

[158] A. Stodola. *Dampf- und gastubrinen (in german)*. Springer, Berlin, 1924 (cit. on p. 78).

[159] A. Ray. Dynamic modelling of power plant turbines for controller design. *Applied mathematical modelling*, 4:109–112, 1980 (cit. on p. 78).

[160] F. P. Incropera and D. P. DeWitt. *Fundamentals of heat and mass transfer*. John Wiley & Sons, Inc., 4th edition, 1996 (cit. on p. 79).

[161] H. Blasius. Das ähnlichkeitsgesetz bei reibungsvorgängen in flüssigkeiten (in german). *Forschungsarbeiten des vdi*, 131, 1913 (cit. on p. 79).

[162] K. Ogriseck. Untersuchung von igcc-kraftwerkskonzepten mit polygeneration (in german). PhD thesis. VDI - Reihe 6, Freiberg, 2006 (cit. on p. 82).

[163] M. Sorgenfrei, M. Penkuhn, and G. Tsatsaronis. Understanding the inefficiencies of an igcc concept with carbon capture based on an advanced exergy analysis. In *28th international conference on efficiency, costs, optimization, simulation and environmental impact of energy systems - ecos*. Pau, France, 2015 (cit. on p. 85).

[164] M. Sorgenfrei and G. Tsatsaronis. Detailed exergetic evaluation of heavy-duty gas turbine systems running on natural gas and syngas. In *27th international conference on efficiency, costs, optimization, simulation and environmental impact of energy systems - ecos*. Turku, Finland, 2014 (cit. on p. 91).

[165] M. Sorgenfrei and G. Tsatsaronis. Detailed exergetic evaluation of heavy-duty gas turbine systems running on natural gas and syngas. *Energy conversion and management*, 107:43–51, 2016 (cit. on p. 91).

[166] G. Tsatsaronis, T. Morosuk, D. Koch, and M. Sorgenfrei. Understanding the thermodynamic inefficiencies in combustion processes. In *3rd international conference on contemporary problems of thermal engineering (cpote)*. Gliwice, Poland, 2012 (cit. on p. 94).

[167] G. Tsatsaronis, T. Morosuk, D. Koch, and M. Sorgenfrei. Understanding the thermodynamic inefficiencies in combustion processes. *Energy*, 62:3–11, 2013. DOI: 10.1016/j.energy.2013.04.075 (cit. on p. 94).

[168] G. Tsatsaronis and F. Cziesla. *Thermoeconomics*. In. Vol. 16. Academic Press, 3rd adition, 2002. part Encyclopedia of Physical Science and Technology, pp. 659–680 (cit. on p. 114).

Appendix A

Temperature Profiles and Flow Diagrams

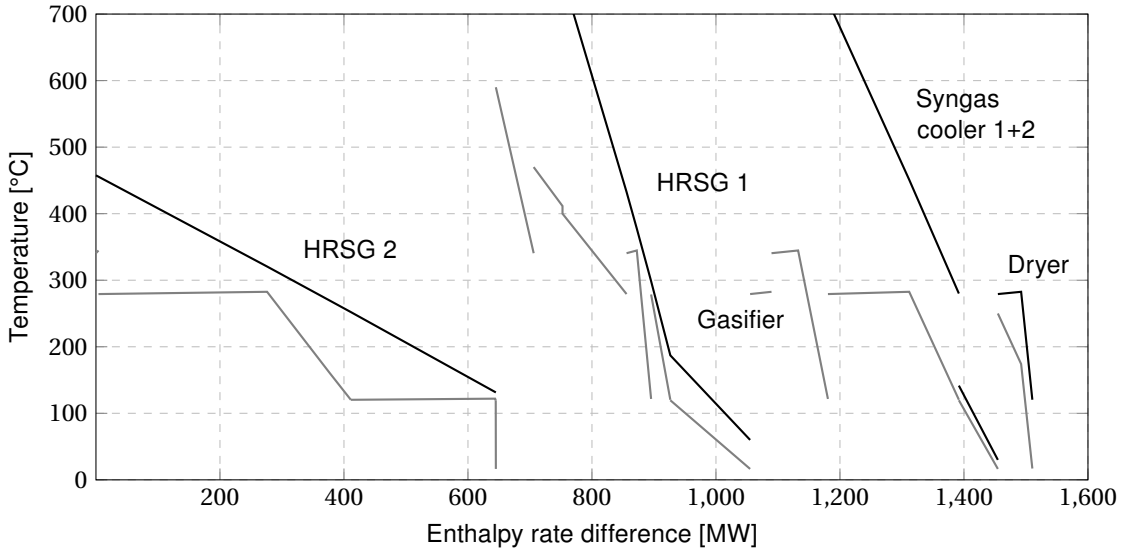

Figure 1.1: Temperature profiles of heat transfer within the IGCC plant using a two-reactor CLC and a Shell gasifier (Case CLC-Ni1).

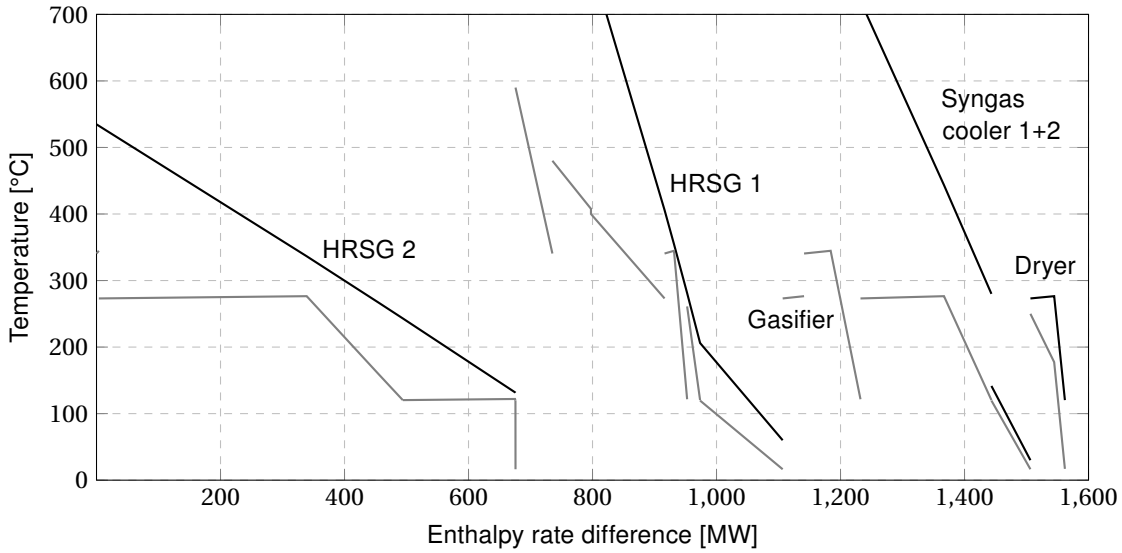

Figure 1.2: Temperature profiles of heat transfer within the IGCC plant using a two-reactor CLC and a Shell gasifier (Case CLC-Ni2).

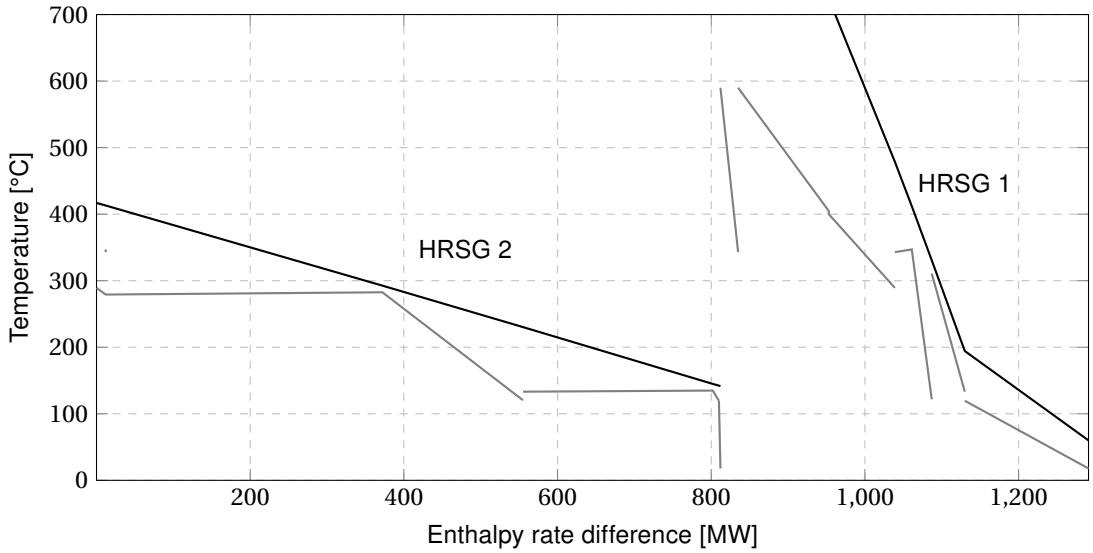

Figure 1.3: Temperature profiles of heat transfer within the IGCC plant using a two-reactor CLC and a Shell gasifier (Case CLC-Ni4).

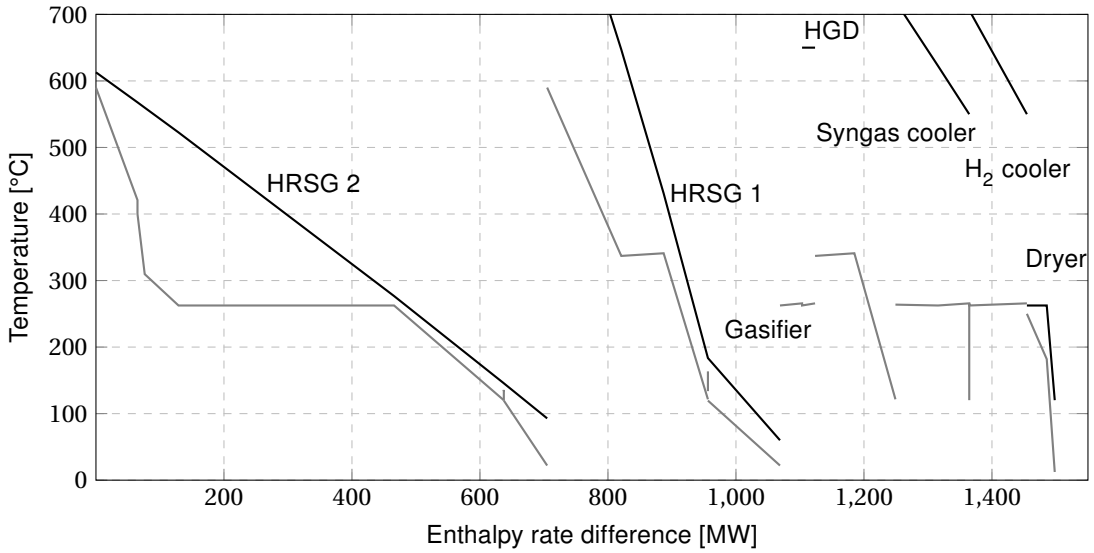

Figure 1.4: Temperature profiles of heat transfer within the IGCC plant using a three-reactor CLC and a Shell gasifier (case CLC-Fe2).

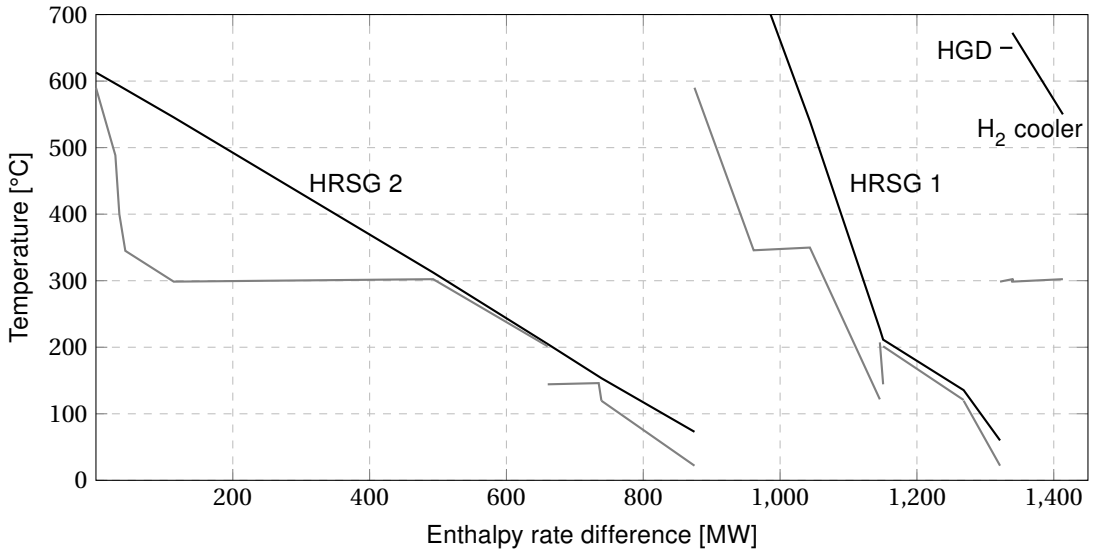

Figure 1.5: Temperature profiles of heat transfer within the IGCC plant using a three-reactor CLC and a BGL gasifier (Case CLC-Fe4).

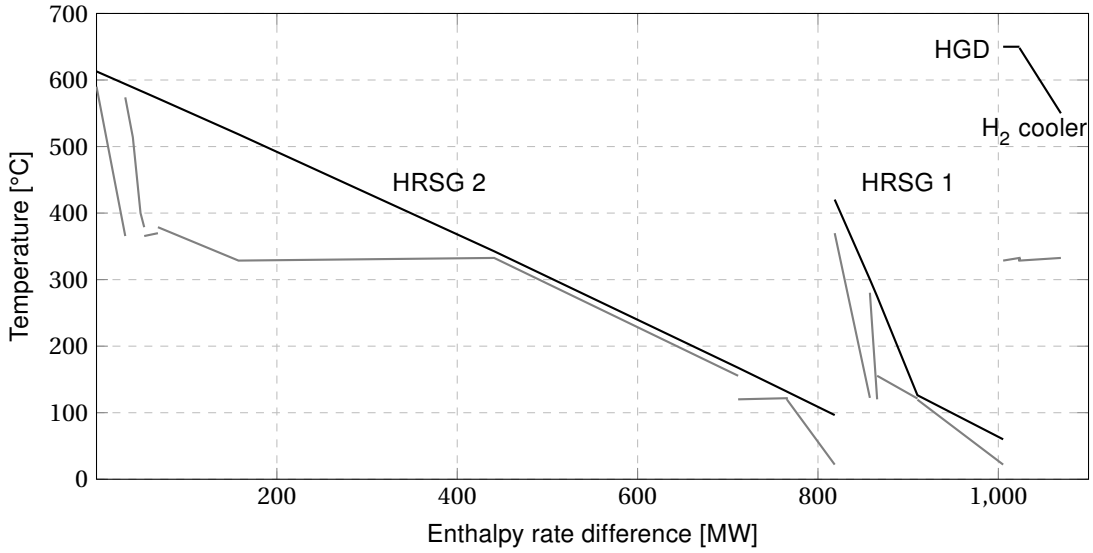

Figure 1.6: Temperature profiles of heat transfer within the IGCC plant using a three-reactor CLC and a BGL gasifier (Case CLC-Fe5).

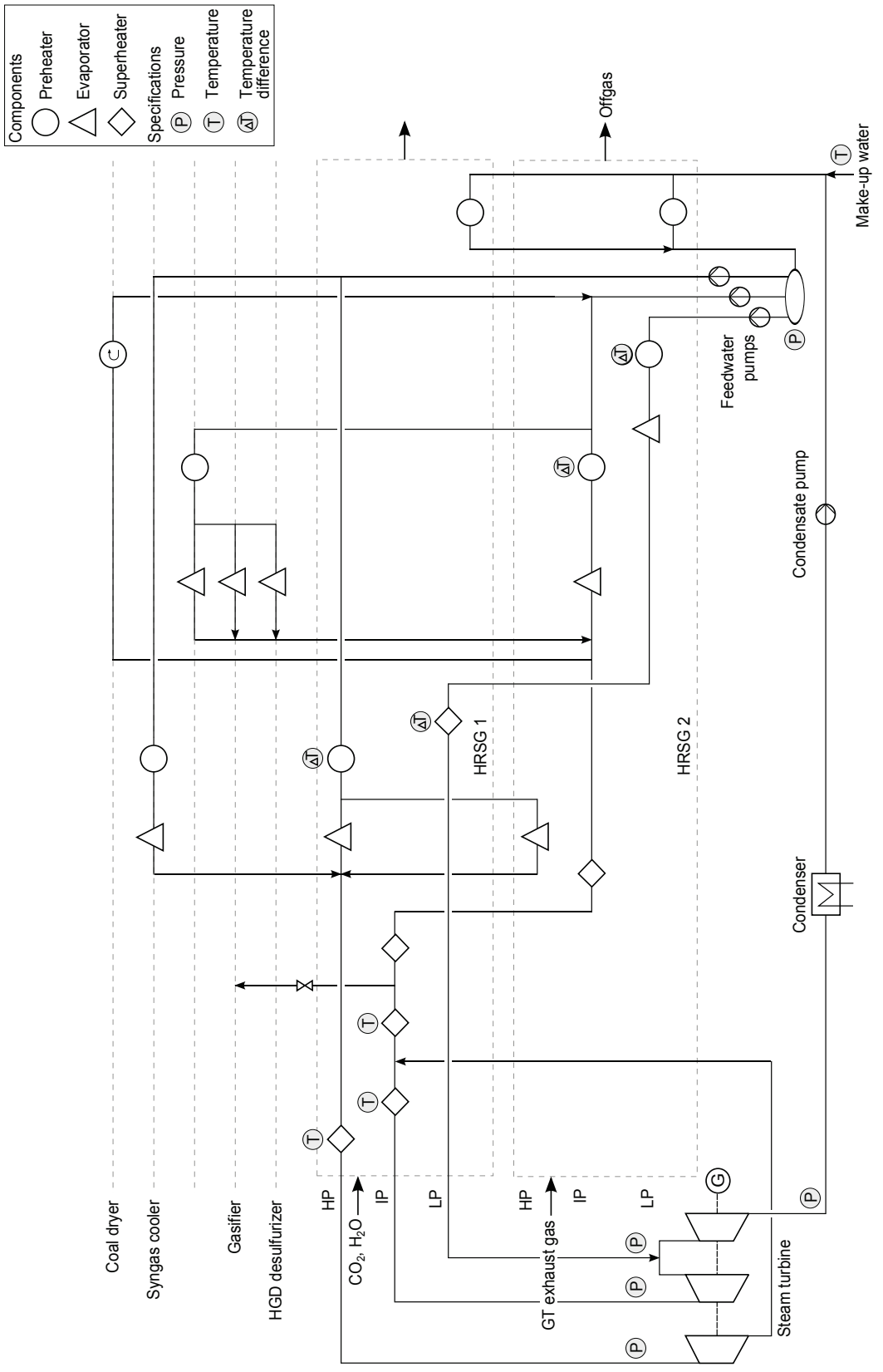

Figure 1.7: Flow diagram of the steam cycle of the cases featuring a Shell gasifier and a 2 reactor CLC unit.

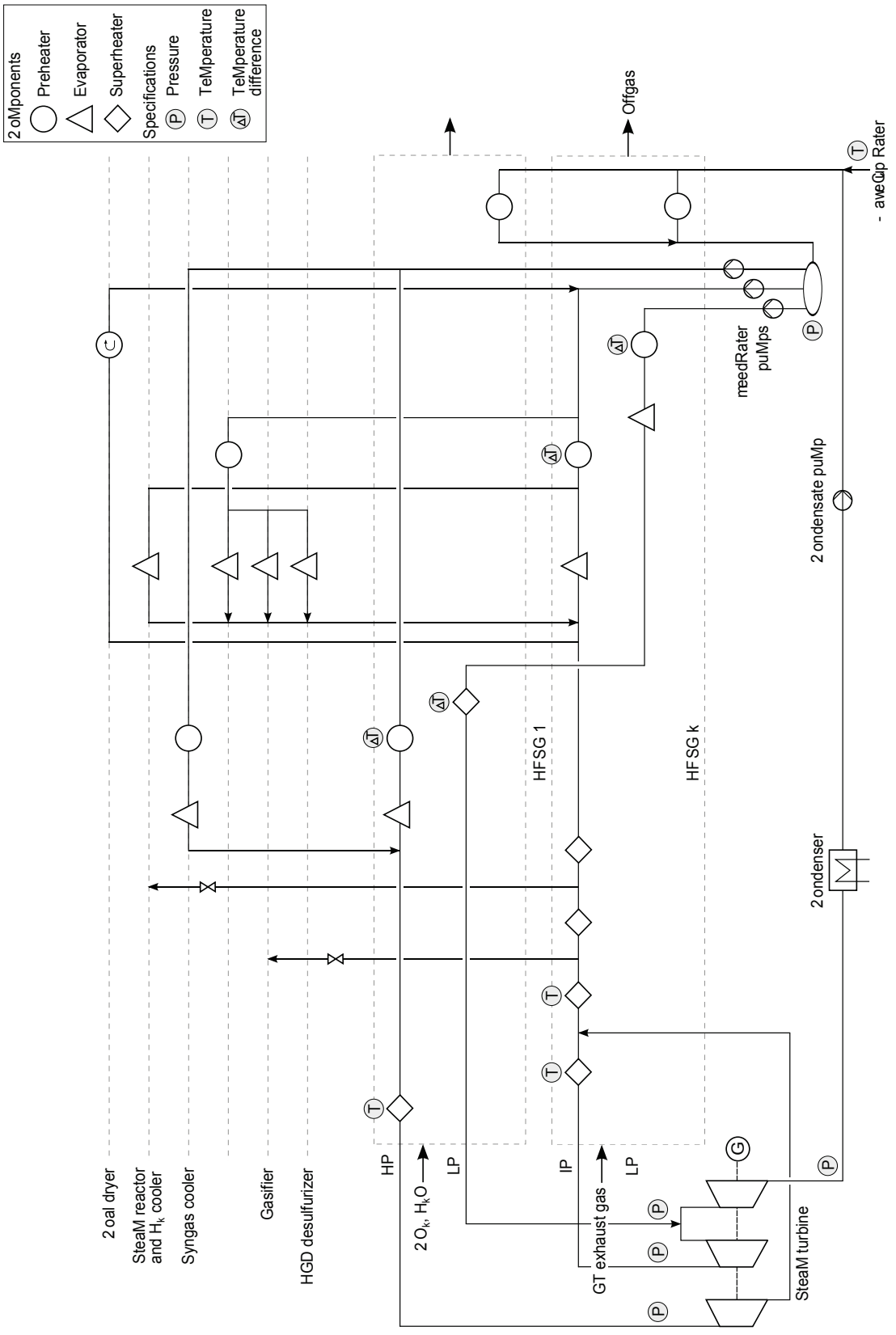

Figure 1.8: Flow diagram of the steam cycle of the cases featuring a Shell gasifier and a 3 reactor CLC unit.

Appendix B

Exergy Analysis

Table 2.1: Results of the conventional and advanced exergy analyses for the ten components with the highest exergy destruction in case IGCC-1.

No.	Component	$\dot{E}_D$ [MW]	y_D [%]	ε [%]	$\dot{E}_D^{UN}$ [MW]	$\dot{E}_D^{AV}$ [MW]	$\dot{E}_D^{EN}$ [MW]	$\dot{E}_D^{EX}$ [MW]	$\dot{E}_D^{AV,EN}$ [MW]	$\dot{E}_D^{AV,EX}$ [MW]
1	Gasifier	644.9	25.06	75.01	569.7	75.1	311.2	333.7	34.0	41.2
2	GT comb. chamber	340.3	13.22	76.01	295.3	44.4	139.7	200.6	18.2	26.2
3	WGS unit	85.9	3.34	91.98	81.1	4.7	31.1	54.7	1.7	3.0
4	GT turbine	77.6	3.02	93.51	63.3	14.3	28.0	49.6	5.2	9.1
5	Syngas cooler	60.1	2.34	69.44	39.6	20.5	21.5	38.6	7.3	13.2
6	H_2S capture cycle	35.7	1.39	–	35.2	0.5	14.3	21.5	0.2	0.3
7	CO_2 capture cycle	35.1	1.37	–	33.1	2.1	13.1	22.0	0.8	1.3
8	GT compressor	27.2	1.06	94.71	21.0	6.3	9.6	17.6	2.2	4.1
9	Gas quench	24.2	0.94	–	24.2	0.0	8.5	15.7	0.0	0.0
10	Condenser	20.5	0.80	–	20.5	0.0	7.2	13.3	0.0	0.0

$\dot{E}_{F,tot} = 2573.4\,MW$

Table 2.2: Exergy destruction of all inefficiencies within the gas turbine system (case IGCC-1).

Inefficiencies	Sum	Air compressor			Comb. chamber	Gas Turbine							Shaft	Gen.*
						Stage 1		Stage 2		Stage 3		Stage 4		
		Stages 1-8	Stages 9-11	Stages 12-13		Vanes	Blades	Vanes	Blades	Vanes	Blades			
Compression	1.79	1.13	0.41	0.25										
Stoichiometric combustion	12.34				12.34									
Addition of excess air	5.33				5.33									
Convective heat transfer	0.40					0.10	0.10	0.06	0.05	0.04	0.05			
Pressure drop	0.75				0.21	0.12		0.13		0.14		0.15		
Expansion and mixing at different temperatures and pressures	5.61				2.80	0.86		0.74		0.66		0.55		
Mixing at different compositions	2.61				1.58	0.38	0.25	0.13	0.09	0.07	0.08	0.03		
Heat loss	0.41				0.41									
Transport of shaft work	0.21												0.21	
Conversion of mechanical into electrical energy	0.41													0.41

* Generator

Table 2.3: Results of the conventional exergy analyses for characteristic cases - part 1.

Component	IGCC-1	CLC-Ni3	CLC-Fe1
Gasification Island	34.29	30.89	29.70
O_2 compressor	0.13	0.13	0.13
N_2 compressor	0.04	-	-
Coal preparation	0.66	1.00	0.77
Gasifier	24.85	25.01	25.44
Gas quench	0.94	0.95	0.58
Syngas cooler 1	2.34	2.40	1.99
Syngas cooler 2	-	0.18	-
Quench gas blower	0.02	0.02	0.05
Cyclone+filter	0.02	0.02	0.07
Scrubber	0.20	0.19	-
Hydrolizer	-	0.002	-
2-stage WGS unit	3.34	-	-
Saturator	0.43	-	-
Claus plant	0.08	0.06	-
Recycle compressor CO_2	-	0.001	0.001
Exergy loss	1.25	0.94	0.68
ASU	1.32	1.34	1.38
Air compressor	0.52	0.52	0.55
Heat exchanger	0.16	0.17	0.16
HP and LP column	0.43	0.40	0.43
Air turbine	0.01	0.01	0.02
O_2 turbine	0.00	0.03	0.01
Heater nitrogen	0.00	0.00	0.00
Heater mixture	0.08	0.08	0.08
Throttling	0.09	0.09	0.09
Exergy loss	0.02	0.03	0.03
AGR/HGD	3.31	1.61	0.42
Heat exchanger	0.001	0.005	-
H_2S capture cycle	1.39	0.62	-
CO_2 capture cycle	1.37	-	-
Refrigeration machine	0.20	0.33	-
Exergy loss	0.36	0.65	-
HGD - desulfurizer	-	-	0.05
HGD - regenerator	-	-	0.34
HGD - compressor	-	-	0.03
CO_2 conditioning	7.10	6.18	5.21
CO_2 compressor	0.75	0.32	0.31
Exergy loss CO_2	6.36	5.87	4.90
CLC unit	-	13.73	10.44
Fuel reactor	-	3.89	2.70
Steam reactor	-	-	1.17
Air reactor	-	9.84	4.62
Air compressor	-	-	1.33
Steam reactor cooler	-	-	0.62

Table 2.4: Results of the conventional exergy analyses for characteristic cases - part 2.

Component	IGCC-1	CLC-Ni3	CLC-Fe1
Gas turbine system	17.65	3.66	12.66
Compressor	1.06	1.28	0.31
Comb. chamber	13.22	-	8.32
Turbine	3.02	2.13	3.54
Exergy loss	0.35	0.25	0.49
Steam cycle	8.21	11.36	10.71
Pumps	0.02	0.02	0.02
Economizer 1	0.08	0.81	0.75
Economizer 2	-	0.00	0.17
Preheater LP	0.00	0.00	0.00
Evaporator LP	0.25	0.55	0.04
Superheater LP	0.01	0.05	0.01
Preheater IP 1	0.22	0.24	0.16
Preheater IP 2	-	0.41	-
Evaporator IP	0.46	1.96	1.38
Superheater IP1	0.13	0.00	0.35
Superheater IP2	0.00	0.80	0.06
Superheater IP3	0.19	0.00	0.00
Superheater IP4	-	0.43	0.17
Preheater HP	-	0.08	0.07
Evaporator HP1	-	0.03	0.05
Evaporator HP2	-	0.03	-
Superheater HP1	0.26	0.53	0.39
Superheater HP2	0.06	-	-
Turbine LP	0.43	0.98	0.28
Turbine IP	0.24	0.41	0.21
Turbine HP	0.12	0.03	0.06
Condenser	0.80	1.36	0.53
Throttles	-	-	0.24
Mixer	0.00	0.04	0.00
Exergy loss	4.93	2.60	5.78

Definitions for the Exergetic Efficiency

Gasifier

$$\dot{E}_{\mathrm{P}} = \dot{E}_{\mathrm{syngas,raw}} - \dot{E}^{\mathrm{PH}}_{\mathrm{coal,dryed}} - \dot{E}^{\mathrm{PH}}_{\mathrm{N_2}} - \dot{E}^{\mathrm{PH}}_{\mathrm{O_2}} - \dot{E}^{\mathrm{PH}}_{\mathrm{H_2O}} + \Delta\dot{E}_{\mathrm{IP\ steam}} \tag{2.1}$$

$$\dot{E}_{\mathrm{F}} = \dot{E}^{\mathrm{CH}}_{\mathrm{coal,dryed}} + \dot{E}^{\mathrm{CH}}_{\mathrm{N_2}} + \dot{E}^{\mathrm{CH}}_{\mathrm{O_2}} + \dot{E}^{\mathrm{CH}}_{\mathrm{H_2O}} - \dot{E}_{\mathrm{carbon}} \tag{2.2}$$

GT combustion chamber

$$\dot{E}_{\mathrm{P}} = \dot{E}^{\mathrm{PH}}_{\mathrm{combustion\ gas}} - \dot{E}^{\mathrm{PH}}_{\mathrm{syngas}} - \dot{E}^{\mathrm{PH}}_{\mathrm{air,in}} \tag{2.3}$$

$$\dot{E}_{\mathrm{F}} = -\dot{E}^{\mathrm{CH}}_{\mathrm{combustion\ gas}} + \dot{E}^{\mathrm{CH}}_{\mathrm{syngas}} + \dot{E}^{\mathrm{CH}}_{\mathrm{air,in}} \tag{2.4}$$

WGS unit

$$\dot{E}_{\mathrm{P}} = e^{\mathrm{CH}}_{\mathrm{H_2}} \cdot \left(\dot{m}_{\mathrm{H_2,in}} - \dot{m}_{\mathrm{H_2,out}}\right) + \Delta\dot{E}_{\mathrm{H_2O,saturator}} + \Delta\dot{E}_{\mathrm{HP\ steam}} + \Delta\dot{E}_{\mathrm{H_2O,Eco}} \tag{2.5}$$

$$\dot{E}_{\mathrm{F}} = \left(\dot{E}_{\mathrm{syngas,raw}} - \dot{E}_{\mathrm{shift\ gas}} - e^{\mathrm{CH}}_{\mathrm{H_2}} \cdot \left(\dot{m}_{\mathrm{H_2,out}} - \dot{m}_{\mathrm{H_2,in}}\right)\right) + \dot{E}_{\mathrm{steam}} - \sum \dot{E}_{\mathrm{condensate}} \tag{2.6}$$

GT turbine

$$\dot{E}_{\mathrm{P}} = |\dot{W}_{\mathrm{el}}| \tag{2.7}$$

$$\dot{E}_{\mathrm{F}} = \dot{E}_{\mathrm{combustion\ gas}} + \sum \dot{E}^{\mathrm{cooling}}_{\mathrm{air,in}} + \sum \dot{E}^{\mathrm{sealing}}_{\mathrm{air,in}} - \sum \dot{E}_{\mathrm{flue\ gas}} \tag{2.8}$$

Syngas cooler

$$\dot{E}_{\mathrm{P}} = \Delta\dot{E}_{\mathrm{HP\ steam}} + \Delta\dot{E}_{\mathrm{IP\ steam}} \tag{2.9}$$

$$\dot{E}_{\mathrm{F}} = \Delta\dot{E}_{\mathrm{syngas,raw}} \tag{2.10}$$

GT compressor

$$\dot{E}_{\mathrm{P}} = \sum \dot{E}^{\mathrm{cooling}}_{\mathrm{air,out}} + \sum \dot{E}^{\mathrm{sealing}}_{\mathrm{air,out}} + \sum \dot{E}^{\mathrm{combustion\ chamber}}_{\mathrm{air,out}} - \dot{E}_{\mathrm{air,in}} \tag{2.11}$$

$$\dot{E}_{\mathrm{F}} = \dot{W}_{\mathrm{el}} \tag{2.12}$$

Calculation algorithm for the advanced exergy analysis

1. Endogenous exergy destruction

$\dot{E}_{D,k}^{EN}$ is calculated by a set of equations assuming that all components except component k are working without exergy destruction. The exergy flows associated with the major streams must be a function of the mass flow rate. The constant exergetic efficiency of the component in regard must be implemented when process variables cross the system boundary.

2. Exogenous exergy destruction

$$\dot{E}_{D,k}^{EX} = \dot{E}_{D,k} - \dot{E}_{D,k}^{EN} \tag{2.13}$$

3. Unavoidable exergy destruction

$$\dot{E}_{D,k}^{UN} = \dot{E}_{P,k} \cdot \left(\dot{E}_{D,k} / \dot{E}_{P,k}\right)^{UN} \tag{2.14}$$

$$\dot{E}_{D,k}^{UN,EN} = \dot{E}_{P,k}^{EN} \cdot \left(\dot{E}_{D,k} / \dot{E}_{P,k}\right)^{UN} \tag{2.15}$$

$$\dot{E}_{D,k}^{UN} = \dot{E}_{D,k}^{UN,EN} \cdot \left(\dot{E}_{P,k} / \dot{E}_{P,k}^{EN}\right) \quad \text{, Eq. 2.14 and 2.15} \tag{2.16}$$

$$\varepsilon = \varepsilon^{EN} \tag{2.17}$$

$$\dot{E}_{P,k} / \dot{E}_{F,k} = \dot{E}_{P,k}^{EN} / \dot{E}_{F,k}^{EN} \tag{2.18}$$

$$\dot{E}_{D,k}^{UN} = \dot{E}_{D,k}^{UN,EN} \cdot \left(\dot{E}_{D,k} / \dot{E}_{D,k}^{EN}\right) \quad \text{, Eq. 2.16 and 2.18} \tag{2.19}$$

4. Avoidable exergy destruction

$$\dot{E}_{D,k}^{AV} = \dot{E}_{D,k} - \dot{E}_{D,k}^{UN} \tag{2.20}$$

5. Avoidable endogenous exergy destruction

$$\dot{E}_{D,k}^{AV,EN} = \dot{E}_{D,k}^{EN} - \dot{E}_{D,k}^{UN,EN} \tag{2.21}$$

6. Avoidable exogenous exergy destruction

$$\dot{E}_{D,k}^{AV,EX} = \dot{E}_{D,k}^{AV} - \dot{E}_{D,k}^{AV,EN} \tag{2.22}$$

7. Unavoidable exogenous exergy destruction

$$\dot{E}_{D,k}^{UN,EX} = \dot{E}_{D,k}^{UN} - \dot{E}_{D,k}^{UN,EN} \tag{2.23}$$

Appendix C

Off-Design

Table 3.1: State variables of the steam cycle under design (case IGCC-2) and off-design conditions (case IGCC-H2/IGCC-H2i) - part 1.

System component		Design			Off-design		
		$\dot{m}$ [kg/s]	p [bar]	T [°C]	$\dot{m}$ [kg/s]	p [bar]	T [°C]
HRSG							
HP superheater 1	in	69.15	170.6	352.6	-	-	-
	out	69.15	164.0	494.2	-	-	-
HP superheater 2	in	69.15	164.0	494.2	-	-	-
	out	69.15	160.3	567.0	-	-	-
IP preheater 1	in	142.20	54.1	160.2	-	-	-
	out	142.20	54.0	160.3	-	-	-
IP preheater 2	in	97.72	53.1	238.4	-	-	-
	out	97.72	52.9	267.4	-	-	-
IP evaporator	in	97.72	52.9	267.4	-	-	-
	out	97.72	50.2	264.2	-	-	-
IP superheater	in	83.73	50.2	264.2	-	-	-
	out	83.73	49.8	292.4	-	-	-
IP reheater	in	106.90	49.8	345.7	-	-	-
	out	106.90	46.5	551.4	-	-	-
LP preheater	in	28.57	7.2	159.4	-	-	-
	out	28.57	7.2	166.1	-	-	-
LP evaporator	in	34.65	7.2	166.1	-	-	-
	out	34.65	6.8	164.0	-	-	-
LP superheater	in	41.83	6.8	164.0	-	-	-
	out	41.83	6.7	236.6	-	-	-
Economizer	in	24.91	6.3	22.0	-	-	-
	out	24.91	6.1	159.4	-	-	-

Table 3.2: State variables of the steam cycle under design (case IGCC-2) and off-design conditions (case IGCC-H2/IGCC-H2i) - part 2.

System component		Design			Off-design		
		$\dot{m}$ [kg/s]	p [bar]	T [°C]	$\dot{m}$ [kg/s]	p [bar]	T [°C]
Gasifier radiant cooler							
HP preheater	in	47.52	187.1	162.3	47.52	187.1	162.3
	out	47.52	179.6	356.8	47.52	179.6	356.8
HP evaporator	in	47.52	179.6	356.8	47.52	179.6	356.8
	out	47.52	170.6	352.6	47.52	170.6	352.6
HT-WGS unit							
HP preheater	in	21.63	187.1	162.3	21.63	187.1	162.3
	out	21.63	179.6	356.8	21.63	179.6	356.8
HP evaporator	in	21.63	179.6	356.8	21.63	179.6	356.8
	out	21.63	170.6	352.6	21.63	170.6	352.6
LP preheater	in	13.27	7.2	159.4	13.27	7.2	159.4
	out	13.27	7.2	166.1	13.27	7.2	166.1
LP evaporator	in	13.27	7.2	166.1	13.27	7.2	166.1
	out	13.27	6.8	164.0	13.27	6.8	164.0
Injection	out	45.94	56.0	300.0	45.94	56.0	300.0
LT-WGS unit							
IP preheater	in	83.73	54.0	160.3	83.73	54.0	160.3
	out	83.73	53.1	238.4	83.73	53.1	238.4
Economizer	in	228.30	6.3	22.0	228.30	6.3	22.0
	out	228.30	6.1	159.4	224.60	6.1	159.4
Saturator							
IP condenser	in	13.99	50.2	264.2	-	-	-
	out	13.99	50.2	264.2	-	-	-
IP subcooler	in	13.99	50.2	264.2	-	-	-
	out	13.99	50.2	238.4	-	-	-
AGR unit							
LP condenser	in	6.08	6.8	164.0	6.08	6.8	164.0
	out	6.08	6.8	164.0	6.08	6.8	164.0
Scrubber							
Injection	out	58.50	75.0	160.0	58.50	75.0	160.0
Boiler							
HP superheater	in	-	-	-	69.15	170.6	352.6
	out	-	-	-	69.15	170.6	397.2
Steam turbine							
HP turbine	in	69.15	160.3	567.0	-	-	-
	out	69.15	49.8	378.6	-	-	-
IP turbine	in	106.90	46.5	551.4	-	-	-
	out	106.90	6.7	270.0	-	-	-
LP turbine	in	148.80	6.7	260.5	23.21	1.0	213.5
	out	148.80	0.035	26.7	23.21	0.035	26.7